

# Deep Discrete Encoders: Identifiable Deep Generative Models for Rich Data with Discrete Latent Layers

Seunghyun Lee and Yuqi Gu

Department of Statistics, Columbia University

## Abstract

In the era of generative AI, deep generative models (DGMs) with latent representations have gained tremendous popularity. Despite their impressive empirical performance, the statistical properties of these models remain underexplored. DGMs are often overparametrized, non-identifiable, and uninterpretable black boxes, raising serious concerns when deploying them in high-stakes applications. Motivated by this, we propose an interpretable deep generative modeling framework for rich data types with discrete latent layers, called *Deep Discrete Encoders* (DDEs). A DDE is a directed graphical model with multiple binary latent layers. Theoretically, we propose transparent identifiability conditions for DDEs, which imply progressively smaller sizes of the latent layers as they go deeper. Identifiability ensures consistent parameter estimation and inspires an interpretable design of the deep architecture. Computationally, we propose a scalable estimation pipeline of a layerwise nonlinear spectral initialization followed by a penalized stochastic approximation EM algorithm. This procedure can efficiently estimate models with exponentially many latent components. Extensive simulation studies validate our theoretical results and demonstrate the proposed algorithms' excellent performance. We apply DDEs to three diverse real datasets for hierarchical topic modeling, image representation learning, response time modeling in educational testing, and obtain interpretable findings.

**Keywords:** Identifiability; Interpretable Artificial Intelligence; Representation Learning; Deep Belief Network; Directed Graphical Model.

## 1 Introduction

In the era of generative AI, deep generative models (DGMs) with latent representations have gained tremendous popularity across various domains. DGMs achieve impressive empirical success due to their rich modeling power and predictive capacity, and are useful tools to generate images, text, and audio ([Hinton et al., 2006](#); [Lee et al., 2009](#); [Kingma and Welling, 2014](#);

---

Corresponding Author: Yuqi Gu. Email: [yuqi.gu@columbia.edu](mailto:yuqi.gu@columbia.edu). Research is partially supported by NSF Grant DMS-2210796.

Salakhutdinov, 2015). However, these models are often subject to statistical issues regarding the model identifiability, interpretability, and parameter estimation reliability. Indeed, most deep learning models are heavily overparametrized black boxes, with more parameters than the number of samples, and are fundamentally non-identifiable. The lack of identifiability means that there may be very different parameter values that give the same marginal distribution of the observed data, leading to inconsistent parameter estimation. In such cases, it is impossible to guarantee the reproducibility of the learned latent representations across different training instances and the validity of the downstream inference. Additionally, the deep layers often merely serve as tools for inducing flexible data distributions but without a meaningful substantive interpretation. These issues raise serious concerns when deploying DGMs in high-stakes applications such as education, medicine, and health care.

We address the above problems from statisticians’ perspectives by proposing a broad family of interpretable and identifiable deep generative models for rich types of data, called *Deep Discrete Encoders* (DDEs). DDEs are directed graphical models with potentially deep discrete latent layers to generate the bottom-layer multivariate observed data. A key feature of DDEs is that the latent layers are discrete and organized in progressively smaller sizes as they go deeper; see Figure 1. This architecture induces very expressive models via the exponentially many mixture components (since each configuration of the discrete latent vector gives a mixture component), and also has the nice interpretation of increasingly more general latent features in deeper layers (Bengio et al., 2013). DDEs are motivated by both popular generative models in deep learning and latent variable models in educational and psychological measurement. While these two areas rarely intersect in the past, we leverage the insights from both fields to inspire the theory and methodology of DDEs.

Figure 1 displays the graphical model representations of a typical DDE alongside a DDE estimated from real data. The right panel of Figure 1 shows that fitting DDEs to a dataset of text documents uncovers interesting hierarchical latent topics as well as an interpretable

word generating mechanism; see more details in Section 6. We emphasize that there is no restriction on the types of observed data; for example, the bottom data layer can be modeled by any exponential family distributions. In the text data example, Poisson distribution is used to model the word counts in documents. Our real data examples in Section 6 range from word *counts* in text documents to *binary* pixel values in images, to *continuous* response times of students in digital educational assessments. Such flexibility makes DDEs attractive for many practical applications ranging from machine learning to domain sciences.

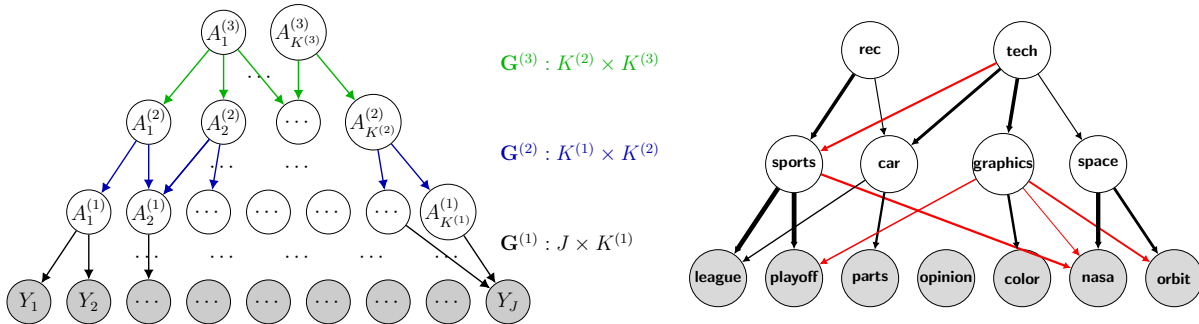


Figure 1: **Left:** Example graphical model representation of DDEs. **Right:** Simplified estimated DDE structure of the latent topics for the 20 newsgroups dataset. Only the shaded nodes are observed. In the right panel, edge widths are proportional to coefficients’ absolute values. The black/red edge colors imply positive/negative coefficients, respectively.

The main contributions in this paper include rigorous identifiability theory and scalable computational pipelines for DDEs. *For identifiability*, we propose general identifiability conditions in terms of the dependence graph structure between adjacent layers in the graphical model (corresponding to the directed arrows in Figure 1). We work under the minimal possible assumptions in order to flexibly cover the various examples mentioned above. Next, we provide an informal statement of the identifiability conditions. Under an identifiable DDE, we also prove that a penalized-likelihood based estimator is consistent for estimating both the continuous parameters as well as the discrete graph structure.

**Theorem** (Informal version of Theorems 1 and 2). *The DDE with a known number of latent variables is identifiable up to latent variable permutation in each layer, as long as each latent variable has at least three exclusive children. Under a weaker notion of “generic*

*identifiability”, this condition can be relaxed to that each latent variable has at least three children that are not necessarily exclusive.*

*For computation*, we propose a scalable estimation pipeline for DDEs. The multiple layers of nonlinear latent variables in DDEs lead to a highly nonconvex optimization landscape with potentially exponentially many local optima. To address this challenging setting, our computational pipeline features a nuanced layerwise nonlinear spectral initialization followed by a penalized stochastic approximation EM algorithm. This procedure can efficiently handle models with a large number of latent variables. We achieve favorable simulation results for as many as  $K^{(1)} = 30$  binary latent variables in the shallowest latent layer, which amount to  $2^{K^{(1)}}$  mixture components and define a very expressive model. Extensive simulation studies not only validate the identifiability results, but also demonstrate the excellent performance of the proposed algorithms. We apply DDEs to real data in three diverse tasks, including hierarchical topic modeling, image representation learning, and response time modeling in digital educational testing. Across these applications, DDEs extract highly interpretable latent structures and learn useful representations for downstream analyses.

We make brief remarks to place DDEs in the rapidly emerging field of generative AI. For the considered unsupervised learning setting, we use “generative model” to refer to probabilistic models where observed data are generated conditional on hidden variables. Classical examples with one hidden layer include mixture models and mixed membership models. Recently, powerful multilayer models have been proposed for more complex tasks, which either consist of multiple latent layers or a single latent layer transformed by deep neural networks. Popular models in machine learning include deep belief networks (Hinton et al., 2006), deep Boltzmann machines (Salakhutdinov and Hinton, 2009), variational autoencoders (Ranzato and Szummer, 2008), generative adversarial networks (Goodfellow et al., 2014), diffusion models (Sohl-Dickstein et al., 2015), and transformer-based models (Vaswani et al., 2017) such as large language models. See Section 2.2 for more discussions.

**Organization.** Section 2 formally defines DDEs and elaborates on its connection with existing models. Section 3 provides identifiability results of DDEs and proves the consistency of a penalized-likelihood estimator. Section 4 presents scalable computational algorithms for estimating DDEs. Section 5 and Section 6 present simulation studies and real-data applications under various data types. Section 7 concludes the paper. All technical proofs, and additional details about computation and data analysis are in the Supplementary Material.

## 2 Deep Discrete Encoders

**Notation.** For a positive integer  $K$ , denote  $[K] = \{1, \dots, K\}$ . For a matrix  $\mathbf{G}$  with  $J$  rows, let  $\mathbf{g}_1, \dots, \mathbf{g}_J$  denote its row vectors. Let  $\mathbf{0}_K, \mathbf{1}_K$  be the all-zero vector and all-one vector of length  $K$ , respectively. Let  $\mathbf{e}_k$  be the  $K$ -dimensional canonical basis vector. Let  $g_{\text{logistic}}(x) := e^x / (1 + e^x)$  denote the logistic/sigmoid function. For a finite set  $I$ , let  $S_I$  denote the collection of all permutation maps of  $I$ , and let  $\text{id}_I$  be the identity permutation on  $I$ . For nonnegative sequences  $\{(a_N, b_N)\}_{N \geq 1}$ , write  $a_N \ll b_N$  when  $a_N/b_N \rightarrow 0$  as  $N \rightarrow \infty$ .

### 2.1 Model Definition

We formally define the  $D$ -latent-layer DDE as a generative model with  $D$  discrete latent layers. For each  $d \in [D]$ , assume that the  $(d - 1)$ th layer is generated conditional on the  $d$ th. Here, only the bottom layer (indexed by  $d = 0$ ) is observed, and all other layers are latent. The bottom layer data can take arbitrary values, but all latent variables are binary, similar to the celebrated deep belief networks (Hinton et al., 2006). Let  $\mathbf{Y} = (Y_1, \dots, Y_J) \in \times_{j=1}^J \mathcal{Y}_j$  denote the  $J$ -dimensional observed responses, where  $\mathcal{Y}_j$  is the sample space for the  $j$ th response; see the end of this subsection for concrete examples. We work under the minimal assumption that each  $\mathcal{Y}_j$  is a separable metric space. Denote the  $d$ th latent layer as  $\mathbf{A}^{(d)} = (A_1^{(d)}, \dots, A_{K^{(d)}}^{(d)}) \in \{0, 1\}^{K^{(d)}}$ , which is a  $K^{(d)}$ -dimensional binary vector. A DDE has a shrinking-ladder-shaped architecture, with the dimension of each layer decreasing as  $d$  increases:  $K^{(D)} < \dots < K^{(1)} < J$ . See Figure 1 for a graphical model representation.

We further specify the distribution of the directed graphical model in a top-down manner. The directed edges in Figure 1 are pointing downward, meaning that the deepest latent variables in the top layer  $d = D$  are generated first. The top layer latent variables are assumed to be independent Bernoullis with parameter  $\mathbf{p} = (p_1, \dots, p_{K^{(D)}})$ :

$$\mathbb{P}(\mathbf{A}^{(D)} = \boldsymbol{\alpha}^{(D)}) = \prod_{k=1}^{K^{(D)}} \mathbb{P}(A_k^{(D)} = \alpha_k^{(D)}) = \prod_{k=1}^{K^{(D)}} p_k^{\alpha_k^{(D)}} (1 - p_k)^{1 - \alpha_k^{(D)}}, \quad \forall \boldsymbol{\alpha}^{(D)} \in \{0, 1\}^{K^{(D)}}. \quad (1)$$

Next, define the *middle latent layers* inductively as follows. For each  $d > 1$ , suppose that  $\mathbb{P}(\mathbf{A}^{(d)})$ , the distribution of the  $d$ th layer, is given. Then, we define the  $(d - 1)$ th layer distribution by assuming the conditional independence of  $A_1^{(d-1)}, \dots, A_{K^{(d-1)}}^{(d-1)}$  given  $\mathbf{A}^{(d)}$ :

$$\mathbb{P}(\mathbf{A}^{(d-1)} = \boldsymbol{\alpha}^{(d-1)} \mid \mathbf{A}^{(d)}) = \prod_{k=1}^{K^{(d-1)}} \mathbb{P}(A_k^{(d-1)} = \alpha_k^{(d-1)} \mid \mathbf{A}^{(d)}), \quad \forall \boldsymbol{\alpha}^{(d-1)} \in \{0, 1\}^{K^{(d-1)}}. \quad (2)$$

Here, we additionally model each conditional distribution in (2) as

$$A_k^{(d-1)} \mid \mathbf{A}^{(d)} \sim \text{Bernoulli}\left(g_{\text{logistic}}\left(\beta_{k,0}^{(d)} + \sum_{l=1}^{K^{(d)}} \beta_{k,l}^{(d)} A_l^{(d)}\right)\right), \quad (3)$$

where  $g_{\text{logistic}}$  is the logistic function that maps the real-valued linear combinations to the  $[0, 1]$ -valued Bernoulli parameters (one may use alternative link functions  $g : \mathbb{R} \rightarrow [0, 1]$ , such as the probit link). Collect the  $\beta_{k,l}$ -parameters in a  $K^{(d-1)} \times (K^{(d)} + 1)$  matrix  $\mathbf{B}^{(d)}$ , whose first column is the intercepts  $(\beta_{k,0}^{(d)})_{k \in [K^{(d-1)}]}$  and remaining parts are  $(\beta_{k,l}^{(d)})_{k \in [K^{(d-1)}], l \in [K^{(d)}]}$ .

Finally, we model the bottom layer for the observed data. The observed  $\mathbf{Y} = (Y_1, \dots, Y_J)$  are modeled by assuming the conditional independence of  $Y_1, \dots, Y_J$  given  $\mathbf{A}^{(1)}$ . As the observations  $\mathbf{Y}$  are not necessarily binary, we replace the Bernoulli conditional distributions in (3) by a general parametric family of the form

$$Y_j \mid \mathbf{A}^{(1)} \sim \text{ParFam}_j\left(g_j\left(\beta_{j,0}^{(1)} + \sum_{k=1}^{K^{(1)}} \beta_{j,k}^{(1)} A_k^{(1)}\right), \gamma_j\right). \quad (4)$$

Here,  $\text{ParFam}_j$  denotes a specific parametric family, and let  $H_j$  denote its parameter space. For convenience, let  $p_j$  be the probability mass/density function of  $\text{ParFam}_j$ . The  $g_j :$

$\mathbb{R} \times [0, \infty) \rightarrow H_j$  is a known link function that maps the linear combinations to the parameters of the given parametric family. Here,  $\gamma_j > 0$  denotes the dispersion parameter, when there exists one. Throughout the paper, we will state all results under the more general assumption that there exists a dispersion parameter in the parametric family in (4). If not, one may ignore the notation  $\gamma$ . We further elaborate on the specific parameterizations in (4) for various response types  $\mathcal{Y}_j$  at the end of this section.

Following the definition of directed graphical models (Koller and Friedman, 2009), we can write the joint distribution of all observed and latent variables based on (1)–(4):

$$\mathbb{P}(\mathbf{Y}, \{\mathbf{A}^{(d)}\}_{d \in [D]}) = \mathbb{P}(\mathbf{Y} \mid \mathbf{A}^{(1)}) \prod_{d=2}^D \mathbb{P}(\mathbf{A}^{(d-1)} \mid \mathbf{A}^{(d)}) \mathbb{P}(\mathbf{A}^{(D)}).$$

The marginal distribution of  $\mathbf{Y}$  is obtained by marginalizing out all of the  $D$  latent layers:

$$\mathbb{P}(\mathbf{Y}) = \sum_{\substack{\boldsymbol{\alpha}^{(d)} \in \{0,1\}^{K^{(d)}} \\ \forall d \in [D]}} \mathbb{P}(\mathbf{Y} \mid \mathbf{A}^{(1)} = \boldsymbol{\alpha}^{(1)}) \prod_{d=2}^D \mathbb{P}(\mathbf{A}^{(d-1)} = \boldsymbol{\alpha}^{(d-1)} \mid \mathbf{A}^{(d)} = \boldsymbol{\alpha}^{(d)}) \mathbb{P}(\mathbf{A}^{(D)} = \boldsymbol{\alpha}^{(D)}). \quad (5)$$

The  $D$ -latent-layer DDE is parametrized by  $(\mathbf{p}, \mathcal{B}, \boldsymbol{\gamma})$ , where  $\mathcal{B} := \{\mathbf{B}^{(d)}\}_{d \in [D]}$  and  $\boldsymbol{\gamma} := (\gamma_1, \dots, \gamma_J)$ . Upon the above marginalization, the induced DDE is a highly expressive model with exponentially many latent mixture components. However, this expressivity also introduces identifiability and computation challenges, which we address in Sections 3 and 4.

In many scenarios, it is desirable for the coefficients  $\mathcal{B}$  to be sparse, as this leads to a more interpretable and parsimonious data-generating mechanism. The interpretability stems from that if a latent variable is connected to only a few, rather than all, variables in the layer below, then these children variables can help pinpoint the interpretation of the latent parent. Similar sparse deep generative architectures have been considered in deep exponential families (Ranganath et al., 2015), Bayesian pyramids (Gu and Dunson, 2023), and deep cognitive diagnostic models (Gu, 2024). Additionally, as will be shown in Section 3.1, the sparsity of the coefficients play a key role in facilitating identifiability. To encode the sparsity of  $\mathbf{B}^{(d)}$ , for each  $d \in [D]$ , define a  $K^{(d-1)} \times K^{(d)}$  binary matrix  $\mathbf{G}^{(d)} = (g_{k,l})$ , where  $g_{k,l} = 1$  if

the corresponding coefficient  $\beta_{k,l}^{(d)}$  is nonzero, and 0 otherwise. Define  $K^{(0)} := J$  for notational convenience. By (2) and (3),  $\mathbf{G}^{(d)}$  can also be viewed as the adjacency matrix or “graphical matrix” between the  $(d-1)$ th layer and the  $d$ th layer in the graphical model representation (see Figure 1). Collect all graphical matrices  $\mathbf{G}^{(d)}$ s by defining  $\mathcal{G} := \{\mathbf{G}^{(d)}\}_{d \in [D]}$ . Now, we formally define  $D$ -latent-layer DDEs, which also incorporate  $\mathcal{G}$  as unknown parameters.

**Definition 1** (DDE). *A  $D$ -latent-layer DDE with parameters  $(\mathbf{p}, \mathcal{B}, \mathcal{G}, \boldsymbol{\gamma})$  is a statistical model with marginal distribution of the observed data as given in (5). When  $\mathcal{K}$  is known and fixed, DDEs can be viewed as parametric families with parameters  $(\Theta, \mathcal{G})$  and probability mass/density functions  $\mathbb{P}_{\Theta, \mathcal{G}}$ , where  $\Theta := (\mathbf{p}, \mathcal{B}, \boldsymbol{\gamma})$  denotes all continuous parameters.*

Next, we give some examples of the various response types  $\mathcal{Y}_j$  allowed in the DDE framework, along with the corresponding link functions  $g$  and parametrizations for (4). As mentioned in the Introduction, the later numerical experiments consider three types of responses: (i) binary, (ii) count, and (iii) continuous. We model each of these responses using (i) Bernoulli with  $g = g_{\text{logistic}}$ , (ii) Poisson with an exponential link  $g(x) = e^x$ , and (iii) Normal with an identity link  $g(x, y) = (x, y)$ , respectively. Modeling other data types is also straightforward. While not required, we typically consider that the data types are the same across the  $p$  features. In such cases, we omit the subscript in  $\mathcal{Y}_j, g_j$ , and write  $\mathcal{Y}$  and  $g$ .

## 2.2 Connections with Existing Models

**Deep Probabilistic Graphical Models in Machine Learning.** There are many deep latent variable models in the machine learning literature, including the popular deep Boltzmann machine (DBM, [Salakhutdinov and Hinton, 2009](#)), deep belief networks (DBNs, [Hinton et al., 2006](#)), and deep exponential families (DEFs, [Ranganath et al., 2015](#)). The DBM and DBN both contain multiple binary latent layers and differ in the directions of the edges; see Figure 2. DBM and DBN have been originally proposed to model binary data and have been later extended to handle continuous or count responses ([Cho et al., 2013](#); [Gan et al.,](#)



2015; Li et al., 2019). We recommend the review Salakhutdinov (2015) for more details and references on DBM and DBNs. DEFs are an unsupervised modeling framework that uses exponential families to model conditional distributions for each layer.

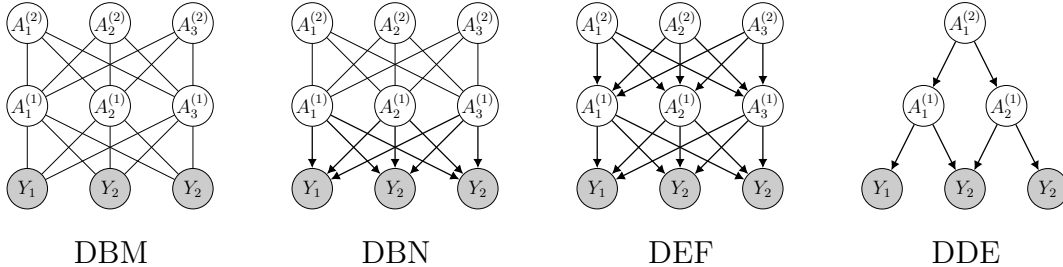


Figure 2: Comparison of the graphical structure of DDEs to relevant deep generative models. DBM: binary data and binary latent. DBN: binary data and binary latent. DEF: exponential family conditional distributions. DDE: general-response data and binary latent.

Despite their numerous empirical successes, the aforementioned machine learning models are usually fundamentally non-identifiable due to an enormous number of latent variables and parameters organized in a complex nonlinear architecture. These models are typically heavily overparametrized, making it challenging to understand and interpret the latent representations. Moreover, popular existing estimation procedures for these models are developed to maximize a tractable but less theoretically understood alternative to the likelihood, such as contrastive divergence or layer-wise variational approximation.

As to be shown later, DDEs resolve all these issues by assuming a shrinking-ladder architecture of entirely discrete latent variables and potentially sparse layerwise connections (see Figure 2). This allows us to establish identifiability and consistency as well as effectively reduce the model dimension and interpret the latent structure. Recently, Gu and Dunson (2023) proposed *Bayesian pyramids*, which are identifiable multilayer discrete latent variable models with a pyramid structure. But the methodology and identifiability theory therein are restricted to multivariate categorical data. DDEs significantly broaden the applicability of Bayesian pyramids by modeling arbitrarily flexible data distributions while still remaining identifiable. For computation, we propose scalable frequentist estimation approaches for DDEs, rather than adopting Bayesian MCMC inference as in Gu and Dunson (2023).

**Psychometrics.** Multidimensional binary latent variables are also popular for modeling students’ item response data in educational measurement (Junker and Sijtsma, 2001; von Davier, 2008; de la Torre, 2011). These psychometric models are known as cognitive diagnostic models (CDMs). A CDM uses a single latent layer of cognitive skills to model a student’s binary responses to many questions in a test, with a sparse loading graph between the observed and latent layers. Here, each binary latent variable represents a student’s mastery or deficiency of a cognitive skill, and the sparse graph between the observed item responses and latent skills encodes which skills each item is designed to measure in the test. The proposed DDEs substantially generalize this modeling idea by allowing (a) multilayer latent variables, which can model one’s knowledge structure at multiple resolutions ranging from fine-grained details to general concepts (Gu, 2024), and (b) modeling a rich class of general responses, going beyond the typical binary correct/incorrect responses in educational tests.

### 3 Theoretical Guarantees for General DDEs

#### 3.1 Model Identifiability

In this section, we establish the identifiability of DDEs. Assuming known numbers of latent variables, we prove that the continuous model parameters and the discrete graph structures between layers can be uniquely identified under certain conditions on the true graphical matrices  $\mathbf{G}^{(d)}$ ’s. We first make an assumption to address some trivial ambiguities.

**Assumption 1.** *Assume that the graphical matrices  $\mathcal{G} = \{\mathbf{G}^{(d)}\}_{d \in [D]}$  and proportion parameters  $\mathbf{p}$  satisfy the following conditions. Here, for notational convenience, let  $K^{(0)} := J$ .*

- (a) *For all  $k \in [K^{(D)}]$ ,  $p_k \in (0, 1)$ .*
- (b) *For all  $d \in [D]$ ,  $\mathbf{G}^{(d)}$  does not have all-zero columns and is faithful in the sense that for any  $k \in [K^{(d-1)}]$ ,  $l \in [K^{(d)}]$ ,  $g_{k,l}^{(d)} = 0$  if and only if  $\beta_{k,l+1}^{(d)} = 0$ .*
- (c) *For any  $d \in [D]$ , all column sums of  $\mathbf{B}^{(d)}$  except for the first column are strictly positive.*

Condition (a) and the first part of (b) is required for the latent dimension  $\mathcal{K}$  to be well-defined, in the sense that removing or adding a latent variable must change the marginal distribution (5). Condition (b) is a standard faithfulness assumption in graphical models (e.g. see Definition 3.8 in [Koller and Friedman, 2009](#)) that follows from our definition of  $\mathbf{G}^{(d)}$ . Condition (c) is introduced to avoid trivial sign-flipping of latent variables. This condition ensures that for each latent variable  $A_k^{(d)}$ , the value  $A_k^{(d)} = 1$  implies a larger coefficient of the  $(k + 1)$ th row of  $\mathbf{B}^{(d)}$ , and may be replaced with other monotonicity assumptions. For example, one can alternatively assume that the first nonzero coefficient in each column of  $\mathbf{B}^{(d)}$  is positive. We emphasize that condition (c) is much weaker compared to the nonnegative coefficient assumption  $\beta_{j,k} \geq 0$ , which is a popular assumption for various identifiable latent variable models ([Donoho and Stodden, 2003](#); [Chen et al., 2020](#); [Lee and Gu, 2024](#)).

Now, we formally define the parameter space and the notion of identifiability. For multilayer latent variable models, there are inevitable latent variable permutation issues within each latent layer. Hence, we introduce the notion of identifiability up to equivalence.

**Definition 2** (Parameter space). *Consider a  $D$ -latent-layer DDE with  $\mathcal{K} = \{K^{(d)}\}_{d \in [D]}$  latent variables. We define the parameter space of the continuous parameters  $\Theta$  given  $\mathcal{G}$  as  $\Omega_{\mathcal{K}}(\Theta; \mathcal{G}) := \{\Theta : \beta_{l,k}^{(d)} \neq 0 \text{ if and only if } g_{l,k}^{(d)} = 1, \gamma_j > 0\}$ . Define the joint parameter space for all parameters to be  $\Omega_{\mathcal{K}}(\Theta, \mathcal{G}) := \{(\Theta, \mathcal{G}) : \Theta \in \Omega_{\mathcal{K}}(\Theta; \mathcal{G})\}$ .*

**Definition 3** (Identifiability up to equivalence). *For a  $D$ -layer DDE with  $\mathcal{K}$  latent variables, we define an equivalence relationship “ $\sim_{\mathcal{K}}$ ” by setting  $(\Theta, \mathcal{G}) \sim_{\mathcal{K}} (\tilde{\Theta}, \tilde{\mathcal{G}})$  if and only if  $\gamma = \tilde{\gamma}$  and there exists permutations  $\sigma^{(d)} \in S_{[K^{(d)}]}$  for all  $d \in [D]$  such that the following hold:*

- $p_k = \tilde{p}_{\sigma^{(D)}(k)}$
- $g_{l,k}^{(d)} = \tilde{g}_{\sigma^{(d-1)}(l), \sigma^{(d)}(k)}^{(d)}$  and  $\beta_{l,k}^{(d)} = \tilde{\beta}_{\sigma^{(d-1)}(l), \sigma^{(d)}(k)}^{(d)}$  for all  $d \in [D]$ ,  $k \in [K^{(d)}]$ ,  $l \in [K^{(d-1)}]$

Here, we set  $\sigma^{(0)} = \text{id}_{[J]}$ . We say that the DDE with true parameters  $(\Theta^*, \mathcal{G}^*)$  is identifiable up to  $\sim_{\mathcal{K}}$  when for any alternate parameter value  $(\Theta, \mathcal{G}) \in \Omega_{\mathcal{K}}(\Theta, \mathcal{G})$  with  $\mathbb{P}_{\Theta, \mathcal{G}} = \mathbb{P}_{\Theta^*, \mathcal{G}^*}$ , it

holds that  $(\Theta, \mathcal{G}) \sim_{\kappa} (\Theta^*, \mathcal{G}^*)$ . Here,  $\mathbb{P}_{\Theta, \mathcal{G}}$  is the marginal distribution of  $\mathbf{Y}$  defined in (5).

Despite the seemingly heavy notation, the equivalence relationship is quite natural. Here, each permutation  $\sigma^{(d)}$  addresses the label-switching issue for indexing the latent variables in the  $d$ th latent layer. Below is a main result on the identifiability of  $D$ -latent-layer DDEs.

**Theorem 1** (Identifiability of DDEs). *Consider the  $D$ -latent-layer DDE with  $\mathcal{K}$  latent variables and true parameters  $(\Theta^*, \mathcal{G}^*)$ . Suppose that for all  $d \leq D - 1$ , the true graphical matrices  $\mathbf{G}^{(d)*}$  and parameters  $\mathbf{B}^{(d)*}$  satisfy the following conditions:*

- A.  $\mathbf{G}^{(d)*}$  contains two identity matrices after permuting the rows. Without the loss of generality, suppose that the first  $2K^{(d)}$  rows of  $\mathbf{G}^{(d)*}$  are  $[\mathbf{I}_{K^{(d)}}, \mathbf{I}_{K^{(d)}}]^\top$ .
- B. For any  $\alpha^{(d)} \neq \alpha'^{(d)} \in \{0, 1\}^{K^{(d)}}$ , there exists  $j > 2K^{(d)}$  such that  $\sum_{k=1}^{K^{(d)}} \beta_{j,k}^{(d)*} (\alpha_k^{(d)} - \alpha_k'^{(d)}) \neq 0$ .

Then, the model components  $(\Theta, \mathcal{G})$  are identifiable.

Our key observation behind proving the identifiability of the complex deep generative structures in DDEs is that, with discrete latent layers, it suffices to establish identifiability for a one-latent-layer model and proceed in a layer-wise manner inductively. To elaborate, consider a “collapsed” DDE where the latent layers indexed by  $d = 2, \dots, D$  are marginalized out to give a probability mass function for the first latent layer:  $\{\mathbb{P}(\mathbf{A}^{(1)} = \alpha^{(1)}) : \alpha^{(1)} \in \{0, 1\}^{K^{(1)}}\}$ . If the collapsed model is proven to be identifiable, that means the conditional distributions  $\mathbb{P}(Y_j | \mathbf{A}^{(1)})$  and the marginal distribution  $\mathbb{P}(\mathbf{A}^{(1)})$  can be uniquely identified from the data distribution  $\mathbb{P}(\mathbf{Y})$ . In this case, we can determine all values of  $\mathbb{P}(\mathbf{A}^{(1)} = \alpha^{(1)})$  for every  $\alpha^{(1)} \in \{0, 1\}^{K^{(1)}}$ . Then, we can theoretically treat the shallowest latent layer  $\mathbf{A}^{(1)}$  as if it were observed, because its probability mass function (pmf) is now identified and known. Then, viewing this pmf as the marginal distribution of  $K^{(1)}$ -dimensional observed variables of a  $(D - 1)$ -latent-layer Bernoulli-DDE, we can inductively identify all parameters via a layerwise argument. Please see Supplementary Material S.1 for the detailed proof.

We interpret the conditions in Theorem 1. Condition A requires each latent variable to have at least two *exclusive children* in the layer below. Condition B is more technical and is introduced to distinguish the different binary latent configurations  $\alpha \neq \alpha'$ . Condition B holds when  $\mathbf{G}^{(d)*}$  also contains exclusive children for all latent variables.

The exclusive children requirements in condition A can be further relaxed under a weaker notion of *generic identifiability*. Generic identifiability allows a measure-zero subset of the parameter space to be non-identifiable, and often holds under weaker conditions than that in Definition 3. As the concept was originally proposed under a continuous parameter space (Allman et al., 2009), we consider the following modified definition that considers a smaller parameter space for the coefficients  $\mathcal{B}$  given the true graphical matrices.

**Definition 4** (Generic identifiability). *Consider a  $D$ -latent-layer DDE with  $\mathcal{K}$  latent variables, graphical matrices  $\mathcal{G}^*$ , and true parameters belonging to  $\Omega_{\mathcal{K}}(\Theta; \mathcal{G}^*)$ . The model is generically identifiable up to  $\sim_{\mathcal{K}}$  when*

$$\{\Theta \in \Omega_{\mathcal{K}}(\Theta; \mathcal{G}^*) : \text{there exists } (\tilde{\Theta}, \tilde{\mathcal{G}}) \not\sim_{\mathcal{K}} (\Theta, \mathcal{G}^*) \text{ such that } \mathbb{P}_{\tilde{\Theta}, \tilde{\mathcal{G}}} = \mathbb{P}_{\Theta, \mathcal{G}^*}\}$$

*is a measure-zero set with respect to  $\Omega_{\mathcal{K}}(\Theta; \mathcal{G}^*)$ .*

We introduce an additional assumption on the parametric families used to model the conditional distribution  $Y_j | \mathbf{A}^{(1)}$  in (4). This is a technical assumption that arises from our proof technique for dealing with measure-zero sets. This assumption holds for all example parametric families described in Section 2.1, and more generally for exponential families with an analytic log-partition function.

**Assumption 2** (Analytic family). *Let  $p(\cdot; \eta, \gamma)$  be the pmf/pdf of a parametric family, indexed by  $\eta, \gamma$  and equipped with a sample space  $\mathcal{Y}$ . We say that  $p$  is analytic when the pmf/pdf  $p(Y; \eta, \gamma)$  is analytic in both  $\eta, \gamma$ , for all  $Y \in \mathcal{Y}$ .*

Now, we are ready to state the generic identifiability result for  $D$ -latent-layer DDEs.

**Theorem 2** (Generic identifiability of DDEs). *Consider the  $D$ -latent-layer DDE with  $\mathcal{K}$  latent variables and true graphical matrices  $\mathcal{G}^*$ , where all parametric families and link function  $g_j$ s are analytic, and the true parameter lives in  $\Omega_{\mathcal{K}}(\Theta; \mathcal{G}^*)$ . Suppose that for all  $d \leq D - 1$ , the true graphical matrices  $\mathbf{G}^{(d)}$  satisfy the following condition C:*

C. *After permuting the rows, we can write  $\mathbf{G}^{(d)*} = [\mathbf{G}_1^{(d)\top}, \mathbf{G}_2^{(d)\top}, \mathbf{G}_3^{(d)\top}]^\top$ , where  $\mathbf{G}_1^{(d)}$  and  $\mathbf{G}_2^{(d)}$  are  $K^{(d)} \times K^{(d)}$  matrices whose diagonal entries are ones:*

$$\mathbf{G}_1^{(d)}, \mathbf{G}_2^{(d)} = \begin{pmatrix} 1 & * & \cdots & * \\ * & 1 & \cdots & * \\ \vdots & \vdots & \ddots & \vdots \\ * & * & \cdots & 1 \end{pmatrix}, \text{ where each } * \text{ denotes an arbitrary value in } \{0, 1\}, \text{ and } \mathbf{G}_3^{(d)} \text{ does not have any all-zero columns.}$$

*Then, the model components  $(\Theta, \mathcal{G})$  are generically identifiable.*

Condition C relaxes conditions A and B in Theorem 1. While condition A requires two exclusive children for each latent variable, condition C does not require any exclusive child and allows more complicated dependence structures. Additionally, condition B for the remaining  $J - 2K^{(d)}$  variables is relaxed to a simple non-zero column condition on  $\mathbf{G}_3^{(d)}$ . Thus, condition C does not concern any continuous parameter values and just depends on the graph structure  $\mathbf{G}^{(d)}$ , and can be used as a practical criterion to assess identifiability.

We place our identifiability results in the literature on the identifiability of generative models and latent variable models. While the identifiability of generative models has attracted increasing attention in machine learning (Hyvarinen et al., 2019; Khemakhem et al., 2020; Moran et al., 2022; Kivva et al., 2022), many of these results require additional information such as auxiliary covariates. More importantly, almost all of these results build on nonlinear independent component analysis (Oja and Hyvarinen, 2000) or variational autoencoders (Ranzato and Szummer, 2008), both of which essentially have only one latent layer of random variables transformed by deterministic deep neural networks. Consequently,

these results cannot be applied to DDEs with multiple latent layers organized in a probabilistic graphical model. Since uncertainty occurs and accumulates in each layer of a DDE, addressing identifiability in such cases requires fundamentally different techniques due to a complicated marginal likelihood. At the high level, our proof techniques are based on transforming the marginal distribution of data into a tensor and invoking the uniqueness of tensor decompositions to establish identifiability. In statistics, the study of identifiability has a long history but also mainly concerns relatively simple latent structures with only one latent layer (Anderson and Rubin, 1956; Koopmans and Reiersol, 1950; Allman et al., 2009; Xu and Shang, 2018). It has been largely unknown whether DGMs with many nonlinear latent layers can be identifiable for general data as considered in this paper.

### 3.2 Estimation Consistency

In this section, we propose a penalized maximum likelihood estimation method for DDEs, and show that the estimator is consistent for both the continuous parameters and the discrete graph structures. Suppose that the numbers of latent variables in all layers are known. We maximize the following objective function to estimate parameters  $\Theta = (\mathbf{p}, \mathcal{B}, \gamma)$ :

$$\widehat{\Theta} \in \underset{\Theta}{\operatorname{argmax}} \left[ \ell(\Theta | \mathbf{Y}) - \sum_{d=1}^D p_{\lambda_N, \tau_N}(\mathbf{B}^{(d)}) \right], \quad (6)$$

where  $\ell(\Theta | \mathbf{Y}) = \sum_{i=1}^N \log \mathbb{P}(\mathbf{Y}_i | \Theta)$  denotes the marginal log-likelihood function given a sample  $\mathbf{Y}_1, \dots, \mathbf{Y}_N$  of size  $N$ , defined based on the marginal distribution of  $\mathbf{Y}$  in (5). From now on, we slightly abuse notation and let  $\mathbf{Y}$  denote the  $N \times J$  data matrix including  $\mathbf{Y}_1, \dots, \mathbf{Y}_N$  as rows. Using the estimated coefficients in  $\widehat{\mathcal{B}} = (\widehat{\beta}_{l,k}^{(d)})$ , the layer-wise graphical matrices in  $\mathcal{G}$  can be estimated by reading off the sparsity pattern of  $\widehat{\mathcal{B}}$ :

$$\widehat{g}_{l,k}^{(d)} := \mathbb{1}(\widehat{\beta}_{l,k}^{(d)} \neq 0) \quad \text{for all } d \in [D], k \in [K^{(d)}], l \in [K^{(d-1)}]. \quad (7)$$

For some tuning parameters  $\lambda_N, \tau_N > 0$ ,  $p_{\lambda_N, \tau_N} : \mathbb{R} \rightarrow [0, \infty)$  is a sparsity-inducing symmetric penalty that is nondecreasing on  $[0, \infty)$ , nondifferentiable at 0, differentiable at  $(0, \tau_N)$ ,

$p_{\lambda_N, \tau_N} \propto \lambda_N / \tau_N$  around 0 and satisfy

$$p_{\lambda_N, \tau_N}(b) = 0, \text{ if } b = 0; \quad p'_{\lambda_N, \tau_N}(b) \leq \frac{C\lambda_N}{\tau_N}, \text{ if } |b| \leq \tau_N; \quad p_{\lambda_N, \tau_N}(b) = \lambda_N, \text{ if } |b| \geq \tau_N.$$

Note that  $\lambda_N$  is the magnitude of the penalty, and  $\tau_N$  is the point of truncation. Our assumption for the penalty  $p_{\lambda_N, \tau_N}$  includes common truncated sparsity-inducing penalties such as the TLP (Truncated Lasso Penalty; Shen et al., 2012) and SCAD (Smoothly Clipped Absolute Deviation; Fan and Li, 2001). With a slight abuse of notation, in (6), we view the penalty  $p_{\lambda_N, \tau_N}$  as a function of matrices by letting it be the sum of the entrywise penalties:

$$p_{\lambda_N, \tau_N}(\mathbf{B}^{(d)}) = \sum_{k \in [K^{(d-1)}], \ell \in [K^{(d)}]} p_{\lambda_N, \tau_N}(\beta_{k, \ell}^{(d)}).$$

Assuming a compact parameter space with bounded coefficients  $\mathbf{B}^{(d)}$ , we prove that the estimator defined in (6) and (7) results in consistent estimation.

**Theorem 3.** *Consider a  $D$ -latent-layer DDE with true parameters  $\Theta^*, \mathcal{G}^*$ . Assume that the model at  $\Theta^*$  is identifiable, has a non-singular Fisher information, and all entries of  $\{\mathbf{B}^{(d)}\}_{d=1}^D$  are bounded. Let  $\hat{\Theta}$  be the estimator resulting from the penalized optimization in (6), where  $\lambda_N$  and  $\tau_N$  depend on  $N$  such that  $1/\sqrt{N} \ll \tau_N \ll \lambda_N/\sqrt{N} \ll 1$ . Then,  $\hat{\Theta}$  is  $\sqrt{N}$ -consistent in the sense that there exists some  $\tilde{\Theta} \sim_{\mathcal{K}} \hat{\Theta}$  such that  $\|\tilde{\Theta} - \Theta^*\| = O_p(1/\sqrt{N})$ . Here,  $\|\cdot\|$  denotes the vectorized  $L^2$  norm. Additionally, the graphical matrices are consistently estimated: for  $\tilde{\mathcal{G}}$  resulting from  $\tilde{\Theta}$  according to (7), we have  $\mathbb{P}(\tilde{\mathcal{G}} \neq \mathcal{G}^*) \rightarrow 0$ .*

**Remark 1.** *One natural question is to whether our estimator would still be consistent when the number of latent variables are unknown. This extension is not straightforward since the number of the top-layer latent variable,  $K^{(D)}$ , determines the number of deepest mixture components of DDEs. Estimating the number of mixture components is a challenging problem even in simple parametric models, and often leads to a slower (than  $1/\sqrt{N}$ ) rate of convergence in parameter estimation (Goffinet et al., 1992; Ho and Nguyen, 2016). Note that for such cases, the Fisher information becomes singular, and Theorem 3 cannot be applied. We will give a practical method to choose  $\mathcal{K}$  at the end of Section 4.*



## 4 Scalable Computation Pipeline

### 4.1 Warm-up Example: Penalized EM Algorithm

This subsection first presents a penalized EM algorithm as a warm-up example, before presenting the scalable computational pipelines in Sections 4.2 (stage one) and 4.3 (stage two).

We describe the methods for two-layer DDEs; they are conceptually easy to generalize to DDEs with more layers. Since the coefficients  $\mathbf{B}^{(1)}$  and  $\mathbf{B}^{(2)}$  are potentially sparse, we propose a penalized EM algorithm (PEM) to compute the penalized maximum likelihood estimator in (6). The PEM is an iterative procedure that consists of an expectation step followed by a penalized maximization step (Green, 1990; Chen et al., 2015). In the  $(t + 1)$ th iteration, the E-step computes the expectation of the complete data penalized-log-likelihood

$$\begin{aligned} \ell_c(\mathbf{Y}, \mathbf{A}^{(1)}, \mathbf{A}^{(2)}; \Theta) - \sum_{d=1}^2 p_{\lambda_N, \tau_N}(\mathbf{B}^{(d)}) &= \sum_{i=1}^N \left[ \log \mathbb{P}(\mathbf{A}_i^{(2)}; \mathbf{p}) + \log \mathbb{P}(\mathbf{A}_i^{(1)} \mid \mathbf{A}_i^{(2)}; \mathbf{B}^{(2)}) \right. \\ &\quad \left. + \log \mathbb{P}(\mathbf{Y}_i \mid \mathbf{A}_i^{(1)}, \mathbf{A}_i^{(2)}; \mathbf{B}^{(1)}, \gamma) \right] - \sum_{d=1}^2 p_{\lambda_N, \tau_N}(\mathbf{B}^{(d)}). \end{aligned}$$

This requires calculating the conditional probability for each latent configuration using the previous parameter estimates; that is, calculating  $\mathbb{P}(\mathbf{A}_i^{(1)} = \boldsymbol{\alpha}^{(1)}, \mathbf{A}_i^{(2)} = \boldsymbol{\alpha}^{(2)} \mid \mathbf{Y}; \Theta^{[t]})$  for all  $i \in [N]$ ,  $\boldsymbol{\alpha}^{(1)} \in \{0, 1\}^{K_1}$ , and  $\boldsymbol{\alpha}^{(2)} \in \{0, 1\}^{K_2}$ . Here, the superscript  $[t]$  denotes the  $t$ th iteration estimates. In the M-step, we update the parameters by maximizing the expectation computed in the E step, which boils down to solving the following three maximizations:

$$\mathbf{p}^{[t+1]} := \operatorname{argmax}_{\mathbf{p}} \sum_{i=1}^N \mathbb{E} \left[ \log \mathbb{P}(\mathbf{A}_i^{(2)}; \mathbf{p}); \mathbf{p}^{[t]} \right], \quad (8)$$

$$\mathbf{B}^{(2), [t+1]} := \operatorname{argmax}_{\mathbf{B}^{(2)}} \sum_{i=1}^N \mathbb{E} \left[ \log \mathbb{P}(\mathbf{A}_i^{(1)} \mid \mathbf{A}_i^{(2)}; \mathbf{B}^{(2)}); \mathbf{B}^{(2), [t]} \right] - p_{\lambda_N, \tau_N}(\mathbf{B}^{(2)}), \quad (9)$$

$$(\mathbf{B}^{(1), [t+1]}, \gamma^{[t+1]}) := \operatorname{argmax}_{\mathbf{B}^{(1)}, \gamma} \sum_{i=1}^N \mathbb{E} \left[ \log \mathbb{P}(\mathbf{Y}_i \mid \mathbf{A}_i^{(1)}, \mathbf{A}_i^{(2)}; \mathbf{B}^{(1), [t]}, \gamma^{[t]}) \right] - p_{\lambda_N, \tau_N}(\mathbf{B}^{(1)}). \quad (10)$$

Here, the optimizations for each layer are separated; we update the top-layer proportion

parameters  $\mathbf{p}$  in (8), the middle latent layer coefficients  $\mathbf{B}^{(2)}$  in (9), and the bottom layer coefficients  $(\mathbf{B}^{(1)}, \boldsymbol{\gamma})$  in (10). Additionally, due to the conditional independence assumption in each layer, the maximizations can be further simplified into low-dimensional optimizations over each row of  $\mathbf{B}$ . Algorithm 1 summarizes the PEM algorithm. The details of the simplified M-step and the implementation are in Supplementary Material S.3.1 and S.3.3.

---

**Algorithm 1:** Penalized EM (PEM) algorithm for the two-latent-layer DDE

---

**Data:**  $\mathbf{Y}, \mathcal{K}$ , tuning parameters  $\lambda_N, \tau_N$ .

Initialize  $\boldsymbol{\Theta}^{[0]}$  using the layerwise initialization in Algorithm 2.

**while** *log-likelihood has not converged* **do**

In the  $[t + 1]$ th iteration,

// **E-step**

**for**  $(i, \boldsymbol{\alpha}^{(1)}, \boldsymbol{\alpha}^{(2)}) \in [N] \times \{0, 1\}^{K^{(1)}} \times \{0, 1\}^{K^{(2)}}$  **do**

$$\varphi_{i, \boldsymbol{\alpha}^{(1)}, \boldsymbol{\alpha}^{(2)}}^{[t+1]} = \mathbb{P}(\mathbf{A}_i^{(1)} = \boldsymbol{\alpha}^{(1)}, \mathbf{A}_i^{(2)} = \boldsymbol{\alpha}^{(2)} \mid \mathbf{Y}; \boldsymbol{\Theta}^{[t]})$$

**end**

// **M-step**

update  $\boldsymbol{\Theta}^{[t+1]} = (\mathbf{p}^{[t+1]}, \mathbf{B}^{(1), [t+1]}, \mathbf{B}^{(2), [t+1]}, \boldsymbol{\gamma}^{[t+1]})$  by solving (8)-(10).

**end**

Estimate  $\mathbf{G}$  based on the sparsity structure of  $\widehat{\mathbf{B}}$  according to (7).

**Output:** Estimated continuous parameters  $\widehat{\boldsymbol{\Theta}}$  and graphical matrices  $\widehat{\mathbf{G}}^{(1)}, \widehat{\mathbf{G}}^{(2)}$ .

---

## 4.2 Stage One: Layerwise Double-SVD Initialization

The multiple layers of nonlinearity in DDEs lead to a highly nonconvex optimization landscape with potentially exponentially many local optima (Sutskever et al., 2013). If the penalized EM algorithm starts with an initialization close to a local optima, it can get stuck and fail to converge to the global maximizer of the penalized log-likelihood function. Hence, for highly complex latent variable models such as DDEs, it is critical to initialize the optimization algorithm wisely. We propose a novel layerwise nonlinear spectral initialization strategy, which enjoys low computational complexity and reasonably high accuracy. This spectral initialization serves as the first stage in the proposed computational pipeline.

Spectral methods have mostly been used for linear low-rank models, and existing approaches are not directly applicable for DDEs with a deep nonlinear structure. To address

this, we propose a nuanced layerwise procedure utilizing the double SVD procedure for de-noising low-rank generalized linear factor models (Zhang et al., 2020) and the SVD-based Varimax to find sparse rotations of the factor loadings (Rohe and Zeng, 2023).

---

**Algorithm 2:** Outline of the Layerwise Double-SVD Initialization

---

**Data:** Data matrix  $\mathbf{Y}_{N \times J}$ , latent dimensions  $\mathcal{K}$ .

1. De-noise the data matrix  $\mathbf{Y}$  using a first SVD, and linearize this matrix by applying the inverse-link function  $(\mu \circ g)^{-1}$  elementwisely. Let  $\hat{\mathbf{Z}}$  denote the inverted matrix.
  2. Let  $\hat{\mathbf{Z}}_0$  be the column-centered version of  $\hat{\mathbf{Z}}$ , and compute its rank- $K^{(1)}$  approximation by a second SVD:  $\hat{\mathbf{Z}}_0 \approx \mathbf{U}_{N \times K^{(1)}} \boldsymbol{\Sigma}_{K^{(1)} \times K^{(1)}} \mathbf{V}_{J \times K^{(1)}}^\top$ .
  3. Rotate  $\mathbf{V}$  according to the Varimax criteria, and denote it as  $\hat{\mathbf{B}}^{(1)}$ . Modify the sign ( $\pm$ ) of each column so that Assumption 2(c) is satisfied.
  4. Use the relationship  $\hat{\mathbf{Z}} \approx [\mathbf{1}_N, \mathbf{A}^{(1)}] \mathbf{B}^{(1)\top}$  to estimate  $\mathbf{A}^{(1)}$ .
  5. Now, suppose that the estimated  $\hat{\mathbf{A}}^{(1)}$  is the “observed data” of a one-latent-layer DDE. Repeat steps 1-4 to estimate  $\mathbf{B}^{(2)}$  and  $\mathbf{A}^{(2)}$ .
- 

Our main idea is to view the responses  $\mathbf{Y}$  as a perturbation of a population expectation  $\mathbb{E}(\mathbf{Y} \mid \mathbf{A}^{(1)}, \mathbf{B}^{(1)}) = (\mu \circ g) ([\mathbf{1}_N, \mathbf{A}^{(1)}] \mathbf{B}^{(1)\top})$ , which is an elementwise (nonlinear) transformation of a low-rank matrix. Here,  $\mu : H \rightarrow \mathcal{Y}$  is the known mean function of the observed-layer parametric family in (4) and  $g : \mathbb{R} \rightarrow H$  is the link function. The function  $(\mu \circ g)$  is equal to  $g_{\text{logistic}}$  for Bernoulli responses, the exponential function for Poisson, and the identity function for Normal. When  $(\mu \circ g)$  is nonlinear, we use the aforementioned double SVD procedure (Zhang et al., 2020). This procedure applies a first SVD to de-noise the data, and then linearizes the data through inverting the link function  $(\mu \circ g)$ , and finally performs a second SVD to find the low-rank matrix  $\hat{\mathbf{Z}} \approx [\mathbf{1}_N, \mathbf{A}^{(1)}] \mathbf{B}^{(1)\top}$ . Next, noting that the true coefficient matrix  $\mathbf{B}^{(1)}$  is sparse, we estimate it by seeking a sparse rotation of the right singular subspace of  $\hat{\mathbf{Z}}$ , using the popular Varimax criterion (Kaiser, 1958; Rohe and Zeng, 2023). This procedure also provides an estimate of the latent variables  $\mathbf{A}^{(1)}$ , which can be treated as the “observed data” to initialize the deeper layer’s  $\mathbf{B}^{(2)}$  and  $\mathbf{A}^{(2)}$  in a similar fashion as described above. This layer-by-layer algorithm readily generalizes to deeper models and is reminiscent of the greedy learning strategy for DBNs (Hinton et al., 2006; Salakhutdinov, 2015).

We summarize the overall procedure in Algorithm 2, and postpone further details of each step to Supplementary Material S.2. In the Supplement, we also illustrate the effectiveness of the spectral initialization by comparing the estimation accuracy of our two-stage computational pipeline to that of the EM algorithm with a random initialization.

### 4.3 Stage Two: Penalized SAEM Algorithm

For DDEs with a large number of latent variables, the E-step in Algorithm 1 requires computing all conditional probabilities  $\mathbb{P}(\mathbf{A}_i^{(1)} = \boldsymbol{\alpha}^{(1)}, \mathbf{A}_i^{(2)} = \boldsymbol{\alpha}^{(2)} \mid \mathbf{Y}; \boldsymbol{\Theta}^{[t]})$  for all  $\boldsymbol{\alpha}^{(1)} \in \{0, 1\}^{K^{(1)}}$  and  $\boldsymbol{\alpha}^{(2)} \in \{0, 1\}^{K^{(2)}}$ . This requires computing and storing  $O(N \times 2^{\sum_{d=1}^D K^{(d)}})$  terms. The exponential dependency in  $K^{(d)}$  is concerning even for moderately large latent dimensions, say  $K^{(d)} = 10$ , and quickly becomes prohibitive for larger  $K^{(d)}$ . Therefore, we propose a penalized Stochastic Approximate EM (SAEM; see Delyon et al., 1999; Kuhn and Lavielle, 2004) by modifying both the E-step and M-step to more scalable versions using approximate sampling. As we illustrate below, this is a method with linear dependence of  $\sum_{d=1}^D K^{(d)}$  on the computing time as well as memory, and is a scalable alternative to Algorithm 1.

We elaborate on the details on how to modify the PEM to derive the SAEM. *First*, we replace the E-step to a simulation step, which consists of simulating only a small number (denoted as  $C$ ) of posterior samples of the latent variables. As exact sampling from the joint distribution  $\mathbb{P}(\mathbf{A}_i^{(1)}, \mathbf{A}_i^{(2)} \mid \mathbf{Y}; \boldsymbol{\Theta}^{[t]})$  is expensive, we sample each latent variable from their complete conditionals. That is, we sample each  $A_{i,k}^{(1),[t+1]}$  from  $\mathbb{P}(A_{i,k}^{(1)} \mid (-), \boldsymbol{\Theta}^{[t]})$ , where  $(-)$  denotes the estimates of all other latent variables from the  $t$ th iteration. Since the latent variables are binary, the conditional distribution is Bernoulli and easy to evaluate. Consequently, the computationally expensive E-step is replaced by the simulation step, which computes and stores only  $O(N \times \sum_{d=1}^D K^{(d)})$  terms. In terms of choosing the number of samples  $C$  in each iteration, we empirically find that taking  $C = 1$  is computationally efficient without sacrificing much accuracy. Additional simulation studies in Supplementary Material S.4.2 demonstrate that taking a larger  $C$  results in only little improvement in

accuracy, but becomes significantly slower. This choice of  $C = 1$  was also suggested in the original paper that proposed the SAEM (Delyon et al., 1999).

*Second*, we modify the M-step objective function by replacing the exact conditional probability values (denoted as  $\varphi^{[t+1]}$  in Algorithm 1) to sample-based quantities, and also stochastically averaging the objective functions. For example, we modify (9) as follows:

$$Q^{(2),[t+1]}(\mathbf{B}^{(2)}) := (1 - \theta_{t+1})Q^{(2),[t]}(\mathbf{B}^{(2)}) + \theta_{t+1} \sum_{i=1}^N \log \mathbb{P}(\mathbf{A}_i^{(1)} = \mathbf{A}_i^{(1),[t+1]} \mid \mathbf{A}_i^{(2)} = \mathbf{A}_i^{(2),[t+1]}; \mathbf{B}^{(2)}), \quad (11)$$

$$\mathbf{B}^{(2),[t+1]} := \operatorname{argmax}_{\mathbf{B}^{(2)}} [Q^{(2),[t+1]}(\mathbf{B}^{(2)}) - p_{\lambda_N, \tau_N}(\mathbf{B}^{(2)})], \quad (12)$$

where  $Q^{(2),[0]} = 0$  and  $\theta_{t+1}$  is a pre-determined step size that decreases in  $t$ . Here, in the log probability term in (11),  $\mathbf{A}_i^{(d)}$  denotes the *latent random variable* and  $\mathbf{A}_i^{(d),[t+1]}$  denotes the *realized sample* from the simulation step in the current  $(t + 1)$ th iteration. In the  $(t + 1)$ th iteration, we update the objective function  $Q^{(2),[t+1]}$  by taking a weighted average of the previous objective function  $Q^{(2),[t]}$ , and the conditional probabilities computed using the current iteration's simulated samples  $\mathbf{A}^{(1),[t+1]}$ . Then, in (12) we compute the parameters that maximize the penalized objective function.

We similarly modify the optimizations in (8)–(10). Algorithm 3 summarizes our final SAEM algorithm with  $C = 1$ , where exact formulas are deferred to Supplement S.3.1. Similar to the PEM algorithm, the M-step updates can be written in terms of low-dimensional maximizations for each row of the coefficient matrices.

**Selecting the latent dimension  $\mathcal{K}$ .** To apply the above computation pipeline to real data, one additionally needs to specify the number of latent variables,  $\mathcal{K}$ . For this purpose, we propose a layer-wise estimation strategy, which can be incorporated into our initialization procedure in Algorithm 2. Recall the denoised data matrix  $\widehat{\mathbf{Z}}$  from Step 1 of Algorithm 2 and let  $\sigma_1, \sigma_2, \dots$  be its singular values in the descending order. Given a candidate grid  $\mathfrak{R}$ , we

---

**Algorithm 3:** Penalized SAEM algorithm for the two-latent-layer DDE
 

---

**Data:**  $\mathbf{Y}, \mathcal{K}$ , tuning parameters  $\lambda_N, \tau_N$ .

Initialize  $\mathbf{A}^{(1),[0]}, \mathbf{A}^{(2),[0]}$  and  $\Theta^{[0]}$  based on Algorithm 2.

**while**  $\|\Theta^{[t]} - \Theta^{[t-1]}\|$  is larger than a threshold **do**

In the  $t$ th iteration,

// **Simulation-step**

**for**  $(i, k) \in [N] \times [K^{(1)}]$  **do**

Sample each  $A_{i,k}^{(1),[t+1]}$  from the complete conditional  $\mathbb{P}(A_{i,k}^{(1)} \mid (-))$  using the previous parameter estimates  $\Theta^{[t]}, \mathbf{A}^{[t]}$

**for**  $(i, l) \in [N] \times [K^{(2)}]$  **do**

Sample each  $A_{i,l}^{(2),[t+1]}$  from the complete conditional  $\mathbb{P}(A_{i,l}^{(2)} \mid (-))$  using the previous parameter estimates  $\Theta^{[t]}, \mathbf{A}^{[t]}$

// **Stochastic approximation M-step**

update the parameters  $\Theta^{[t+1]}$  by maximizing the stochastic averaged objectives (e.g. see (12))

Estimate  $\mathbf{G}$  based on the sparsity structure of  $\widehat{\mathbf{B}}$  according to (7).

**Output:** Estimated continuous parameters  $\widehat{\Theta}$ , estimated graphical matrices  $\mathcal{G}$ .

---

estimate the number of latent variables in the first layer based on the largest spectral ratio:  $\widehat{K}^{(1)} := \operatorname{argmax}_{k \in \mathbb{R}} (\sigma_k / \sigma_{k+1}) - 1$ . Now, given  $\widehat{K}^{(1)}$ , we proceed with the remaining steps of Algorithm 2 to estimate the first-layer latent variables  $\mathbf{A}^{(1)}$ . By treating the estimated  $\mathbf{A}^{(1)}$  as the observed variables of a one-latent-layer DDE, we can repeat the above procedure to estimate  $\widehat{K}^{(2)}$ . See Supplement S.3.2 for alternative selection criteria for  $\mathcal{K}$ .

## 5 Simulation Studies

We conduct extensive simulation studies in various settings to assess the performance of the proposed computation pipeline (Algorithms 2 and 3) and validate our identifiability conditions (in Section 3.1). We generate data from two-latent-layer DDEs, exploring a total of 90 true settings by varying the following:

- (a) three *parametric families*: Bernoulli, Poission, Normal,
- (b) three *paramter dimensions*:  $(J, K^{(1)}, K^{(2)}) = (18, 6, 2), (54, 18, 6), (90, 30, 10)$ ,
- (c) two *parameter values*: see (13) below,
- (d) five varying *sample sizes*:  $N = 500, 1000, 2000, 4000, 8000$ .

Given a value of  $K^{(2)}$ , set  $K^{(1)} = 3K^{(2)}$  and  $J = 9K^{(2)}$ , which allows a large latent dimension with as many as  $K^{(1)} = 30$  binary latent variables in the shallowest latent layer.

In terms of the true parameter values, we consider two sets of values based on the strict and generic identifiability conditions in Theorems 1 and 2, respectively. In particular, we define  $\mathcal{B}_s = \{\mathbf{B}_s^{(d)}\}_{d=1,2}$  that satisfy Theorem 1 as follows:

$$\mathbf{B}_s^{(d)} = \begin{pmatrix} -21_{K^{(d)}} & 4\mathbf{I}_{K^{(d)}} \\ -41_{K^{(d)}} & 4\mathbf{I}_{K^{(d)}} \\ -21_{K^{(d)}} & \mathbf{B}_1^{(d)} \end{pmatrix}, \quad \text{where } \beta_{1;j,k}^{(d)} := \begin{cases} 4 & \text{if } k = j, \\ 4/3 & \text{else if } |k - j| = K^{(d)}/2, \\ 0 & \text{otherwise.} \end{cases} \quad (13)$$

We also consider  $\mathcal{B}_g = \{\mathbf{B}_g^{(d)}\}_{d=1,2}$  that satisfy Theorem 2, whose exact values are displayed in Supplement S.4.1. We set the top-layer proportion parameters as  $p_k = 0.5$  for all  $k \in [K^{(2)}]$ , and set the dispersion parameters for the Normal distribution as  $\gamma_j = \sigma_j^2 = 1$  for all  $j \in [J]$ .

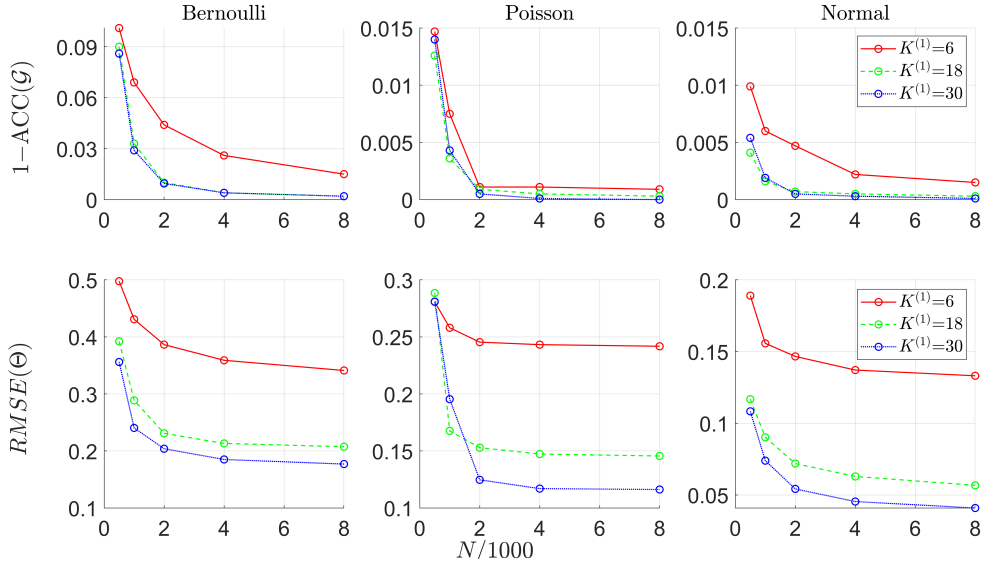


Figure 3: Estimation error for  $\mathcal{G}$  and  $\Theta$  under the two-latent-layer DDE with parameters  $\mathcal{B}_s$  and various observed-layer parametric families.

For each scenario, we run 100 independent simulations, and display the estimation results in Figure 3. The results under the generic identifiable parameters  $\mathcal{B}_g$  and computation times are included in Supplementary Material S.4.1. We measure the estimation accuracy of

the graphical matrices  $\mathcal{G}$  by computing the average entrywise accuracy. For the continuous parameters  $\Theta$ , we report the root mean squared error (RMSE). Under all response types and parameter values, the estimation errors for both  $\mathcal{G}$  and  $\Theta$  decrease as the sample size  $N$  increases. This empirically justifies the identifiability and consistency results. Additionally, by comparing the estimation accuracy across different parametric families, we observe that the Bernoulli is the most challenging to estimate, and the Normal is the easiest. Regarding the true parameters, the sparse model with coefficients  $\mathcal{B}_s$  is easier to estimate. This is because sparsity helps the initialization and reduces the effective parameter dimension. Finally, under coefficients  $\mathcal{B}_s$ , estimation accuracy improves as the latent and observed dimensions increase, which is a consequence of the decreasing percentage of nonzero entries in  $\mathcal{B}$ .

In Supplementary Material S.4.3, we present simulation results where the latent dimension  $\mathcal{K}$  is unknown. We illustrate that the spectral-gap estimator has near-perfect selection accuracy for a large  $N$  (e.g., larger than 4000), and is superior in terms of both accuracy and computation time compared to alternative estimation strategies.

## 6 Real Data Applications

We illustrate DDEs’ interpretability, representation power, and downstream prediction accuracy on three diverse real-world datasets. Supplementary Material S.5.1 gives the preprocessing details of all datasets.

### 6.1 Binary Data: Bernoulli-DDE for MNIST Handwritten Digits

The MNIST dataset for handwritten digits is very popular for classification as well as unsupervised learning (Deng, 2012). We fit the two-latent-layer DDE with binary responses (Bernoulli-DDE), where the observed layer distributions in (4) are  $Y_j \mid (\mathbf{A}^{(1)} = \boldsymbol{\alpha}^{(1)}) \sim \text{Ber}(g_{\text{logistic}}(\beta_{j,0}^{(1)} + \sum_{k \in [K^{(1)}]} \beta_{j,k}^{(1)} \alpha_k^{(1)}))$ . This resembles existing generative models for images such as DBN and DBM, but we instead consider a much low-dimensional shrinking-ladder shaped latent structure that is identifiable and interpretable. For easier presentation, we



Basis image						
Positive part						
Negative part						

Table 1: From left to right: Estimated basis images  $\beta_{0,0}^{(1)}, \beta_{0,1}^{(1)}, \beta_{0,2}^{(1)}, \beta_{0,3}^{(1)}, \beta_{0,4}^{(1)}, \beta_{0,5}^{(1)}$  from the MNIST data, which define sparse subregions in the  $28 \times 28$  image. The second and third row shows the most significant portion of the basis images by thresholding at the value  $\pm 1.5$ .

consider the subset of images whose true digit labels are 0, 1, 2, and 3. After preprocessing, our training set consists of  $N = 20,679$  images each with  $J = 264$  binary pixels. Compared to many existing works that analyzed MNIST, we are considering a more challenging fully-unsupervised setting by holding out all other information about the images, such as the true labels, number of classes, and the spatial location among the pixels.

We fit the two-latent-layer DDE using Algorithm 1 with the latent dimensions set to  $K^{(1)} = 5$  and  $K^{(2)} = 2$  (see the Supplementary Material S.5.2 for the rationale for this choice). Table 1 displays the first-layer coefficients  $\mathbf{B}^{(1)}$  by rearranging the each column into the original  $28 \times 28$  grid. Note that the value of  $\mathbf{B}^{(1)}$  is in the logit-scale, so the negative coefficients make the corresponding pixel more likely to be zero. From the reshaped columns  $\beta_{0,0}^{(1)}, \beta_{0,1}^{(1)}, \dots, \beta_{0,5}^{(1)}$  of  $\mathbf{B}^{(1)}$ , we can interpret the meaning of each latent variable:  $A_1^{(1)} = 1$  indicates a zero-like shape,  $A_5^{(1)} = 1$  indicates symmetric curves on the upper-left and bottom-right corners, and the other latent variables represent different rotations. Additionally, using the deeper graphical matrix  $\mathbf{G}^{(2)}$  displayed in the Supplementary Material S.5.4, we can also interpret the top layer latent variables as broader information about the images. For example,  $A_1^{(2)}$  indicates large pixel density and  $A_2^{(2)}$  indicates symmetry with respect to the x-axis.

The learned shallower and deeper latent representations  $(\hat{\mathbf{A}}^{(1)}, \hat{\mathbf{A}}^{(2)})$  are evaluated under

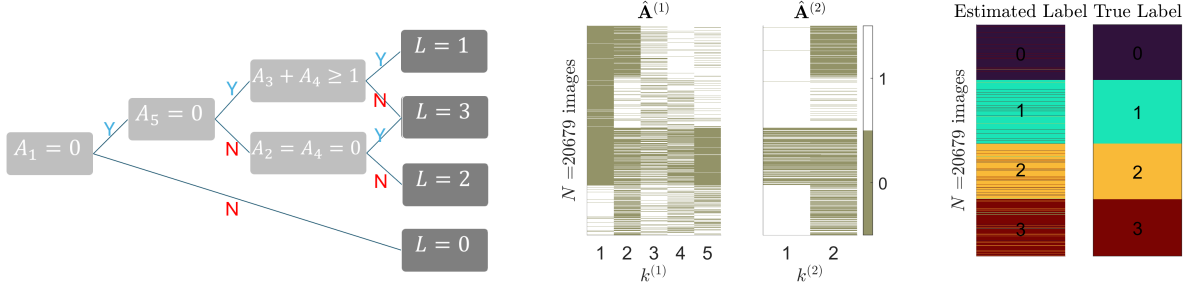


Figure 4: **Left:** Decision tree to estimate the digit  $L = 0, 1, 2, 3$ . **Center:** Estimated latent representations  $\hat{\mathbf{A}}^{(1)}, \hat{\mathbf{A}}^{(2)}$ . **Right:** Estimated and true digits in the train set.

two measures of performance: *classification accuracy* and *reconstruction accuracy*. We first estimate the latent variables using the  $\varphi$  matrix in the EM algorithm:

$$(\hat{\mathbf{A}}_i^{(1)}, \hat{\mathbf{A}}_i^{(2)}) = \underset{\boldsymbol{\alpha}^{(1)} \in \{0,1\}^{K_1}, \boldsymbol{\alpha}^{(2)} \in \{0,1\}^{K_2}}{\operatorname{argmax}} \varphi_{i, \boldsymbol{\alpha}^{(1)}, \boldsymbol{\alpha}^{(2)}}; \quad \boldsymbol{\alpha}^{(\ell)} \in \{0, 1\}^{K_\ell}, \ell = 1, 2. \quad (14)$$

Then, a decision tree that classifies the binary latent representations to the categorical label is built by using the misclassification error as the splitting criteria; see the left panel of Figure 4. The center and right panels display the estimated latent traits and estimated labels. Our classifier leads to a high train/test accuracy of 92.0%/92.6%, even though our model is not fine-tuned for image classification. Although the state-of-art machine learning methods can achieve an accuracy as high as 97% (Monnier et al., 2020), we point out that the main goal here is not classification, but on interpretability and parsimony; indeed, the DDE uses more limited information and is a less complex but more interpretable model that provides the generative process for the image. In Table 3, we compare the classification accuracy and pixel-wise reconstruction accuracy of the two-latent-layer DDE with alternative interpretable models, such as the latent class model (LCM) and the one-latent-layer DDE. The results show that the two-latent-layer DDE performs the best. We also display example generated images alongside their latent configurations in Table 2, which illustrates various handwriting styles for each digit. Supplementary Material S.5.4 additionally displays sample reconstructed images based on these three methods, and illustrates that the LCM and the one-latent-layer DDE generate noisier and less flexible images than the two-latent-layer DDE.

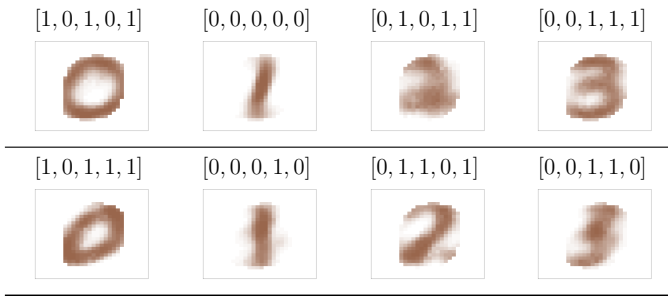


Table 2: Example generated images from the two-latent-layer DDE and their latent representations.

Accuracy	LCM	1-DDE	2-DDE
Train classif. (%)	89.5	84.8	92.0
Test classif. (%)	90.9	86.2	92.6
Train recon. (%)	48.2	79.5	79.6
Test recon. (%)	48.5	79.1	79.9

Table 3: Classification accuracy and pixel-wise reconstruction accuracy for the MNIST dataset.

## 6.2 Count Data: Poisson-DDE Hierarchical Topic Modeling

Next, we apply DDEs to learn hierarchical latent topics from text documents. Within the field of topic modeling, it is natural for the topics to be correlated with each other (Blei and Lafferty, 2006), and hierarchical topic modeling is often adopted (Griffiths et al., 2003; Paisley et al., 2014; Chakraborty et al., 2024). While many of the existing works assume a tree-structured hierarchy, DDEs flexibly allow multiple parents for each variable.

We analyze the text corpus from the 20 newsgroups dataset (Lang, 1995), which was previously analyzed by other topic models with binary latent variables (Srivastava et al., 2013; Gan et al., 2015). The training set of the corpus consists of approximately 11,000 documents and 2,000 words, and is based on the email messages across 20 newsgroups. After preprocessing by focusing on 12 newsgroups and removing stop words and infrequent words, the dataset consists of  $N = 5,883$  documents and  $J = 653$  words. While not used for fitting the DDE, the label (newsgroup) of each document is also provided in the dataset, alongside three larger categories: recreation, computer, and science.

We fit the two-latent-layer DDE with a Poisson-distributed data layer (Poisson-DDE)  $Y_j \mid (\mathbf{A}^{(1)} = \boldsymbol{\alpha}^{(1)}) \sim \text{Poi}(\exp[\beta_{j,0}^{(1)} + \sum_{k \in [K^{(1)}]} \beta_{j,k}^{(1)} \alpha_k^{(1)}])$ , and display the estimated latent structure in Figure 5. We set  $K^{(1)} = 8$  based on the spectral ratio estimator and  $K^{(2)} = 2$  based on the identifiability conditions and better interpretability. Additional details behind this choice are given in Supplementary Material S.5.2. Our choice of  $K^{(2)} = 2$  is also

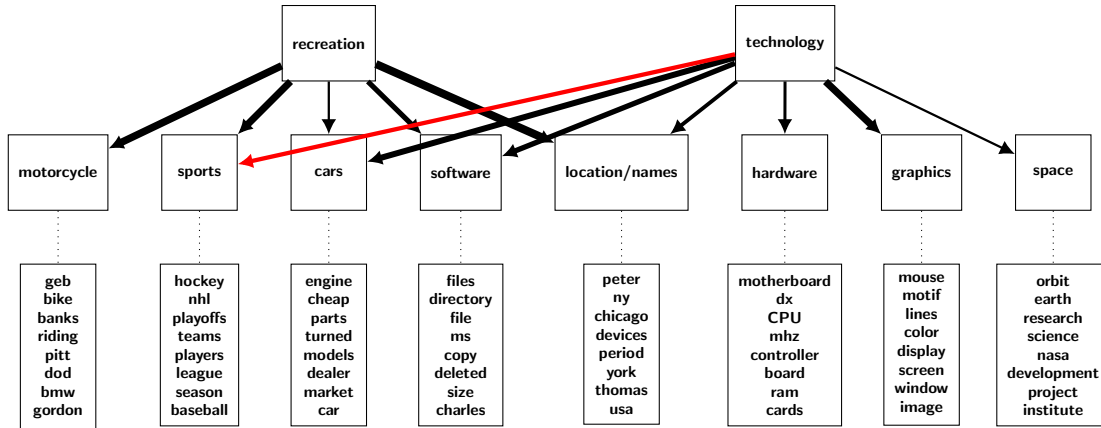


Figure 5: DDE estimated from the 20 newsgroups dataset. For each shallow layer latent variable, we display the top eight representative words. The width of the upper layer arrows is proportional to the corresponding coefficients and the red arrow indicates negative values.

consistent with the correlation structure discovered in Gan et al. (2015). To better interpret individual latent variables, we define representative words for each topic  $k$  based on the discrepancy between  $\beta_{j,k}$  and all other coefficients,  $(\beta_{j,l})_{l \neq k}$ . That is, for each index  $k$ , we choose the words  $j$  with the largest values of  $\max\{\min\{\beta_{j,k} - \beta_{j,l} : l \neq k\}, 0\}$ . We display the representative words for each latent variable in the bottom row of Figure 5. Here, each latent variable is named based on the representative words and the held-out newsgroup categories.

Compared to the held-out tree structure of the 12 newsgroup labels (see Figure S.7 in the Supplement), one can see that the DDE has discovered a lower-dimensional structure in Figure 5. The latent structure in DDEs allow multiple parents for each topic and effectively model the complex label dependence. For example, ‘cars’, ‘software’, ‘location/names’ have both ‘recreation’ and ‘technology’ as parents, and many bottom-layer words are assigned to multiple topics. We also observe that similar true labels are combined into a single latent variable, for example ‘computer’ and ‘science’ are combined into ‘technology’ in the second latent layer, and ‘baseball’ and ‘hockey’ are combined as ‘sports’ in the bottom latent layer.

We also compare our model fit to existing directed graphical models with matching latent dimensions: LDA (Blei et al., 2003) and DPFA-SBN (Gan et al., 2015). LDA has a single latent layer with mixed membership scores as continuous latent variables, and DPFA-SBN

is a multilayer model with binary latent variables similar to DDEs. We consider the following three metrics widely used in topic modeling to measure different aspects of fit (Chen et al., 2023). The first measure is the *perplexity*, measuring the predictive likelihood of the words in the held-out set. While there are multiple notions of perplexities, we choose the definition that was adopted in similar Poisson-based models (Zhou et al., 2012; Gan et al., 2015; Ranganath et al., 2015, see Supplementary Material S.5.3 for more details). In addition to the train perplexity, we also display the test perplexity. The second measure is the average negative *coherence*, measuring the quality within each topic by computing  $-\frac{1}{K^{(1)}} \sum_{k=1}^{K^{(1)}} \sum_{v_1, v_2 \in V_k} \log((\text{freq}(v_1, v_2) + 1)/\text{freq}(v_2))$ , where  $V_k$  is the top 15 representative words for the  $k$ th topic, and the function “freq” counts the number of documents containing the words specified in the input argument. The third measure is the *similarity*, computing the number of overlapping words within representative words across different topics:  $\sum_{1 \leq k_1 < k_2 \leq K^{(1)}} \sum_{v_1 \in V_{k_1}, v_2 \in V_{k_2}} I(v_1 = v_2)$ . For all three measures, smaller values are better.

Table 4 summarizes the results and shows the promising fit of DDE. Compared to other models with the same latent dimensions, DDEs have better test perplexity and similarity. The similarity measure shows that while the other model fits exhibit common representative words among different topics, the representative words learned from DDE are entirely disjoint and effectively represent different topics. In terms of coherence, the DDE fit is better than LDA but worse than DPFA. We have also fit models with larger dimensions for comparison, by considering LDA with 256 latent variables, and DPFA with  $K^{(1)} = 128, K^{(2)} = 64$  latent variables. The dimension for LDA is motivated by that the DDE has  $2^8 = 256$  mixture components; while for DPFA, this is the same latent dimension specified in the original paper (Gan et al., 2015). We can see that while considering a larger latent dimension may help in terms of perplexity, this leads to a loss of the within-topic coherence as well as dilutes the boundary of each topic, and hence gives less interpretable results.

Model	Dimension $\mathcal{K}$	Train perplexity	Test perplexity	Neg. coherence	Similarity
LDA	8	499	512	276	43
LDA	256	269	515	321	(41450)
DPFA	8 – 2	289	499	211	5
DPFA	128 – 64	175	232	280	(3378)
DDE	8 – 2	322	398	270	0
DDE	8 – 3	322	399	275	0

Table 4: Train and test perplexity scores of different models on the 20 Newsgroups dataset. For all measures, smaller values are better. We parenthesize similarity scores for the models with different dimensions, as the measure is not normalized.

### 6.3 Continuous Data: Lognormal-DDE for Response Times

We apply the DDE to a response time dataset from the Trends in International Mathematics and Science Study (TIMSS) (Fishbein et al., 2021). We analyze the eighth-grade students’ response time for an internet-based mathematics assessment. After preprocessing, the dataset consists of  $N = 526$  students’ response times for  $J = 29$  questions. Here, we fit the two-latent-layer DDE where a lognormal distribution is used to model the continuous positive response times (Lognormal-DDE):  $Y_j \mid (\mathbf{A}^{(1)} = \boldsymbol{\alpha}^{(1)}) \sim \text{lognormal}(\beta_{j,0}^{(1)} + \sum_{k \in [K^{(1)}]} \beta_{j,k}^{(1)} \alpha_k^{(1)}, \gamma_j)$ . This dataset includes additional information regarding the latent structure  $\mathbf{G}^{(1)}$ , which is the so-called  $Q$ -matrix in the cognitive diagnostic modeling literature (von Davier, 2008; Lee and Gu, 2024). The provisional  $\mathbf{G}^{(1)}$  matrix specifies  $K^{(1)} = 7$  latent cognitive skills (Number, Algebra, Geometry, Data and Probability, Knowing, Applying, and Reasoning) as well as the skills that are required to solve each item. That is,  $g_{j,k}^{(1)} = 1$  if item  $j$  requires latent skill  $k$  to solve it. Hence, following the confirmatory latent variable modeling convention in psychometrics, we estimate the DDE parameters by fixing  $\mathbf{G}^{(1)}$  to this given structure.

Response \ Latent skill	$A_1^{(2)}$	$A_1^{(1)}$ : Number	$A_2^{(1)}$ : Algebra	$A_3^{(1)}$ : Geometry	$A_4^{(1)}$ : Data and Prob
Agree a lot	0.83	0.72	0.88	0.86	0.87
Agree a little	0.80	0.72	0.85	0.84	0.85
Disagree a little	0.76	0.74	0.85	0.84	0.84
Disagree a lot	0.69	0.67	0.76	0.75	0.78

Table 5: Average latent variable estimate for each response category for the question “Mathematics is one of my favorite subjects”.

We fit the two-latent-layer DDE with  $K^{(1)} = 7$ ,  $K^{(2)} = 1$ , and estimate the latent skills based on the posterior probability using (14). We compare the estimated latent variables with the held-out information of each student’s categorical response to a survey question: “Mathematics is one of my favorite subjects”, and display the results in Table 5. The first column shows that the higher-order latent variable,  $A_1^{(2)}$ , is highly correlated with the magnitude that students like math. This suggests that  $A_1^{(2)}$  can be interpreted as a general indicator for the students’ interest in math, while the fine-grained latent variables  $\mathbf{A}^{(1)}$  represent more specific skill mastery for each domain. In addition, we observe that the students who enjoy math tend to have a higher probability of mastering specific skills as well. This is coherent with the fact that the estimated  $\mathbf{B}^{(1)}$ -coefficients are all positive.

## 7 Discussion

This paper makes contributions to core AI problems from statisticians’ perspectives by proposing a broad family of interpretable DGMs with solid identifiability guarantees, scalable computation pipelines, and promising application potential. It also opens up interesting directions for future research. Theoretically, it would be desirable to extend our identifiability and consistency results to the challenging setting with an unknown number of latent variables. We conjecture that one may be able to identify  $\mathcal{K}$  under additional restrictions on the parameter space or considering specific parametric families. Second, it would be interesting to theoretically justify the good performance of the spectral-gap estimator for estimating the latent dimensions under general nonlinear link functions. Another interesting problem pertains to high-dimensional settings, where the number of observed responses,  $J$ , may grow with the sample size  $N$ . Our current notion of identifiability focuses on identifying the population model parameters under the traditional asymptotics with a fixed  $J$ , where the latent variables are marginalized out in the likelihood. As modern datasets often comes with a large number of observed features, it would be interesting to explore whether our identifiability and estimability results can be generalized to such settings.

In terms of the methodology and applications, an immediate future direction is working to effectively estimate and deploy deeper DDEs with  $D \geq 3$  latent layers. The current theory and computational pipeline conceptually readily generalizes to deeper architectures than considered in this initial paper. It remains to test and refine these deeper models' performance in larger-scale real-world data. Also, it would be interesting to extend DDEs to datasets with additional covariates. For example, the MNIST dataset comes with the actual digit labels as well as the spatial structure of the pixels in the image. In addition, many real datasets contain multiple modalities of data. For example, one may consider a dataset consisting of images uploaded in social media alongside text data such as tags. It is worthwhile to generalize DDEs to model such modern multimodal data. Finally, it would be interesting to extend DDEs for identifiable causal representation learning (Schölkopf et al., 2021) to uncover causal structures among the higher-order latent variables.

**Supplementary Material.** The Supplement contains all technical proofs, additional theoretical results, and additional details about algorithms, simulations, and real data analyses.

## References

- Allman, E. S., Matias, C., and Rhodes, J. A. (2009). Identifiability of parameters in latent structure models with many observed variables. *The Annals of Statistics*, 37(6A):3099–3132.
- Anderson, T. and Rubin, H. (1956). Statistical inference in factor analysis. In *Proceedings of the Berkeley Symposium on Mathematical Statistics and Probability*, page 111. University of California Press.
- Bengio, Y., Courville, A., and Vincent, P. (2013). Representation learning: A review and new perspectives. *IEEE Transactions on Pattern Analysis and Machine Intelligence*, 35(8):1798–1828.
- Blei, D. and Lafferty, J. (2006). Correlated topic models. *Advances in neural information processing systems*, 18:147.
- Blei, D. M., Ng, A. Y., and Jordan, M. I. (2003). Latent Dirichlet allocation. *Journal of Machine Learning Research*, 3(Jan):993–1022.
- Chakraborty, S., Lei, R., and Nguyen, X. (2024). Learning topic hierarchies by tree-directed latent variable models. *arXiv preprint arXiv:2408.14327*.



- Chen, J. and Chen, Z. (2008). Extended Bayesian information criteria for model selection with large model spaces. *Biometrika*, 95(3):759–771.
- Chen, Y., Culpepper, S., and Liang, F. (2020). A sparse latent class model for cognitive diagnosis. *Psychometrika*, 85(1):121–153.
- Chen, Y., He, S., Yang, Y., and Liang, F. (2023). Learning topic models: Identifiability and finite-sample analysis. *Journal of the American Statistical Association*, 118(544):2860–2875.
- Chen, Y. and Li, X. (2022). Determining the number of factors in high-dimensional generalized latent factor models. *Biometrika*, 109(3):769–782.
- Chen, Y., Liu, J., Xu, G., and Ying, Z. (2015). Statistical analysis of Q-matrix based diagnostic classification models. *Journal of the American Statistical Association*, 110(510):850–866.
- Chetverikov, D., Liao, Z., and Chernozhukov, V. (2021). On cross-validated lasso in high dimensions. *The Annals of Statistics*, 49(3):1300–1317.
- Cho, K. H., Raiko, T., and Ilin, A. (2013). Gaussian-bernoulli deep Boltzmann machine. In *The 2013 International Joint Conference on Neural Networks (IJCNN)*, pages 1–7. IEEE.
- de la Torre, J. (2011). The generalized DINA model framework. *Psychometrika*, 76(2):179–199.
- Delyon, B., Lavielle, M., and Moulines, E. (1999). Convergence of a stochastic approximation version of the EM algorithm. *Annals of Statistics*, pages 94–128.
- Deng, L. (2012). The mnist database of handwritten digit images for machine learning research [best of the web]. *IEEE Signal Processing Magazine*, 29(6):141–142.
- Donoho, D. and Stodden, V. (2003). When does non-negative matrix factorization give a correct decomposition into parts? *Advances in neural information processing systems*, 16.
- Fan, J. and Li, R. (2001). Variable selection via nonconcave penalized likelihood and its oracle properties. *Journal of the American Statistical Association*, 96(456):1348–1360.
- Fishbein, B., Foy, P., and Yin, L. (2021). TIMSS 2019 user guide for the international database. *Hentet fra <https://timssandpirls.bc.edu/timss2019/international-database>*.
- Gan, Z., Chen, C., Henao, R., Carlson, D., and Carin, L. (2015). Scalable deep Poisson factor analysis for topic modeling. In *International Conference on Machine Learning*, pages 1823–1832. PMLR.
- Goffinet, B., Loisel, P., and Laurent, B. (1992). Testing in normal mixture models when the proportions are known. *Biometrika*, 79(4):842–846.

- Goodfellow, I., Pouget-Abadie, J., Mirza, M., Xu, B., Warde-Farley, D., Ozair, S., Courville, A., and Bengio, Y. (2014). Generative adversarial nets. *Advances in Neural Information Processing Systems*, 27.
- Green, P. J. (1990). On use of the EM algorithm for penalized likelihood estimation. *Journal of the Royal Statistical Society Series B: Statistical Methodology*, 52(3):443–452.
- Griffiths, T., Jordan, M., Tenenbaum, J., and Blei, D. (2003). Hierarchical topic models and the nested chinese restaurant process. *Advances in Neural Information Processing Systems*, 16.
- Grün, B. and Hornik, K. (2011). topicmodels: An r package for fitting topic models. *Journal of Statistical Software*, 40:1–30.
- Gu, Y. (2024). Going deep in diagnostic modeling: Deep cognitive diagnostic models (Deep-CDMs). *Psychometrika*, 89(1):118–150.
- Gu, Y. and Dunson, D. B. (2023). Bayesian pyramids: Identifiable multilayer discrete latent structure models for discrete data. *Journal of the Royal Statistical Society: Series B*, 85(2):399–426.
- Hinton, G. E., Osindero, S., and Teh, Y.-W. (2006). A fast learning algorithm for deep belief nets. *Neural Computation*, 18(7):1527–1554.
- Ho, N. and Nguyen, X. (2016). On strong identifiability and convergence rates of parameter estimation in finite mixtures. *Electronic Journal of Statistics*, 10(1):271 – 307.
- Hyvarinen, A., Sasaki, H., and Turner, R. (2019). Nonlinear ICA using auxiliary variables and generalized contrastive learning. In *The 22nd International Conference on Artificial Intelligence and Statistics*, pages 859–868. PMLR.
- Junker, B. W. and Sijtsma, K. (2001). Cognitive assessment models with few assumptions, and connections with nonparametric item response theory. *Applied Psychological Measurement*, 25(3):258–272.
- Kaiser, H. F. (1958). The varimax criterion for analytic rotation in factor analysis. *Psychometrika*, 23(3):187–200.
- Ke, Z. T. and Wang, M. (2024). Using SVD for topic modeling. *Journal of the American Statistical Association*, 119(545):434–449.
- Khemakhem, I., Kingma, D., Monti, R., and Hyvarinen, A. (2020). Variational autoencoders and nonlinear ica: A unifying framework. In *Artificial Intelligence and Statistics*, pages 2207–2217. PMLR.
- Kingma, D. P. and Welling, M. (2014). Stochastic gradient VB and the variational auto-encoder. In *Second international conference on learning representations, ICLR*, volume 19, page 121.

- Kivva, B., Rajendran, G., Ravikumar, P., and Aragam, B. (2022). Identifiability of deep generative models without auxiliary information. *Advances in Neural Information Processing Systems*, 35:15687–15701.
- Koller, D. and Friedman, N. (2009). *Probabilistic graphical models: principles and techniques*. MIT press.
- Koopmans, T. C. and Reiersol, O. (1950). The identification of structural characteristics. *The Annals of Mathematical Statistics*, 21(2):165–181.
- Kruskal, J. B. (1977). Three-way arrays: rank and uniqueness of trilinear decompositions, with application to arithmetic complexity and statistics. *Linear Algebra and Its Applications*, 18(2):95–138.
- Kuhn, E. and Lavielle, M. (2004). Coupling a stochastic approximation version of EM with an MCMC procedure. *ESAIM: Probability and Statistics*, 8:115–131.
- Kuhn, H. W. (1955). The Hungarian method for the assignment problem. *Naval Research Logistics Quarterly*, 2(1-2):83–97.
- Lang, K. (1995). Newsweeder: Learning to filter netnews. In *Proceedings of the Twelfth International Conference on Machine Learning*, pages 331–339.
- Lee, H., Grosse, R., Ranganath, R., and Ng, A. Y. (2009). Convolutional deep belief networks for scalable unsupervised learning of hierarchical representations. In *Proceedings of the 26th annual international conference on machine learning*, pages 609–616.
- Lee, S. and Gu, Y. (2024). New paradigm of identifiable general-response cognitive diagnostic models: beyond categorical data. *Psychometrika*, 89:1304–1336.
- Li, Z., Cai, X., Liu, Y., and Zhu, B. (2019). A novel Gaussian–Bernoulli based convolutional deep belief networks for image feature extraction. *Neural Processing Letters*, 49:305–319.
- Melnykov, V. and Melnykov, I. (2012). Initializing the EM algorithm in Gaussian mixture models with an unknown number of components. *Computational Statistics & Data Analysis*, 56(6):1381–1395.
- Mityagin, B. S. (2020). The zero set of a real analytic function. *Mathematical Notes*, 107(3-4):529–530.
- Monnier, T., Groueix, T., and Aubry, M. (2020). Deep transformation-invariant clustering. *Advances in neural information processing systems*, 33:7945–7955.
- Moran, G. E., Sridhar, D., Wang, Y., and Blei, D. M. (2022). Identifiable deep generative models via sparse decoding. *Transactions on Machine Learning Research*.
- Oja, E. and Hyvarinen, A. (2000). Independent component analysis: algorithms and applications. *Neural networks*, 13(4-5):411–430.

- Paisley, J., Wang, C., Blei, D. M., and Jordan, M. I. (2014). Nested hierarchical Dirichlet processes. *IEEE transactions on pattern analysis and machine intelligence*, 37(2):256–270.
- Ranganath, R., Tang, L., Charlin, L., and Blei, D. (2015). Deep exponential families. In *Artificial Intelligence and Statistics*, pages 762–771. PMLR.
- Ranzato, M. and Szummer, M. (2008). Semi-supervised learning of compact document representations with deep networks. In *Proceedings of the 25th international conference on Machine learning*, pages 792–799.
- Robbins, H. and Monro, S. (1951). A stochastic approximation method. *The Annals of Mathematical Statistics*, pages 400–407.
- Rohe, K. and Zeng, M. (2023). Vintage factor analysis with varimax performs statistical inference. *Journal of the Royal Statistical Society Series B: Statistical Methodology*, 85(4):1037–1060.
- Salakhutdinov, R. (2015). Learning deep generative models. *Annual Review of Statistics and Its Application*, 2(1):361–385.
- Salakhutdinov, R. and Hinton, G. (2009). Deep Boltzmann machines. In *Artificial Intelligence and Statistics*, pages 448–455. PMLR.
- Schölkopf, B., Locatello, F., Bauer, S., Ke, N. R., Kalchbrenner, N., Goyal, A., and Bengio, Y. (2021). Toward causal representation learning. *Proceedings of the IEEE*, 109(5):612–634.
- Shen, X., Pan, W., and Zhu, Y. (2012). Likelihood-based selection and sharp parameter estimation. *Journal of the American Statistical Association*, 107(497):223–232.
- Shen, X. and Wong, W. H. (1994). Convergence rate of sieve estimates. *The Annals of Statistics*, pages 580–615.
- Sohl-Dickstein, J., Weiss, E., Maheswaranathan, N., and Ganguli, S. (2015). Deep unsupervised learning using nonequilibrium thermodynamics. In *International Conference on Machine Learning*, pages 2256–2265. PMLR.
- Srivastava, N., Salakhutdinov, R. R., and Hinton, G. E. (2013). Modeling documents with deep Boltzmann machines. *arXiv preprint arXiv:1309.6865*.
- Sutskever, I., Martens, J., Dahl, G., and Hinton, G. (2013). On the importance of initialization and momentum in deep learning. In *International conference on machine learning*, pages 1139–1147. PMLR.
- Van der Vaart, A. W. (2000). *Asymptotic statistics*, volume 3. Cambridge university press.
- Vaswani, A., Shazeer, N., Parmar, N., Uszkoreit, J., Jones, L., Gomez, A. N., Kaiser, L. u., and Polosukhin, I. (2017). Attention is All you Need. In Guyon, I., Luxburg, U. V., Bengio, S., Wallach, H., Fergus, R., Vishwanathan, S., and Garnett, R., editors, *Advances in Neural Information Processing Systems*, volume 30. Curran Associates, Inc.

- von Davier, M. (2008). A general diagnostic model applied to language testing data. *British Journal of Mathematical and Statistical Psychology*, 61(2):287–307.
- Wilks, S. S. (1938). The large-sample distribution of the likelihood ratio for testing composite hypotheses. *The Annals of Mathematical Statistics*, 9(1):60–62.
- Xu, G. and Shang, Z. (2018). Identifying latent structures in restricted latent class models. *Journal of the American Statistical Association*, 113(523):1284–1295.
- Zhang, H., Chen, Y., and Li, X. (2020). A note on exploratory item factor analysis by singular value decomposition. *Psychometrika*, 85:358–372.
- Zhou, M., Hannah, L., Dunson, D., and Carin, L. (2012). Beta-negative binomial process and Poisson factor analysis. In *Artificial Intelligence and Statistics*, pages 1462–1471. PMLR.

# Supplementary Material

This Supplementary Material is organized as follows. Section S.1 proves all main theorems and provides additional identifiability results under one-layer saturated models and variants. Section S.2 provides details regarding the spectral initialization algorithm. Section S.3 gives details regarding the EM algorithms (Algorithms 1 and 3) such as M-step update formulas, implementation details, and selection of the number of latent variables. Section S.4 provides various additional simulation results under (a) generically identifiable true parameters, (b) varying numbers of Monte Carlo samples in the SAEM algorithm, (c) unknown latent dimensions. Finally, Section S.5 gives additional data analysis details such as preprocessing, latent dimension selection, and additional visualizations.

## S.1 Proof of Theorems

Recall from Section 3.1 that our identifiability results for general DDEs with multiple latent layers build upon the identifiability of a model with only one latent layer (the shallowest latent layer), where the deeper latent layers have been marginalized out. Here, we formally state identifiability conditions for such one-latent-layer saturated models in Section S.1.1, before proving the identifiability results for general DDEs in Section S.1.2. We prove the claims stated for the one-latent-layer models in Section S.1.3, and Theorem 3 in Section S.1.4. Additional identifiability results under related models with interaction effects (instead of the main-effect DDEs introduced in the main paper) are presented in Section S.1.5.

### S.1.1 Identifiability Under One-latent-layer Saturated Models

The *one-latent-layer saturated model* is defined as follows.

**Definition S.1** (One-latent-layer saturated model). *The one-latent-layer saturated model with  $K^{(1)}$  latent variables, responses  $\mathbf{Y} \in \prod_{j \in [J]} \mathcal{Y}_j$ , and parameters  $(\Theta^{(1)}, \mathbf{G}^{(1)})$  is defined*

by the distribution of  $\mathbf{Y} \mid \mathbf{A}^{(1)}$  in (4), and the saturated latent distribution

$$\mathbb{P}(\mathbf{A}^{(1)} = \boldsymbol{\alpha}) = \pi_{\boldsymbol{\alpha}}, \quad \text{for all } \boldsymbol{\alpha} \in \{0, 1\}^{K^{(1)}}. \quad (\text{S.1})$$

Here, the parameter  $\boldsymbol{\pi} := (\pi_{\boldsymbol{\alpha}})_{\boldsymbol{\alpha}}$  satisfies  $\pi_{\boldsymbol{\alpha}} \in (0, 1)$  and  $\sum_{\boldsymbol{\alpha}} \pi_{\boldsymbol{\alpha}} = 1$ . The notation  $\boldsymbol{\Theta}^{(1)} := (\boldsymbol{\pi}, \mathbf{B}^{(1)}, \boldsymbol{\gamma})$  collects all continuous parameters. We define the parameter spaces  $\Omega_{K^{(1)}}(\boldsymbol{\Theta}^{(1)}; \mathbf{G}^{(1)})$  and  $\Omega_{K^{(1)}}(\tilde{\boldsymbol{\Theta}}^{(1)}, \tilde{\mathbf{G}}^{(1)})$  similar to Definition 2 in the main paper.

Here, the term ‘‘saturated’’ indicates that no additional distributional assumptions are imposed on the latent variables, except that they are discrete. Similar to Definition 3, we define an equivalence relationship  $\sim_{K^{(1)}}$  when the parameters are identical up to label switching, and use it to define identifiability.

**Definition S.2** (Equivalence relation). *For the one-latent-layer saturated model, define an equivalence relationship ‘‘ $\sim_{K^{(1)}}$ ’’ by setting  $(\boldsymbol{\Theta}^{(1)}, \mathbf{G}^{(1)}) \sim_{K^{(1)}} (\tilde{\boldsymbol{\Theta}}^{(1)}, \tilde{\mathbf{G}}^{(1)})$  if and only if  $\boldsymbol{\gamma} = \tilde{\boldsymbol{\gamma}}$  and there exist a permutation  $\sigma^{(1)} \in S_{[K^{(1)}]}$  such that the following conditions hold:*

- $\boldsymbol{\pi}_{(\alpha_{\sigma^{(1)}}, \dots, \alpha_{\sigma^{(1)}(K^{(1)})})} = \tilde{\boldsymbol{\pi}}_{\boldsymbol{\alpha}}$  for all  $\boldsymbol{\alpha} \in \{0, 1\}^{K^{(1)}}$
- $g_{j,k}^{(1)} = \tilde{g}_{j, \sigma^{(1)}(k)}^{(1)}$  and  $\beta_{j,k}^{(1)} = \tilde{\beta}_{j, \sigma^{(1)}(k)}^{(1)}$  for all  $k \in [K^{(1)}], j \in [J]$ .

We say that the one-latent-layer saturated model with true parameters  $(\boldsymbol{\Theta}^{(1)\star}, \mathbf{G}^{(1)\star})$  is identifiable up to  $\sim_{K^{(1)}}$ , if for any alternate parameter value  $(\boldsymbol{\Theta}^{(1)}, \mathbf{G}^{(1)}) \in \Omega_{K^{(1)}}(\boldsymbol{\Theta}^{(1)}, \mathbf{G}^{(1)})$  with  $\mathbb{P}_{\boldsymbol{\Theta}^{(1)}, \mathbf{G}^{(1)}} = \mathbb{P}_{\boldsymbol{\Theta}^{(1)\star}, \mathbf{G}^{(1)\star}}$ , it holds that  $(\boldsymbol{\Theta}^{(1)}, \mathbf{G}^{(1)}) \sim_{\mathcal{K}} (\boldsymbol{\Theta}^{(1)\star}, \mathbf{G}^{(1)\star})$ . Here,  $\mathbb{P}_{\boldsymbol{\Theta}^{(1)}, \mathbf{G}^{(1)}}$  is the marginal distribution of  $\mathbf{Y}$ , which follows from (4) and (S.1).

Under these definitions, we state identifiability results for the one-latent-layer saturated model. Proposition 1 and Proposition 2 are one-layer analogues of Theorem 1 and Theorem 2, respectively. We postpone the proofs of these results to Section S.1.3.

**Proposition 1.** *Given the knowledge of  $K^{(1)}$ , the one-latent-layer saturated model with parameters  $(\boldsymbol{\Theta}^{\star}, \mathbf{G}^{(1)\star}) \in \Omega_{K^{(1)}}(\boldsymbol{\Theta}^{(1)}, \mathbf{G}^{(1)})$  is identifiable up to  $\sim_{K^{(1)}}$  when the true parameters*

$\mathbf{B}^{(1)\star}, \mathbf{G}^{(1)\star}$  satisfy conditions A, B from Theorem 1. In particular, condition B holds when  $\mathbf{G}^{(1)\star}$  contains another identity matrix.

**Proposition 2.** Consider the one-latent-layer saturated model where all parametric families and link functions  $g_j$ s in (4) are analytic, and the true parameter lives in  $\Omega_{K^{(1)}}(\Theta^{(1)}; \mathbf{G}^{(1)\star})$ . Then, the model is generically identifiable when  $\mathbf{G}^{(1)\star}$  satisfies condition C from Theorem 2.

### S.1.2 Proof of Theorems 1 and 2

We prove the identifiability results for DDEs using Propositions 1 and 2.

*Proof of Theorem 1.* Our argument is based on applying Proposition 1 in a layer-wise manner. First, consider the bottom two layers with

$$\pi_{\alpha^{(1)}}^{(1)} = \mathbb{P}(\mathbf{A}^{(1)} = \alpha^{(1)}), \quad \forall \alpha^{(1)} \in \{0, 1\}^{K_1} \quad (\text{S.2})$$

defined by marginalizing out the deeper latent layers. Now, we can consider this as the one-layer model with proportion parameters  $\boldsymbol{\pi}^{(1)} = (\pi_{\alpha^{(1)}}^{(1)}, \alpha^{(1)} \in \{0, 1\}^{K_1})$ . Then, Proposition 1 gives the identifiability of  $\mathbf{B}^{(1)}, \mathbf{G}^{(1)}, \boldsymbol{\pi}^{(1)}$  up to  $\sim_{K^{(1)}}$ .

Having identified  $\boldsymbol{\pi}^{(1)}$ , the marginal distribution of the shallowest latent layer  $\mathbf{A}^{(1)}$  is uniquely identified. We generalize the notation in (S.2) and define  $\boldsymbol{\pi}^{(d)}$  similarly. Inductively, for  $1 \leq d < D$ , we apply Proposition 1 by considering  $\mathbf{A}^{(d)}$  and  $\boldsymbol{\pi}^{(d)}$  as the “observed” binary response vector and its proportion parameters that characterize its marginal probability mass function:

$$\pi_{\alpha^{(d)}}^{(d)} = \mathbb{P}(\mathbf{A}^{(d)} = \alpha^{(d)}), \quad \forall \alpha^{(d)} \in \{0, 1\}^{K_d}.$$

Consequently, the parameters  $\mathbf{B}^{(d+1)}, \mathbf{G}^{(d+1)}, \boldsymbol{\pi}^{(d+1)}$  between the  $d$ th and  $(d+1)$ th layers are identified up to  $\sim_{K^{(d+1)}}$ . In particular, when  $d = D - 1$ , it remains to determine  $\mathbf{p}$  from the unstructured proportion parameter vector  $\boldsymbol{\pi}^{(D)}$ . Since we already have identified the  $D$ th



layer labels up to  $\sim_{K^{(D)}}$ , this simply follows by marginalizing out the irrelevant coordinates:

$$p_k = \mathbb{P}(A_k^{(D)} = 1) = \sum_{\boldsymbol{\alpha}^{(D)}: \alpha_k^{(D)}=1} \pi_{\boldsymbol{\alpha}^{(D)}}^{(D)}.$$

The proof is complete.  $\square$

*Proof of Theorem 2.* Proposition 2 shows that the non-identifiable measure-zero set of the one-latent-layer saturated model only depends on the coefficients  $\mathbf{B}^{(1)}$  and  $\boldsymbol{\gamma}$ . By marginalizing out all layers except the bottom two layers, the DDE becomes a one-latent-layer saturated model with parameters  $\boldsymbol{\Theta}^{(1)} := (\pi^{(1)}, \mathbf{B}^{(1)}, \mathbf{G}^{(1)}, \boldsymbol{\gamma})$ . Since we assume that  $\mathbf{G}^{(1)}$  satisfies condition C, the parameters  $\boldsymbol{\Theta}^{(1)}$  are identifiable (upto a permutation  $\sigma^{(1)} \in S_{[K^{(1)}]}$ ) as long as  $(\mathbf{B}^{(1)}, \boldsymbol{\gamma}) \notin N^{(1)}$ . Here,  $N^{(1)}$  is a measure-zero subset of the coefficient space  $\Omega(\mathbf{B}^{(1)}, \boldsymbol{\gamma}; \mathbf{G}^{(1)})$ .

Now, assuming  $\mathbf{B}^{(1)} \notin N^{(1)}$ , we can use a similar argument for deeper layers inductively. For  $2 \leq d \leq D-1$ , let  $N^{(d)}$  be the non-identifiable measure-zero subset of the  $d$ th layer coefficient space  $\Omega(\mathbf{B}^{(d)}; \mathbf{G}^{(d)})$ . Note that we can still apply Proposition 2 since the conditional distribution of  $\mathbf{A}^{(d)} \mid \mathbf{A}^{(d+1)}$  is modeled as a Bernoulli distribution with a logistic link  $g_{\text{logistic}}$ , which is indeed analytic and satisfy Assumption 2. Consequently, as long as  $\mathbf{B}^{(d)} \notin N^{(d)}$  for all  $1 \leq d \leq D-1$ , the  $D$ -layer DDE is identifiable up to permutations of the latent variables within each layer. The proof is complete since  $\cup_{d=1}^D (N^{(d)})^c$  is a union of a finite number of measure-zero sets, and hence again measure-zero.  $\square$

### S.1.3 Proof of Propositions 1 and 2

#### S.1.3.1 Additional Notations

We introduce additional notations that will be used to prove identifiability results for the one-latent-layer saturated model. Most of these notations are consistent with Lee and Gu (2024). First, we omit the superscript “(1)” that indicates the first latent layer when dealing with the one-latent-layer saturated model. Let  $j, k, \boldsymbol{\alpha}$  denote typical indices for  $j \in [J], k \in [K], \boldsymbol{\alpha} \in \{0, 1\}^K$ . Write  $\mathbf{G} = \mathbf{G}^{(1)} = \{\mathbf{g}_1^\top, \dots, \mathbf{g}_J^\top\}^\top$  and let  $H_j := \{k \in [K] : G_{j,k} = 1\}$  be

the index of the parent latent variables for  $Y_j$ . Recall that for each  $j$ , the sample space  $\mathcal{Y}_j$  is a separable metric space. Let  $m_j$  be a base measure on  $\mathcal{Y}_j$ , this will be the counting measure for discrete sample spaces and the Lebesgue measure for continuous cases. Given  $j$  and  $\boldsymbol{\alpha}$ , define the measure  $\mathbb{P}_{j,\boldsymbol{\alpha}}$  on  $\mathcal{Y}_j$  by setting

$$\mathbb{P}_{j,\boldsymbol{\alpha}}(S) := \mathbb{P}(Y_j \in S \mid \mathbf{A} = \boldsymbol{\alpha}) = \int_S p_j(y; \beta_{j,0} + \sum_k \beta_{j,k} \alpha_k, \gamma_j) dm_j(y). \quad (\text{S.3})$$

In other words,  $\mathbb{P}_{j,\boldsymbol{\alpha}}$  denotes the conditional distribution of  $Y_j \mid \mathbf{A} = \boldsymbol{\alpha}$  in (4).

For each  $j \in [J]$ , construct measurable subsets  $S_{1,j}, \dots, S_{\kappa_j,j} \subseteq \mathcal{Y}_j$  with  $\kappa_j \geq 2$ , where the collection of vectors  $\mathbf{s}_j(\boldsymbol{\alpha}) := (\mathbb{P}_{j,\boldsymbol{\alpha}}(S_{1,j}), \dots, \mathbb{P}_{j,\boldsymbol{\alpha}}(S_{\kappa_j,j}))_{\boldsymbol{\alpha} \in \{0,1\}^K}$  is “faithful” in the following sense:

- (a) for  $\boldsymbol{\alpha}, \boldsymbol{\alpha}'$  with  $\boldsymbol{\alpha}_{H_j} = \boldsymbol{\alpha}'_{H_j}$ , it holds that  $\mathbf{s}_j(\boldsymbol{\alpha}) = \mathbf{s}_j(\boldsymbol{\alpha}')$ ,
- (b) there exists  $\boldsymbol{\alpha}, \boldsymbol{\alpha}'$  with  $\boldsymbol{\alpha}_{H_j} \neq \boldsymbol{\alpha}'_{H_j}$  such that  $\mathbf{s}_j(\boldsymbol{\alpha}) \neq \mathbf{s}_j(\boldsymbol{\alpha}')$ .

This construction is possible since Assumption 1(a) on the parameter space lead to a faithful graphical model. Without loss of generality, suppose that  $S_{\kappa_j,j} = \mathcal{Y}_j$  for all  $j$ . Also, define the following (unordered) set

$$\mathcal{S}_j := \left\{ \mathbf{s}_j(\boldsymbol{\alpha}) : \boldsymbol{\alpha} \in \{0,1\}^K \right\}. \quad (\text{S.4})$$

Define  $\mathbf{N}_1$  to be a  $\kappa_1 \dots \kappa_K \times 2^K$  matrix by setting

$$\mathbf{N}_1((l_1, \dots, l_K), \boldsymbol{\alpha}) := \mathbb{P}(Y_1 \in S_{l_1,1}, \dots, Y_K \in S_{l_K,K} \mid \boldsymbol{\alpha}).$$

Here, we index the  $2^K$  columns of  $\mathbf{N}_1$  using the binary vector  $\boldsymbol{\alpha} \in \{0,1\}^K$ , and the rows by  $\xi_1 = (l_1, \dots, l_K)$ , where  $l_j \in [\kappa_j]$ . Similarly, let  $\mathbf{N}_2$  be a  $\kappa_{K+1} \dots \kappa_{2K} \times 2^K$  matrix whose  $((l_{K+1}, \dots, l_{2K}), \boldsymbol{\alpha})$ -th entry is  $\mathbb{P}(Y_{K+1} \in S_{l_{K+1},K+1}, \dots, Y_{2K} \in S_{l_{2K},2K} \mid \boldsymbol{\alpha})$ , and  $\mathbf{N}_3$  be a  $\kappa_{2k+1} \dots \kappa_J \times 2^K$  matrix whose  $((l_{2K+1}, \dots, l_J), \boldsymbol{\alpha})$ -th entry is  $\mathbb{P}(Y_{2K+1} \in S_{l_{2K+1},1}, \dots, Y_J \in S_{l_J,J} \mid \boldsymbol{\alpha})$ . Similar to  $\mathbf{N}_1$ , we index the rows of  $\mathbf{N}_2$  and  $\mathbf{N}_3$  by  $\xi_2 = (l_{K+1}, \dots, l_{2K})$  and  $\xi_3 = (l_{2K+1}, \dots, l_J)$ , respectively. For notational simplicity, let  $v_1 = \prod_{k=1}^K \kappa_k$ ,  $v_2 =$

$\prod_{k=K+1}^{2K} \kappa_k$ ,  $v_3 = \prod_{k=2K+1}^J \kappa_k$ . Note that the assumption  $S_{\kappa_j, j} = \mathcal{Y}_j$  implies forces the last row in all  $\mathbf{N}_a$ s to be  $\mathbf{1}_{2K}^\top$ .

Next, let  $\mathbf{P}_0$  be a 3-way marginal probability tensor with size  $v_1 \times v_2 \times v_3$ , defined as

$$\begin{aligned} \mathbf{P}_0(\xi_1, \xi_2, \xi_3) &= \mathbb{P}(Y_1 \in S_{l_1}, \dots, Y_J \in S_{l_J}) \\ &= \sum_{\boldsymbol{\alpha}} \pi_{\boldsymbol{\alpha}} \mathbf{N}_1((l_1, \dots, l_K), \boldsymbol{\alpha}) \mathbf{N}_2((l_{K+1}, \dots, l_{2K}), \boldsymbol{\alpha}) \mathbf{N}_3((l_{2K+1}, \dots, l_J), \boldsymbol{\alpha}). \end{aligned}$$

We introduce an additional notation for tensor products as follows. For  $a = 1, 2, 3$ , consider  $v_a \times r$  matrices  $\mathbf{M}_a$  whose  $l$ th column is indexed as  $\mathbf{m}_{a,l}$ . Also, let  $\circ$  denote the outer product between vectors. Then, we define the tensor product of  $\mathbf{M}_1, \mathbf{M}_2, \mathbf{M}_3$  as

$$[\mathbf{M}_1, \mathbf{M}_2, \mathbf{M}_3] := \sum_{l=1}^r \mathbf{m}_{1,l} \circ \mathbf{m}_{2,l} \circ \mathbf{m}_{3,l}.$$

Using this notation, we can write  $\mathbf{P}_0$  as follows:

$$\mathbf{P}_0 = [\mathbf{N}_1 \text{Diag}(\boldsymbol{\pi}), \mathbf{N}_2, \mathbf{N}_3]. \quad (\text{S.5})$$

Now, our notation is almost identical to that in the proof of Theorem 1 in [Lee and Gu \(2024\)](#). Under conditions A and B from Theorem 1, we can apply *step 3* and the first two paragraphs of *step 4* there to argue that the decomposition (S.5) is unique up to a column permutation. We summarize this in the below Lemma S.1.

**Lemma S.1** (Theorem 1 in [Lee and Gu \(2024\)](#)). *Consider the one-latent-layer saturated model, where the true parameters satisfy conditions A and B. Let  $\mathbf{P}_0$  be the 3-way marginal probability tensor under these parameters. Then, the tensor decomposition  $\mathbf{P}_0 = [\mathbf{M}_1, \mathbf{M}_2, \mathbf{M}_3]$  is unique up to a common column permutation. Here,  $\mathbf{M}_a$ s are  $v_a \times 2^K$  matrices, whose last rows are the all-one vector  $\mathbf{1}_{2K}^\top$  for  $a = 2, 3$ . Additionally, assuming that the graphical matrix  $\mathbf{G}$  is known, the model parameters  $(\boldsymbol{\Theta}, \mathbf{G})$  are identifiable up to sign-flipping.*

### S.1.3.2 Proof of Proposition 1

The following Lemma will be crucially utilized to identify and recover  $\tilde{\mathbf{G}}$ . We present its proof after proving the main Proposition.

**Lemma S.2.** *Suppose that the parameters  $(\mathbf{B}, \mathbf{G})$  satisfy part (a) in Assumption 1. For any  $j$ , define  $H_j, \mathcal{S}_j, \mathbf{s}_j(\boldsymbol{\alpha})$  as above.*

(a)  $|H_j|$  and  $|\mathcal{S}_j|$  satisfies:

- $|H_j| = 0$  if and only if  $|\mathcal{S}_j| = 1$
- $|H_j| = 1$  if and only if  $|\mathcal{S}_j| = 2$
- $|H_j| \geq 2$  if and only if  $|\mathcal{S}_j| \geq 3$ .

(b)  $\left\{ \mathbf{s}_j(\boldsymbol{\alpha}) : \alpha_k = 1 \right\} = \left\{ \mathbf{s}_j(\boldsymbol{\alpha}) : \alpha_k = 0 \right\}$  if and only if  $g_{j,k} = 0$ .

*Proof of Proposition 1.* Our proof builds upon Lemma S.1, which proved a more general notion of nonparametric identifiability of the one-layer model, but under a given graphical matrix  $\mathbf{G}$ . The cited Theorem 1 proves that the continuous parameters are identifiable up to sign flipping, given  $\mathbf{G}$ . In our setting, Assumption 1(c) resolves the sign flipping issue and the continuous parameters can be uniquely determined. Consequently, it suffices to show that  $\mathbf{G}$  is identifiable up to the equivalence relation  $\underset{K^{(1)}}{\sim}$ . We separate this proof into two steps.

*Step 1: Tensor decomposition and setup.* Consider a one-latent-layer saturated model with true parameters  $(\boldsymbol{\Theta}, \mathbf{G})$  that satisfies conditions A, B. Suppose there exists an alternative set of parameters  $(\tilde{\boldsymbol{\Theta}}, \tilde{\mathbf{G}})$  that define a same marginal distribution of  $\mathbf{Y}$ . Define the notation  $\tilde{\mathbb{P}}_{j, \tilde{\boldsymbol{\alpha}}}$  similar as  $\mathbb{P}_{j, \boldsymbol{\alpha}}$  in (S.3), and also define  $\tilde{\mathbf{N}}_1, \tilde{\mathbf{N}}_2, \tilde{\mathbf{N}}_3$  as the conditional probability matrices that specify the value of

$$\mathbb{P}((Y_1, \dots, Y_K) \mid \mathbf{A} = \tilde{\boldsymbol{\alpha}}), \quad \mathbb{P}((Y_{K+1}, \dots, Y_{2K}) \mid \mathbf{A} = \tilde{\boldsymbol{\alpha}}), \quad \mathbb{P}((Y_{2K+1}, \dots, Y_J) \mid \mathbf{A} = \tilde{\boldsymbol{\alpha}})$$

under the alternative parameters. Here, each column of  $\tilde{\mathbf{N}}_a$  is denoted by  $\tilde{\boldsymbol{\alpha}} \in \{0, 1\}^K$ , and the last row of each  $\tilde{\mathbf{N}}_a$  is the all-one vector  $\mathbf{1}_{2^K}^\top$ . Then, the marginal probability tensor  $\mathbf{P}_0$  defined in (S.5) can be written as

$$\mathbf{P}_0 = [\mathbf{N}_1 \text{diag}(\boldsymbol{\pi}), \mathbf{N}_2, \mathbf{N}_3] = [\tilde{\mathbf{N}}_1 \text{diag}(\tilde{\boldsymbol{\pi}}), \tilde{\mathbf{N}}_2, \tilde{\mathbf{N}}_3]. \quad (\text{S.6})$$

By applying Lemma S.1, the tensor decomposition in (S.6) is unique, so  $\tilde{\mathbf{N}}_1 \text{diag}(\boldsymbol{\pi}), \tilde{\mathbf{N}}_2, \tilde{\mathbf{N}}_3$  and  $\mathbf{N}_1 \text{diag}(\boldsymbol{\pi}), \mathbf{N}_2, \mathbf{N}_3$  are identical up to a common column permutation, say  $\mathfrak{S} \in S_{\{0,1\}^K}$ . In particular, as the last row of  $\tilde{\mathbf{N}}_1 \text{diag}(\tilde{\boldsymbol{\pi}})$  and  $\mathbf{N}_1 \text{diag}(\boldsymbol{\pi})$  is exactly  $\tilde{\boldsymbol{\pi}}^\top$  and  $\boldsymbol{\pi}^\top$ ,  $(\tilde{\boldsymbol{\pi}}, \tilde{\mathbf{N}}_1)$  and  $(\boldsymbol{\pi}, \mathbf{N}_1)$  are also identical up to the same permutation  $\mathfrak{S}$ .

We use this observation to prove that  $\tilde{\mathbf{G}}$  is equivalent to  $\mathbf{G}$  under  $\underset{K^{(1)}}{\sim}$ . One subtlety for identifying  $\mathbf{G}$  is that there is no information about the  $2^K$  column indices of  $\tilde{\mathbf{N}}_1, \tilde{\mathbf{N}}_2, \tilde{\mathbf{N}}_3$ , so we cannot read off the conditional dependence structure directly. We tackle this problem based on the key observation that the unordered set  $\mathcal{S}_j$  (defined in (S.4)) can be written as

$$\begin{aligned} \mathcal{S}_j &= \left\{ (\mathbb{P}_{j,\boldsymbol{\alpha}}(S_{1,j}), \dots, \mathbb{P}_{j,\boldsymbol{\alpha}}(S_{\kappa_j,j})) : \boldsymbol{\alpha} \in \{0, 1\}^K \right\} & (\text{S.7}) \\ &= \left\{ (\mathbf{N}_{a_j}((\kappa_1, \dots, \kappa_{j-1}, 1, \kappa_{j+1}, \dots, \kappa_J), \boldsymbol{\alpha}), \dots, \mathbf{N}_{a_j}((\kappa_1, \dots, \kappa_{j-1}, \kappa_j, \kappa_{j+1}, \dots, \kappa_J), \boldsymbol{\alpha})) : \boldsymbol{\alpha} \right\} \\ &= \left\{ (\tilde{\mathbf{N}}_{a_j}((\kappa_1, \dots, \kappa_{j-1}, 1, \kappa_{j+1}, \dots, \kappa_J), \tilde{\boldsymbol{\alpha}}), \dots, \tilde{\mathbf{N}}_{a_j}((\kappa_1, \dots, \kappa_{j-1}, \kappa_j, \kappa_{j+1}, \dots, \kappa_J), \tilde{\boldsymbol{\alpha}})) : \tilde{\boldsymbol{\alpha}} \right\} \\ &= \left\{ (\tilde{\mathbb{P}}_{j,\tilde{\boldsymbol{\alpha}}}(S_{1,j}), \dots, \tilde{\mathbb{P}}_{j,\tilde{\boldsymbol{\alpha}}}(S_{\kappa_j,j})) : \tilde{\boldsymbol{\alpha}} \right\}, & (\text{S.8}) \end{aligned}$$

and provides enough information about  $\tilde{\mathbf{g}}_j$ . Here, the index  $a_j = 1, 2, 3$  can be understood from the context, for example  $a_j = 1$  when  $j \leq K$ ,  $a_j = 2$  when  $K < j \leq 2K$ .

*Step 2: Proving the equivalence by constructing a column permutation.* Now, we show that there exists a permutation  $\sigma \in S_{[K]}$  such that  $\tilde{g}_{j,k} = g_{j,\sigma(k)}$  for all  $j \in [J], k \in [K]$ . We first construct such a permutation  $\sigma$  by observing  $\mathcal{S}_1, \dots, \mathcal{S}_K$ . For  $k \in [K]$ , (S.7) implies  $|\mathcal{S}_k| = 2$ , and part (a) of Lemma S.2 constraints  $\tilde{\mathbf{g}}_k$  to be a standard basis vector. Hence, we can define  $\sigma(k)$  such that  $\tilde{\mathbf{g}}_k = \mathbf{e}_{\sigma(k)}$ . To see that  $\sigma$  is indeed a permutation, we have to show that  $\sigma(k) \neq \sigma(l)$  for  $k \neq l$ . But this is immediate by noting that the cardinality of the pmf

vector of  $\{\mathbb{P}(Y_k \in S_{1,k}, Y_l \in S_{1,l} \mid \mathbf{A} = \boldsymbol{\alpha}) : \boldsymbol{\alpha}\}$  is 2 if and only if  $k = l$ . For future purposes, let us partition the  $2^K$  row indices  $\tilde{\boldsymbol{\alpha}}$  in (S.8) into two groups  $T_k$  and  $T_k^c$  based on the value of  $(\tilde{\mathbb{P}}_{j,\tilde{\boldsymbol{\alpha}}}(S_{1,j}), \dots, \tilde{\mathbb{P}}_{j,\tilde{\boldsymbol{\alpha}}}(S_{\kappa_j,j}))$ . Then, the columns of  $\tilde{\mathbf{N}}$  that correspond to the  $\tilde{\boldsymbol{\alpha}} \in T_k$  must be identical to the columns of  $\mathbf{N}$  indexed by  $\boldsymbol{\alpha}$ s such that  $\alpha_{\sigma(k)} = 0$  (or 1).

Now, for each  $j > K$  and  $k \in [K]$ , we show that  $\tilde{g}_{j,k} = g_{j,\sigma(k)}$  and complete the proof. By part (b) of Lemma S.2, we have  $\tilde{g}_{j,k} = 0$  if and only if

$$\{(\tilde{\mathbb{P}}_{j,\tilde{\boldsymbol{\alpha}}}(S_{1,j}), \dots, \tilde{\mathbb{P}}_{j,\tilde{\boldsymbol{\alpha}}}(S_{\kappa_j,j})) : \tilde{\boldsymbol{\alpha}} \in T_k\} = \{(\tilde{\mathbb{P}}_{j,\tilde{\boldsymbol{\alpha}}}(S_{1,j}), \dots, \tilde{\mathbb{P}}_{j,\tilde{\boldsymbol{\alpha}}}(S_{\kappa_j,j})) : \tilde{\boldsymbol{\alpha}} \notin T_k\}. \quad (\text{S.9})$$

For notational simplicity, let  $\boldsymbol{\alpha}_\sigma := (\alpha_{\sigma(1)}, \dots, \alpha_{\sigma(k)})$ . Then, by the construction of  $T_k$ , (S.9) simplifies to

$$\{(\mathbb{P}_{j,\boldsymbol{\alpha}_\sigma}(S_{1,j}), \dots, \mathbb{P}_{j,\boldsymbol{\alpha}_\sigma}(S_{\kappa_j,j})) : \alpha_{\sigma(k)} = 1\} = \{(\mathbb{P}_{j,\boldsymbol{\alpha}_\sigma}(S_{1,j}), \dots, \mathbb{P}_{j,\boldsymbol{\alpha}_\sigma}(S_{\kappa_j,j})) : \alpha_{\sigma(k)} = 0\}.$$

Another application of part (b) of Lemma S.2 shows that this is equivalent to  $g_{j,\sigma(k)} = 0$ . Hence,  $\tilde{g}_{j,k} = g_{j,\sigma(k)}$  and the proof is complete.  $\square$

Below, we provide a short proof of Lemma S.2.

*Proof of Lemma S.2.* (a) The proof is immediate from the faithfulness of the graphical matrix  $\mathbf{G}$ . For example, the third bullet point follows from noting that  $|H_j| \geq 2$  implies  $|\{\sum_{k \in H_j} \beta_{j,k} \alpha_k : \boldsymbol{\alpha}\}| \geq 3$ , and that  $|\{\sum_{k \in H_j} \beta_{j,k} \alpha_k : \boldsymbol{\alpha}\}| \leq 2$  implies  $|H_j| \leq 1$ .

(b) The “if” part immediately follows by conditional independence. For the “only if” part, by considering the contrapositive statement, it suffices to show that  $g_{j,k} = 1$  implies

$$\{\mathbf{s}_j(\boldsymbol{\alpha}) : \alpha_k = 1\} \neq \{\mathbf{s}_j(\boldsymbol{\alpha}) : \alpha_k = 0\}.$$

By writing out the parametrization and using the identifiability of the parametric family in (4), it suffices to show that  $\{\sum_{l \neq k} \beta_{j,l} \alpha_l + \beta_{j,k}\} \neq \{\sum_{l \neq k} \beta_{j,l} \alpha_l\}$ . But this is immediate since  $\beta_{j,k} \neq 0$ .

$\square$

### S.1.3.3 Proof of Proposition 2

For the sake of notational simplicity, for a given coefficient matrix  $\mathbf{B}$ , define

$$\eta_{j,\boldsymbol{\alpha}} := \beta_{j,0} + \sum_{k=1}^K \beta_{j,k} \alpha_k \quad (\text{S.10})$$

for each  $j$  and  $\boldsymbol{\alpha} \in \{0, 1\}^K$ . For an alternative coefficient matrix  $\tilde{\mathbf{B}}$ , we similarly define

$$\tilde{\eta}_{j,\tilde{\boldsymbol{\alpha}}} := \tilde{\beta}_{j,0} + \sum_{k=1}^K \tilde{\beta}_{j,k} \tilde{\alpha}_k$$

for  $\tilde{\boldsymbol{\alpha}} \in \{0, 1\}^K$ .

Before presenting the proof of Proposition 2, we state two lemmas whose proof is postponed to the end of the subsection. Our first lemma is a relaxation of Lemma S.1, and guarantees an *almost sure* unique tensor decomposition of  $\mathbf{P}_0$ . Recall the definition of  $\mathbf{P}_0$  from (S.5).

**Lemma S.3** (Modification of Theorem 2 in Lee and Gu (2024)). *Consider the one-latent-layer saturated model with a true graphical matrix  $\mathbf{G}^{(1)\star}$  that satisfies condition C, and analytic parametric families  $p(\cdot; \eta, \gamma)$  and link functions  $g_j$ . Then, the rank  $2^K$  tensor decomposition  $\mathbf{P}_0 = [\mathbf{M}_1, \mathbf{M}_2, \mathbf{M}_3]$  is unique up to column permutations for  $\Omega_K(\boldsymbol{\Theta}^{(1)}; \mathbf{G}^{(1)\star}) \setminus \mathcal{N}_1$ . Here,  $\mathbf{M}_a$ s are  $v_a \times 2^K$  matrices, whose last rows are the all-one vector  $\mathbf{1}_{2^K}^\top$  for  $a = 2, 3$ . The set  $\mathcal{N}_1$  is a measure-zero subset of  $\Omega_K(\boldsymbol{\Theta}^{(1)}; \mathbf{G}^{(1)\star})$  that only imposes restrictions on  $\mathbf{B}, \gamma$  and not on the mixture proportion parameters  $\boldsymbol{\pi}$ .*

Our next lemma provides additional structure regarding the  $2^K$  column indices in the tensor decomposition in Lemma S.3. This is a nontrivial problem as we wish to identify the parameters up to a label switching of  $K$  binary latent variables. Here, to formally state the label switching, recall the notation of  $\sim_K$  Definition S.2 and write  $\mathbf{B} \sim_K \tilde{\mathbf{B}}, \mathbf{G} \sim_K \tilde{\mathbf{G}}, \boldsymbol{\alpha} \sim_K \tilde{\boldsymbol{\alpha}}$  when there exists a permutation  $\sigma \in S_{[K]}$  such that  $\beta_{j,l} = \tilde{\beta}_{j,\sigma(l)}, g_{j,l} = \tilde{g}_{j,\sigma(l)}$ , and  $\boldsymbol{\alpha} = (\tilde{\alpha}_{\sigma(1)}, \dots, \tilde{\alpha}_{\sigma(K)})$ .

**Lemma S.4.** *Suppose that there exist two sets of parameters  $(\mathbf{B}, \mathbf{G})$ ,  $(\tilde{\mathbf{B}}, \tilde{\mathbf{G}})$  that satisfies Assumption 1 and defines an identical  $\eta_{j,\alpha}$  in the following sense: there exists a permutation  $\mathfrak{S} \in S_{\{0,1\}^K}$  such that*

$$\eta_{j,\alpha} = \tilde{\eta}_{j,\mathfrak{S}(\alpha)}, \quad (\text{S.11})$$

for all  $j$ ,  $\alpha$ . Then, we have  $(\mathbf{B}, \mathbf{G}, \alpha) \sim_K (\tilde{\mathbf{B}}, \tilde{\mathbf{G}}, \mathfrak{S}(\alpha))$  for “generic” parameters  $\mathbf{B} \notin \Omega(\mathbf{B}; \mathbf{G}) \setminus \mathcal{N}_2$ , where  $\mathcal{N}_2$  is a measure-zero subset of  $\Omega(\mathbf{B}; \mathbf{G})$ .

*Proof of Proposition 2.* We work under the same notations introduced at the beginning of the section. We make one additional assumption regarding the finite subsets  $\mathcal{D}_j := (S_{1,j}, \dots, S_{\kappa_j,j})$  of the sample space  $\mathcal{Y}_j$  as follows. We assume that  $\mathcal{D}_j \subset \mathcal{C}_j$ , where  $\mathcal{C}_j$  is a countable separating class whose values determine probability measure on  $\mathcal{Y}_j$ . The existence of such a separating class is a consequence of  $\mathcal{Y}_j$  being a separating metric space; see Step 1 in the proof of Theorem 1 in Lee and Gu (2024) for a proof.

Suppose that  $\mathbf{G}$  satisfy condition C,  $\Theta \in \Omega_{\mathcal{K}}(\Theta; \mathbf{G})$ , and that there exists an alternate parameter  $\tilde{\Theta}, \tilde{\mathbf{G}}$  that defines the same marginal likelihood. Here, we are dropping all superscripts in  $\mathbf{G} = \mathbf{G}^{(1)*}$  for simplicity. We show that  $(\Theta, \mathbf{G}) \sim_{\mathcal{K}} (\tilde{\Theta}, \tilde{\mathbf{G}})$  for  $\Theta \in \Omega_{\mathcal{K}}(\Theta; \mathbf{G}) \setminus (\mathcal{N}_1 \cup \mathcal{N}_2)$ , where  $\mathcal{N}_1, \mathcal{N}_2$  are measure-zero sets that will be defined later. Recall that for  $a = 1, 2, 3$ ,  $\mathbf{N}_a$  are the  $v_a \times 2^K$  conditional probability matrices that describe  $\mathbf{Y} \mid (\mathbf{A} = \alpha)$  under the true parameters  $\Theta, \mathbf{G}$ . Similarly, define  $\tilde{\mathbf{N}}_a$  as the corresponding matrices under the alternative parameters  $\tilde{\Theta}, \tilde{\mathbf{G}}$ . Similar to the proof of Proposition 1, we start from the rank  $2^K$  decomposition of the marginal probability tensor in (S.5). By applying Lemma S.3, the decomposition

$$\mathbf{P}_0 = [\mathbf{N}_1 \text{diag}(\boldsymbol{\pi}), \mathbf{N}_2, \mathbf{N}_3] = [\tilde{\mathbf{N}}_1 \text{diag}(\tilde{\boldsymbol{\pi}}), \tilde{\mathbf{N}}_2, \tilde{\mathbf{N}}_3] \quad (\text{S.12})$$

is unique up to (the  $2^K$ ) column permutations, for true parameters  $\Theta \in \Omega_{\mathcal{K}}(\Theta; \mathbf{G}) \setminus \mathcal{N}_1$ . Here,  $\mathcal{N}_1$  is a measure-zero subset of  $\Omega_{\mathcal{K}}(\Theta; \mathbf{G})$  that is defined in Lemma S.3. This implies



that  $(\boldsymbol{\pi}, \mathbf{N}_1, \mathbf{N}_2, \mathbf{N}_3)$  and  $(\tilde{\boldsymbol{\pi}}, \tilde{\mathbf{N}}_1, \tilde{\mathbf{N}}_2, \tilde{\mathbf{N}}_3)$  are identical up to a common column permutation  $\mathfrak{S} \in S_{\{0,1\}^K}$ . In other words, for any  $\boldsymbol{\alpha} \in \{0,1\}^K$ , the  $\boldsymbol{\alpha}$ th column in  $\mathbf{N}_a$  is identical to the  $\mathfrak{S}(\boldsymbol{\alpha})$ th column of  $\tilde{\mathbf{N}}_a$  and  $\pi_{\boldsymbol{\alpha}} = \tilde{\pi}_{\mathfrak{S}(\boldsymbol{\alpha})}$ .

By considering the row of  $\mathbf{N}_a$  that corresponds to the set  $S_{l_j,j}$ , we have

$$\begin{aligned} \mathbb{P}_{j,\boldsymbol{\alpha}}(S_{l_j,j}) &= \mathbf{N}_a(\kappa_{\cdot}, \dots, \kappa_{j-1}, l_j, \kappa_{j+1}, \dots, \kappa_{\cdot}, \boldsymbol{\alpha}) \\ &= \tilde{\mathbf{N}}_a(\kappa_{\cdot}, \dots, \kappa_{j-1}, l_j, \kappa_{j+1}, \dots, \kappa_{\cdot}, \mathfrak{S}(\boldsymbol{\alpha})) = \tilde{\mathbb{P}}_{j,\mathfrak{S}(\boldsymbol{\alpha})}(S_{l_j,j}) \end{aligned} \quad (\text{S.13})$$

for all  $j, l_j \in [\kappa_j]$ , and  $\boldsymbol{\alpha}$ . Furthermore, note that this identity holds for any finite subset  $\mathcal{D}_j$  of  $\mathcal{C}_j$ , as the column indices of  $\tilde{\mathbf{N}}_a$  are determined by the alternative model and do not depend on the discretization  $\mathcal{D}_j$ . Hence, (S.13) holds for all  $S_{l_j,j} \in \mathcal{C}_j$ . Since  $\mathcal{C}_j$  is a separating class, we have  $\mathbb{P}_{j,\boldsymbol{\alpha}} = \tilde{\mathbb{P}}_{j,\mathfrak{S}(\boldsymbol{\alpha})}$ . Recalling that  $\mathbb{P}_{j,\boldsymbol{\alpha}} = \text{ParFam}_j(\eta_{j,\boldsymbol{\alpha}}, \gamma_j)$  for some identifiable parametric family (see (S.3)), we must have  $\eta_{j,\boldsymbol{\alpha}} = \tilde{\eta}_{j,\mathfrak{S}(\boldsymbol{\alpha})}$  and  $\gamma_j = \tilde{\gamma}_j$  for all  $j, \boldsymbol{\alpha}$ .

Now, additionally assuming that  $\boldsymbol{\Theta} \notin \mathcal{N}_2$ , we can apply Lemma S.4. Here,  $\mathcal{N}_2$  is the null set defined in Lemma S.4. Then, we have  $(\mathbf{B}, \mathbf{G}) \sim_K (\tilde{\mathbf{B}}, \tilde{\mathbf{G}})$ . Also, because  $\boldsymbol{\alpha} \sim_K \mathfrak{S}(\boldsymbol{\alpha})$ ,  $\tilde{\pi}_{\mathfrak{S}(\boldsymbol{\alpha})} = \pi_{\boldsymbol{\alpha}}$  implies  $\tilde{\boldsymbol{\pi}} \sim_K \boldsymbol{\pi}$  and the proof is complete.  $\square$

We finally present the postponed proof of Lemmas S.3 and S.4. While the main proof idea of Lemma S.3 is similar to that of Theorem 2 in Lee and Gu (2024), we provide a detailed proof for the sake of completeness.

*Proof of Lemma S.3.* For a matrix  $\mathbf{N}$ , let  $rk_k(\mathbf{N})$  be the Kruskal column-rank of  $\mathbf{N}$ , that is, the largest integer  $r$  such that any  $r$  columns of  $\mathbf{N}$  are linearly independent. We claim that it suffices to show that

$$rk_k(\mathbf{N}_1) = 2^K, \quad rk_k(\mathbf{N}_2) = 2^K, \quad rk_k(\mathbf{N}_3) \geq 2$$

for generic parameters in  $\Omega(\boldsymbol{\Theta}; \mathbf{G}) \setminus \mathcal{N}$ . Assuming this, one can apply Kruskal's Theorem (Kruskal, 1977), which guarantees the uniqueness of the three-way tensor decomposition of  $\mathbf{P}_0$  up to a universal column permutation and gives the desired result. Along the way, we

show that the candidate set of non-identifiable parameters,  $\mathcal{N}$ , only imposes restrictions on  $\mathbf{B}$  and  $\boldsymbol{\gamma}$  but not on  $\boldsymbol{\pi}$ .

For the remainder of the proof, let  $\boldsymbol{\beta}_{I_1, I_2}$  denote the sub-matrix of the  $J \times (K + 1)$  coefficient matrix  $\boldsymbol{\beta}$  whose rows and columns are indexed by  $I_1$  and  $I_2$ , respectively. Similarly,  $\boldsymbol{\gamma}_{I_1}$  denotes the sub-vector of  $\boldsymbol{\gamma}$  by collecting the entries indexed by  $I_1$ .

**Proof of  $rk_k(\mathbf{N}_1) = 2^K$ .** First, write the parameter space

$$\Omega(\boldsymbol{\beta}_{1:K, 0:K}, \boldsymbol{\gamma}_{1:K}; \mathbf{G}_1) = \{\boldsymbol{\beta}_{1:K, 0:K}, \boldsymbol{\gamma}_{1:K} : \beta_{j,k} \neq 0 \text{ for } g_{j,k} = 1\}$$

as a finite union of open, connected subsets of Euclidean space  $\mathbb{R}^{\sum_{j,k \leq K} g_{j,k}} \times \mathbb{R}^K$ . Without loss of generality, let

$$\Omega_{\text{positive}}(\boldsymbol{\beta}_{1:K, 0:K}, \boldsymbol{\gamma}_{1:K}; \mathbf{G}_1) := \{\boldsymbol{\beta}_{1:K, 0:K}, \boldsymbol{\gamma}_{1:K} : \beta_{j,k} > 0 \text{ for } g_{j,k} = 1\}$$

be our domain. Here, we consider  $\mathbf{N}_1 = \mathbf{N}_1(\boldsymbol{\beta}_{1:K, 0:K}, \boldsymbol{\gamma}_{1:K})$  to be a matrix-valued function of  $(\boldsymbol{\beta}_{1:K, 0:K}, \boldsymbol{\gamma}_{1:K})$ . Because  $\mathbf{N}_1$  has full column rank if and only if  $\det(\mathbf{N}_1^\top \mathbf{N}_1) \neq 0$ , it suffices to show that

$$\{\boldsymbol{\beta}_{1:K, 0:K} \in \Omega_{\text{positive}}(\boldsymbol{\beta}_{1:K, 0:K}, \boldsymbol{\gamma}_{1:K}; \mathbf{G}_1) : \det(\mathbf{N}_1^\top \mathbf{N}_1) = 0\}$$

is a measure-zero set in  $\Omega(\boldsymbol{\beta}_{1:K, 0:K}, \boldsymbol{\gamma}_{1:K}; \mathbf{G}_1)$ . Note that the following argument also holds for other connected sub-domains of  $\Omega(\boldsymbol{\beta}_{1:K, 0:K}, \boldsymbol{\gamma}_{1:K}; \mathbf{G}_1)$ , and the union of a finite number of measure-zero sets are still measure-zero.

In particular, when  $\mathbf{G}_1 = \mathbf{I}_K$ , the proof of Theorem 1 in [Lee and Gu \(2024\)](#) showed that  $\mathbf{N}_1(\boldsymbol{\beta}_{1:K, 0:K}, \boldsymbol{\gamma}_{1:K})$  always have full column rank. We use technical real analysis arguments to claim that this statement can be generalized to an arbitrary  $\mathbf{G}_1$  that satisfies  $\text{diag}(\mathbf{G}_1) = \mathbf{I}_K$ . Consider the mapping

$$(\det(\mathbf{N}_1^\top \mathbf{N}_1))(\boldsymbol{\beta}_{1:K, 0:K}, \boldsymbol{\gamma}_{1:K}) : \Omega(\boldsymbol{\beta}_{1:K, 0:K}, \boldsymbol{\gamma}_{1:K}; \mathbf{G}_1) \rightarrow \mathbb{R}. \quad (\text{S.14})$$

Observe that  $\det(\mathbf{N}_1^\top \mathbf{N}_1)$  defined in (S.14) is a polynomial of entries of  $\mathbf{N}_1$ . Each entry in

$\mathbf{N}_1$  can be written in the form of

$$\mathbf{N}_1((l_1, \dots, l_K), \boldsymbol{\alpha}) = \prod_{j=1}^K \int_{S_{l_j, j}} p_j(y_j; g_j(\beta_{j,0} + \sum_k \beta_{j,k} \alpha_k), \gamma_j) m(dy_j).$$

Since we assume that the density  $p_j$  and link function  $g_j$  are analytic, each entry of  $\mathbf{N}_1$  is analytic. Consequently,  $\det(\mathbf{N}_1^\top \mathbf{N}_1)$  is also analytic.

Next, note that  $\det(\mathbf{N}_1^\top \mathbf{N}_1)$  cannot be identically zero, in other words, there exists  $(\boldsymbol{\beta}_{1:K,0:K}^*, \boldsymbol{\gamma}_{1:K}^*)$  such that  $\det(\mathbf{N}_1^\top \mathbf{N}_1)(\boldsymbol{\beta}_{1:K,0:K}^*, \boldsymbol{\gamma}_{1:K}^*) \neq 0$ . This is because one can make small perturbations from a parameter value in  $\Omega(\boldsymbol{\beta}_{1:K,0:K}, \boldsymbol{\gamma}_{1:K}; \mathbf{I}_K)$  by setting  $\beta_{j,k} = \epsilon$  for indices with  $g_{j,k} = 1$  without making the determinant become zero. Hence, by the following technical Lemma, we conclude that

$$\{\boldsymbol{\beta}_{1:K,0:K}, \boldsymbol{\gamma}_{1:K} \in \Omega(\boldsymbol{\beta}_{1:K,0:K}, \boldsymbol{\gamma}_{1:K}; \mathbf{G}_1) : (\det(\mathbf{N}_1^\top \mathbf{N}_1))(\boldsymbol{\beta}_{1:K,0:K}, \boldsymbol{\gamma}_{1:K}) = 0\}$$

is a null set in  $\Omega(\boldsymbol{\beta}_{1:K,0:K}, \boldsymbol{\gamma}_{1:K}, \mathbf{G}_1)$ . The conclusion  $rk_k(\mathbf{N}_2) = 2^K$  automatically follows.

**Lemma S.5** (Mityagin (2020)). *Let  $f : \Omega \rightarrow \mathbb{R}$  be a real analytic function defined on an open, connected domain  $\Omega \in \mathbb{R}^d$  that is not identically zero. Then,  $\{\omega \in \Omega : f(\omega) = 0\}$  is a measure-zero set in  $\Omega$ .*

**Proof of  $rk_k(\mathbf{N}_3) \geq 2$ .** Theorem 1 in Lee and Gu (2024) showed that  $rk_k(\mathbf{N}_3) \geq 2$  under condition B. Hence, it suffices to show that condition B holds for generic parameters in  $\Omega(\boldsymbol{\beta}_{2K+1:J,1:K}; \mathbf{G}_3)$ . Fix any  $\boldsymbol{\alpha} \neq \boldsymbol{\alpha}'$ , and let  $l = l(\boldsymbol{\alpha}, \boldsymbol{\alpha}')$  be an index among  $[K]$  such that  $\alpha_l \neq \alpha'_l$ . Since we assume that all columns of  $\mathbf{G}_3$  are nonzero, there exists  $j = j(\boldsymbol{\alpha}, \boldsymbol{\alpha}') > 2K$  such that  $g_{j,l} = 1$ . As  $\beta_{j,l}(\alpha_l - \alpha'_l) \neq 0$ ,

$$\{\boldsymbol{\beta}_{j,1:K} \in \Omega(\boldsymbol{\beta}_{j,1:K}; \mathbf{g}_j) : \sum_{k=1}^K \beta_{j,k} g_{j,k}(\alpha_k - \alpha'_k) = 0\}$$

is a measure-zero set in  $\Omega(\boldsymbol{\beta}_{j,1:K}; \mathbf{g}_j)$ . Consequently,

$$\Phi_{\boldsymbol{\alpha}, \boldsymbol{\alpha}'} := \{\boldsymbol{\beta}_{2K+1:J,1:K} \in \Omega(\boldsymbol{\beta}_{2K+1:J,1:K}; \mathbf{G}_3) : \sum_{k=1}^K \beta_{j,k} g_{j(\boldsymbol{\alpha}, \boldsymbol{\alpha}'), k}(\alpha_k - \alpha'_k) = 0\}$$

is a measure-zero set in  $\Omega(\beta_{2K+1:J,1:K}; \mathbf{G}_3)$ . The proof is complete by taking a union over all  $\alpha \neq \alpha'$ .  $\square$

*Proof of Lemma S.4.* We first assume that the true parameter  $\mathbf{B}$  belongs in the coefficient space

$$\Omega^g(\mathbf{B}; \mathbf{G}) := \{\mathbf{B} : \text{for each } j, \text{ all elements of the form } \sum_{k \in H_j} \beta_{j,k} a_k, a_k = 0, 1, \text{ are distinct}\}.$$

It is clear that the complement  $\Omega(\mathbf{B}; \mathbf{G}) \setminus \Omega^g(\mathbf{B}; \mathbf{G})$  can be spelled out as a finite union of lower dimensional subspaces, and has measure-zero with respect to  $\Omega(\mathbf{B}; \mathbf{G})$ . The following proof is somewhat technical, but the main idea is to show that one can entirely recover  $\mathbf{B}, \mathbf{G}, \mathfrak{S}$  up to label switching, based on the *values* of  $\eta_{j,\alpha}$  while *not using the indices*  $\alpha$ . Steps 1 and 2 characterizes the coefficients  $\mathbf{B}$  based on the values  $\{\eta_{j,\alpha}\}_\alpha$ , which allows us to prove equivalence of  $\mathbf{B}, \mathbf{G}$  and  $\tilde{\mathbf{B}}, \tilde{\mathbf{G}}$  in step 3.

**Step 1: recovering  $|H_j|$  and  $|\mathbf{B}|$ .** We first claim that for each  $j$ , there uniquely exists an integer  $I_j$ , coefficients  $c_{j,0}, c_{j,1} > \dots > c_{j,I_j} > 0$  that satisfy

$$\eta_{j,\alpha} = \beta_{j,0} + \sum_{l \in H_j} \beta_{j,l} \alpha_l = c_{j,0} + \sum_{k \leq I_j} c_{j,k} (\mathfrak{T}_j(\alpha))_k \quad (\text{S.15})$$

for all  $\alpha$  and some permutation  $\mathfrak{T}_j \in S_{\{0,1\}^\kappa}$ . Here, we also prove that that  $I_j = |H_j|$ .

The *existence* directly follows as we can take  $I_j = |H_j|$  and define  $\{c_{j,k} : k \leq I_j\}$  to be the coefficients  $\{|\beta_{j,l}| : l \in H_j\}$  in decreasing order. Then, for each  $k \leq I_j$ , there must be an  $l_k \in H_j$  such that  $c_{j,k} = |\beta_{j,l_k}| > 0$ . Consequently, we can construct the permutation  $\mathfrak{T}_j$  by setting

$$(\mathfrak{T}_j(\alpha))_k := \begin{cases} \alpha_{l_k} & \text{if } \beta_{j,l_k} > 0 \\ 1 - \alpha_{l_k} & \text{if } \beta_{j,l_k} < 0, \end{cases}$$

for  $k \leq I_j$  and arbitrarily defining the remaining coordinates. By plugging in these defini-

tions, we get

$$\begin{aligned} \sum_{k \leq I_j} c_{j,k} (\mathfrak{T}_j(\boldsymbol{\alpha}))_k &= \sum_{l \in H_j} \text{sgn}(\beta_{j,l}) |\beta_{j,l}| \alpha_l + \sum_{l \in H_j, \beta_{j,l} < 0} |\beta_{j,l}| \\ &= \sum_{l \in H_j} \beta_{j,l} \alpha_l - \sum_{l \in H_j, \beta_{j,l} < 0} \beta_{j,l}. \end{aligned}$$

Hence, (S.15) holds for  $c_{j,0} := \beta_{j,0} + \sum_{l \in H_j, \beta_{j,l} < 0} \beta_{j,l}$ .

For *uniqueness*, we provide an inductive characterization of the  $c_{j,k}$ s based on the values  $U_j := \{\eta_{j,\boldsymbol{\alpha}} : \boldsymbol{\alpha} \in \{0,1\}^K\}$ . First,  $c_{j,0}$  must be the minimum of the set  $U_j$ . Next, we define  $c_{j,I_j}$  by noting that  $c_{j,0} + c_{j,I_j}$  should be the smallest element in  $\{\eta_{j,\boldsymbol{\alpha}} : \eta_{j,\boldsymbol{\alpha}} > c_{j,0}\}$ . Inductively for each  $k < I_j$ , given  $c_{j,0}$  and  $c_{j,k+1}, \dots, c_{j,I_j}$ ,  $c_{j,0} + c_{j,k}$  must be the smallest element in  $U_j \setminus \{c_{j,0} + \sum_{l>k} c_{j,l} a_l : a_l = 0, 1\}$ . We continue the induction until the set  $U_j \setminus \{c_{j,0} + \sum_{l>k} c_{j,l} a_l : a_l = 0, 1\}$  is empty. By considering the true parameterization and the fact that  $\mathbf{B} \in \Omega^g(\mathbf{B}; \mathbf{G})$ , we have  $|U_j| = 2^{|H_j|}$ , and hence  $|H_j| = I_j$ . Additionally, this observation gives  $c_{j,1} > \dots > c_{j,|H_j|} > 0$ .

**Step 2: Recovering the indexing  $\boldsymbol{\alpha}$ .** While we have recovered the absolute values of the coefficients  $|\beta_{j,k}|$  in Step 1, they are ordered based on their absolute values. Thus, the ordering is different across different  $j$ . In this step, we fully recover  $\beta_{j,k}$  up to a column permutation  $\tau \in S_{[K]}$ , by representing each  $\beta_{j,k}$  in terms of  $\eta$  and  $c$ -values. To this end, we inductively construct sets  $T_{j,k}, V_{j,k} \subseteq [2^K]$  for all  $j \in [J]$  and  $k \leq |H_j|$ . We claim that they correspond to  $\boldsymbol{\alpha}$ s with identical  $\alpha_{\sigma_j(k)}$  values, for some injective mapping  $\sigma_j : [|H_j|] \rightarrow [K]$  (see (S.18) for a precise statement). This claim will be crucially utilized to recover the coefficients  $\beta_{j,k}$ .

First, fix  $j \in [J]$ ,  $k \leq |H_j|$ , and define  $T_{j,k}^{(1)} = \{\boldsymbol{\alpha} : \eta_{j,\boldsymbol{\alpha}} = c_{j,0}\}$  and  $V_{j,k}^{(1)} = \{\boldsymbol{\alpha} : \eta_{j,\boldsymbol{\alpha}} = c_{j,0} + c_{j,k}\}$ . Since there exists a unique index  $l_k$  such that  $|\beta_{j,l_k}| = c_{j,k} > 0$ , these two sets have distinct  $\alpha_l$  values if and only if  $l = l_k$ . Define  $\sigma_j(k)$  as this  $l_k$ . Since  $l_k \neq l_{k'}$  for  $k \neq k'$ ,  $\sigma_j$  is injective. Without the loss of generality, suppose  $\beta_{j,l_k} > 0$ . This is only for the sake of

explicitly characterizing the sets  $T_{j,k}$  and  $V_{j,k}$ , and does not affect their construction. Under this assumption,  $\boldsymbol{\alpha} \in T_{j,k}^{(1)}$  must satisfy  $\alpha_{\sigma_j(k)} = 0$ ,  $\boldsymbol{\alpha} \in V_{j,k}^{(1)}$  must satisfy  $\alpha_{\sigma_j(k)} = 1$ . Also, as the values of  $\alpha_l$  for  $l \notin H_j$  does not change the value of  $\eta_{j,\boldsymbol{\alpha}}$ , we have  $|T_{j,k}^{(1)}| = |V_{j,k}^{(1)}| = 2^{K-|H_j|}$ .

Inductively for  $t > 1$ , let

$$\mathcal{T}_{j,k}^{[t]} := \{\boldsymbol{\alpha} \notin T_{j,k}^{(t-1)}, V_{j,k}^{(t-1)} : \eta_{j,\boldsymbol{\alpha}} = \min_{\boldsymbol{\alpha}' \notin T_{j,k}^{(t-1)}, V_{j,k}^{(t-1)}} \eta_{j,\boldsymbol{\alpha}'}\}, \quad (\text{S.16})$$

$$\mathcal{V}_{j,k}^{[t]} := \{\boldsymbol{\alpha} \notin T_{j,k}^{(t-1)}, V_{j,k}^{(t-1)} : \eta_{j,\boldsymbol{\alpha}} = \min_{\boldsymbol{\alpha}' \notin T_{j,k}^{(t-1)}, V_{j,k}^{(t-1)}} \eta_{j,\boldsymbol{\alpha}'} + c_{j,k}\}, \quad (\text{S.17})$$

and define  $T_{j,k}^{[t]} = T_{j,k}^{(t-1)} \cup \mathcal{T}_{j,k}^{[t]}$  and  $V_{j,k}^{[t]} = V_{j,k}^{(t-1)} \cup \mathcal{V}_{j,k}^{[t]}$ . By the construction in (S.16) and (S.17), again because  $\beta_{j,\sigma_j(k)} > 0$ , we must have  $\alpha_{\sigma_j(k)} = 0$  for  $\boldsymbol{\alpha} \in \mathcal{T}_{j,k}^{[t]}$ , and  $\alpha_{\sigma_j(k)} = 1$  for  $\boldsymbol{\alpha} \in \mathcal{V}_{j,k}^{[t]}$ . We also have  $|\mathcal{T}_{j,k}^{[t]}| = |\mathcal{V}_{j,k}^{[t]}| = 2^{K-|H_j|}$ , which inductively gives  $|T_{j,k}^{[t]}| = |V_{j,k}^{[t]}| = 2^{K-|H_j|}t$ . We continue the construction until  $T_{j,k}^{[t]} \cup V_{j,k}^{[t]} = \{0, 1\}^K$ , that is when  $t = 2^{|H_j|-1}$ .

Finally, we define  $T_{j,k} := T_{j,k}^{(2^{|H_j|-1})}$  and  $V_{j,k} := V_{j,k}^{(2^{|H_j|-1})}$  as the final induction outputs. Then,  $\{T_{j,k}, V_{j,k}\}$  is a partition of  $\{0, 1\}^K$  with equal cardinality, where  $T_{j,k} = \{\boldsymbol{\alpha} : \alpha_{\sigma_j(k)} = 0\}$  and  $V_{j,k} = \{\boldsymbol{\alpha} : \alpha_{\sigma_j(k)} = 1\}$ . In general, without the positivity assumption  $\beta_{j,\sigma_j(k)} > 0$ , we can conclude that

$$\{T_{j,k}, V_{j,k}\} = \{\{\boldsymbol{\alpha} : \alpha_{\sigma_j(k)} = 0\}, \{\boldsymbol{\alpha} : \alpha_{\sigma_j(k)} = 1\}\}, \quad (\text{S.18})$$

as an *unordered* set. As all columns of  $\mathbf{G}$  are not empty (see Assumption 1 (b)), for each  $l$ , we must have at least one  $j$  such that  $g_{j,l} = 1$ . Hence, the set of all possible partitions  $\{\{T_{j,k}, V_{j,k}\} : j \in [J], k \in [|H_j|]\}$  must take exactly  $K$  distinct values. Let us index each element by  $\{T_l, V_l\}$  for  $l \in [K]$ , and let  $\tau \in S_{[K]}$  be a permutation such that

$$\{T_l, V_l\} = \{\{\boldsymbol{\alpha} : \alpha_{\tau(l)} = 0\}, \{\boldsymbol{\alpha} : \alpha_{\tau(l)} = 1\}\}. \quad (\text{S.19})$$

Without loss of generality, suppose that  $T_l$  and  $V_l$  are defined so that the mean of the vector  $(\eta_{j,\boldsymbol{\alpha}} : \boldsymbol{\alpha} \in T_l)$  is strictly smaller than the mean of  $(\eta_{j,\boldsymbol{\alpha}} : \boldsymbol{\alpha} \in V_l)$ . Then, the monotonicity

assumption Assumption 1(c) implies that

$$T_l = \{\boldsymbol{\alpha} : \alpha_{\tau(l)} = 0\}, \quad V_l = \{\boldsymbol{\alpha} : \alpha_{\tau(l)} = 1\}, \quad (\text{S.20})$$

and resolves the sign-flipping for the latent variable  $A_{\tau(l)}$ . Next, to recover the parameter  $\beta_{j,\tau(l)}$  for each  $j$  and  $l$ , we claim that

(a) if  $\{T_l, V_l\} \notin \{\{T_{j,k}, V_{j,k}\} : k \leq |H_j|\}$ ,  $\beta_{j,\tau(l)} = 0$ .

(b) if  $\{T_l, V_l\} = \{T_{j,k}, V_{j,k}\}$  for some  $k \leq |H_j|$ ,  $|\beta_{j,\tau(l)}| = c_{j,k}$  and

$$\text{sgn}(\beta_{j,\tau(l)}) = \begin{cases} 1 & \text{if } T_l = T_{j,k}, \\ -1 & \text{if } T_l = V_{j,k}. \end{cases}$$

Here, to show (a), suppose  $\{T_l, V_l\} \notin \{\{T_{j,k}, V_{j,k}\} : k \leq |H_j|\}$ . Then, by the characterization in (S.18) and (S.19), we must have  $\sigma_j(k) \neq \tau(l)$  for all  $k \leq |H_j|$ . Recalling that  $\sigma_j$  collects all indices such that  $|\beta_{j,\sigma_j(k)}| > 0$ , we must have  $\beta_{j,\tau(l)} = 0$ . To prove part (b), note that the assumption implies  $\sigma_j(k) = \tau(l)$ , so  $|\beta_{j,\tau(l)}| = |\beta_{j,\sigma_j(k)}| = c_{j,k}$ . The claim regarding the sign holds because  $T_{j,k}$  has a smaller average of  $\eta_{j,\cdot}$  values than  $V_{j,k}$  by construction. Thus,  $T_l = T_{j,k}$  if and only if  $\beta_{j,\tau(l)} > 0$ .

**Step 3: explicit representation of all parameters.** Finally, we prove the desired result by applying the same characterization of the parameters under the alternative values  $\tilde{\eta}_{j,\tilde{\alpha}}$ . Here, note that  $\mathbf{B} \in \Omega^g(\mathbf{B}; \mathbf{G})$  implies that  $\tilde{\mathbf{B}} \in \Omega^g(\mathbf{B}; \mathbf{G})$ . We apply steps 1-2 using  $\tilde{\eta}_{j,\tilde{\alpha}}$  instead of  $\eta_{j,\alpha}$ . Step 1 holds without any change, and we obtain the same coefficients  $c_{j,k}$ s as well as  $|H_j| = |\tilde{H}_j|$ . Next, in step 2, the definition of  $T_{j,k}, V_{j,k}$  in (S.16), (S.17) needs to be modified to be the collection of  $\tilde{\alpha}$ s instead of  $\alpha$ s. Let  $\tilde{T}_{j,k}$  and  $\tilde{V}_{j,k}$  be the corresponding sets under the alternative parametrization. As the coefficients  $c_{j,k}$  are identical,  $(T_{j,k}, V_{j,k})$  and  $(\tilde{T}_{j,k}, \tilde{V}_{j,k})$  are consistent in the sense that

$$\tilde{T}_{j,k} = \mathfrak{S}(T_{j,k}), \quad \tilde{V}_{j,k} = \mathfrak{S}(V_{j,k}). \quad (\text{S.21})$$

In other words, by viewing  $T_{j,k}$  as the collection of *indices*  $\alpha$  in  $\eta_{j,\alpha}$ ,  $\tilde{T}_{j,k}$  and  $T_{j,k}$  are the same collection of indices. Thus, in terms of defining  $\tilde{T}_l$  and  $\tilde{V}_l$ , we can take the same indexing for  $l \in [K]$  as in (S.19) by letting  $\tilde{T}_l := \mathfrak{S}(T_l)$  and  $\tilde{V}_l := \mathfrak{S}(V_l)$ . Hence, for some permutation  $\tilde{\tau} \in S_{[K]}$ , we must have

$$\tilde{T}_l = \{\tilde{\alpha} : \tilde{\alpha}_{\tilde{\tau}(l)} = 0\} = \mathfrak{S}(\{\alpha : \alpha_{\tau(l)} = 0\}) = \mathfrak{S}(T_l), \quad (\text{S.22})$$

$$\tilde{V}_l = \{\tilde{\alpha} : \tilde{\alpha}_{\tilde{\tau}(l)} = 1\} = \mathfrak{S}(\{\alpha : \alpha_{\tau(l)} = 1\}) = \mathfrak{S}(V_l). \quad (\text{S.23})$$

Now, we finish the proof by proving  $\mathbf{B} \sim \tilde{\mathbf{B}}$  and  $\alpha \sim \mathfrak{S}(\alpha)$ . By taking  $\sigma := \tilde{\tau} \cdot \tau^{-1}$  in the definition of the equivalence relations, it suffices to show  $\beta_{j,\tau(l)} = \tilde{\beta}_{j,\tilde{\tau}(l)}$  for all  $j, l$ , and  $\alpha_{\tau(l)} = (\mathfrak{S}(\alpha))_{\tilde{\tau}(l)}$  for all  $\alpha, l$ . The conclusion for  $\beta_{j,\tau(l)}$  follows from its characterization in Step 2. For any  $j, l$ , the relationship (S.21) and (S.22) shows that  $\{T_l, V_l\} \in \{\{T_{j,k}, V_{j,k}\} : k \leq |H_j|\}$  if and only if  $\{\tilde{T}_l, \tilde{V}_l\} \in \{\{\tilde{T}_{j,k}, \tilde{V}_{j,k}\} : k \leq |H_j|\}$ . For case (a), we have  $\beta_{j,\tau(l)} = \tilde{\beta}_{j,\tilde{\tau}(l)} = 0$ . For case (b), we have  $|\beta_{j,\tau(l)}| = c_{j,k} = |\tilde{\beta}_{j,\tilde{\tau}(l)}|$  as well as  $\text{sgn}(\beta_{j,\tau(l)}) = \text{sgn}(\tilde{\beta}_{j,\tilde{\tau}(l)})$ , thus  $\beta_{j,\tau(l)} = \tilde{\beta}_{j,\tilde{\tau}(l)}$ . We next show the claim for  $\alpha$ . Without loss of generality, suppose  $\alpha_{\tau(l)} = 0$ . Then, by applying (S.20) and (S.22), we have  $\mathfrak{S}(\alpha) \in \tilde{T}_l$  and  $(\mathfrak{S}(\alpha))_{\tilde{\tau}(l)} = 0$ . Similarly, for  $\alpha_{\tau(l)} = 1$ , we get  $(\mathfrak{S}(\alpha))_{\tilde{\tau}(l)} = 1$  and the proof is complete.  $\square$

### S.1.4 Proof of Theorem 3

*Proof.* For simplicity, we omit displaying the dependence of data in the likelihood  $\ell(\Theta) = \ell(\Theta | \mathbf{Y})$  and omit the subscript in the equivalence relation  $\sim_{\mathcal{K}}$ . We also define the objective function in (6) as

$$Q_N(\Theta) := \frac{1}{N} \left[ -\ell(\Theta) + \sum_{d=1}^D p_{\lambda_N, \tau_N}(\mathbf{B}^{(d)}) \right].$$

Below, we separately prove the consistency of the continuous parameters  $\Theta$  and discrete parameters  $\mathcal{G}$ . In the proof, we use the usual Bachmann-Landau asymptotic notations for deterministic sequences as well as its analog for random sequences.

We first show that  $\hat{\Theta}$  is consistent up to label permutations. This follows by modifying



the usual consistency proof of M-estimators (Van der Vaart, 2000) under our identifiability notion. Fix  $\epsilon > 0$ , and define the pointwise limit of  $Q_N(\Theta)$  as

$$Q_\infty(\Theta) := -\mathbb{E}_{\Theta^*} \log \mathbb{P}(\mathbf{Y} \mid \Theta).$$

Define the  $\epsilon$ -ball around  $\Theta^*$  under the equivalence relation  $\sim$  as

$$B_\sim(\epsilon, \Theta^*) := \{\Theta : \|\Theta' - \Theta^*\| \leq \epsilon \text{ for some } \Theta' \sim \Theta\}.$$

Also, define the constant  $\eta := \inf_{\Theta \notin B_\sim(\epsilon, \Theta^*)} Q_\infty(\Theta) - Q_\infty(\Theta^*)$ . Since we assume the model identifiability up to  $\sim$ , we must have  $Q_\infty(\Theta) - Q_\infty(\Theta^*) = \text{KL}(\mathbb{P}(\cdot \mid \Theta) \parallel \mathbb{P}(\cdot \mid \Theta^*)) > 0$  for all  $\Theta \not\sim \Theta^*$ . Here, KL denotes the Kullback–Leibler divergence. Then, we get  $\eta > 0$ , as we are considering a compact parameter space. By a standard argument, we have

$$\mathbb{P}(\min_{\Theta' \sim \hat{\Theta}} \|\Theta' - \Theta^*\| > \epsilon) \leq \mathbb{P}\left(\min_{\Theta \notin B_\sim(\epsilon, \Theta^*)} Q_N(\Theta) \leq Q_N(\Theta^*)\right) \quad (\text{S.24})$$

$$\leq \mathbb{P}\left(\min_{\Theta \notin B_\sim(\epsilon, \Theta^*)} Q_N(\Theta) \leq Q_N(\Theta^*), \sup_{\Theta} |Q_N(\Theta) - Q_\infty(\Theta)| < \frac{\eta}{2}\right) + o(1). \quad (\text{S.25})$$

Here, (S.24) uses the definition that  $\hat{\Theta}$  is a minimizer of  $Q_N(\Theta)$ . The inequality in (S.25) follows from the uniform law of large numbers, which holds under a compact parameter space and a vanishing penalty with  $\lambda_N = o(N)$ . Now, the proof is complete by noting that the first term in (S.25) is zero, since  $\Theta \notin B_\sim(\epsilon, \Theta^*)$  and  $\sup_{\Theta} |Q_N(\Theta) - Q_\infty(\Theta)| < \frac{\eta}{2}$  implies

$$Q_N(\Theta) > Q_\infty(\Theta) - \frac{\eta}{2} \geq Q_\infty(\Theta^*) + \frac{\eta}{2} > Q_N(\Theta^*).$$

Hence, there exists some  $\tilde{\Theta} \sim \hat{\Theta}$  that is consistent for  $\Theta^*$ .

Now, we prove that  $\tilde{\Theta}$  is  $\sqrt{N}$ -consistent, additionally using the assumption on the Fisher information. We first re-write the inequality  $Q_N(\tilde{\Theta}) \leq Q_N(\Theta^*)$  as

$$-\ell(\tilde{\Theta}) + \ell(\Theta^*) \leq p_{\lambda_N, \tau_N}(\mathbf{B}_0) - p_{\lambda_N, \tau_N}(\tilde{\mathbf{B}}). \quad (\text{S.26})$$

By a Taylor expansion, we can bound the LHS of (S.26) as

$$\begin{aligned} -\ell(\tilde{\Theta}) + \ell(\Theta^*) &= -(\tilde{\Theta} - \Theta^*)^\top \ell'(\Theta^*) + \frac{1}{2}(\tilde{\Theta} - \Theta^*)^\top (NI(\Theta^*) + o_p(N))(\tilde{\Theta} - \Theta^*) \\ &\geq \|\tilde{\Theta} - \Theta^*\|_2 O_p(\sqrt{N}) + N \|\tilde{\Theta} - \Theta^*\|_2^2 \left( \frac{\lambda_{\min}(I(\Theta^*))}{2} + o_p(1) \right). \end{aligned}$$

Here,  $\lambda_{\min}(I(\Theta^*)) > 0$  denotes the smallest eigenvalue of the positive definite Fisher information  $I(\Theta^*)$ . On the other hand, the RHS of (S.26) must be negative since  $\tau_N \rightarrow 0$ . Indeed, for  $\beta_{l,k}^{(d)*} \neq 0$  and a large enough  $N$ , consistency gives  $|\tilde{\beta}_{l,k}^{(d)}| = |\beta_{l,k}^{(d)*}| + o_p(1) > \tau_N$ , and the bound

$$p_{\lambda_N, \tau_N}(\mathbf{B}_0^{(d)}) - p_{\lambda_N, \tau_N}(\tilde{\mathbf{B}}^{(d)}) \leq \sum_{l,k: \beta_{l,k}^{(d)*} \neq 0} \left[ p_{\lambda_N, \tau_N}(\beta_{l,k}^{(d)*}) - p_{\lambda_N, \tau_N}(\tilde{\beta}_{l,k}^{(d)}) \right] = 0$$

holds with high probability. Hence, we have

$$\|\tilde{\Theta} - \Theta^*\|_2 O_p(\sqrt{N}) + \frac{\lambda_{\min}(I(\Theta^*))}{2} N \|\tilde{\Theta} - \Theta^*\|_2^2 \leq 0$$

with high probability, which is impossible when  $\|\tilde{\Theta} - \Theta^*\|_2 \gg \frac{1}{\sqrt{N}}$ . Thus,  $\|\tilde{\Theta} - \Theta^*\|_2 = O_p\left(\frac{1}{\sqrt{N}}\right)$ .

Finally, we prove the estimation consistency for the discrete graph structures  $\mathbf{G}^{(d)}$ s. It suffices to show that for any fixed  $d, l, k$ ,  $\tilde{g}_{l,k}^{(d)} = g_{l,k}^{(d)}$  with high probability. As a first case, suppose that  $g_{0;l,k}^{(d)} = 1$ . Then, the consistency result implies  $\tilde{\beta}_{l,k}^{(d)} \xrightarrow{p} \beta_{0;l,k}^{(d)} \neq 0$ . Hence,  $\tilde{\beta}_{l,k}^{(d)} \neq 0$  with high probability, so  $\tilde{g}_{l,k}^{(d)} = 1$ . Next, consider the case when  $g_{0;l,k}^{(d)} = 1$ . Assume the converse, and suppose  $\tilde{\beta}_{l,k}^{(d)} \neq 0$ . By the  $\sqrt{N}$ -consistency and the assumption that  $\tau_N \gg \frac{1}{\sqrt{N}}$ , we must have  $|\tilde{\beta}_{l,k}^{(d)}| \ll \tau_N$  with high probability. Then, the first-order conditions (KKT conditions) give that

$$\partial_{\beta_{l,k}^{(d)}} \ell(\tilde{\Theta}) := \frac{\partial \ell(\Theta)}{\partial \beta_{l,k}^{(d)}} \Big|_{\Theta = \tilde{\Theta}} = p'_{\lambda_N, \tau_N}(\tilde{\beta}_{l,k}^{(d)}) = \Theta_p \left( \frac{\lambda_N}{\tau_N} \right).$$

But we have a contradiction because a Taylor expansion of the partial derivative gives

$$\partial_{\beta_{l,k}^{(d)}} \ell(\tilde{\Theta}) = \partial_{\beta_{l,k}^{(d)}} \ell(\Theta^*) + NO_p(\tilde{\Theta} - \Theta^*) = O_p(\sqrt{N}),$$

and  $\sqrt{N} \ll \lambda_N/\tau_N$ . Hence, we must have  $\tilde{g}_{l,k}^{(d)} = 0$ , and the proof is complete.  $\square$

### S.1.5 Detour: Identifiability of One-latent-layer Saturated Models With Interaction Effects of Binary Latent Variables

One may ask whether the linear/additive parametrization  $\beta_{j,0} + \sum_{k \in [K]} \beta_{j,k} A_k$  in the one-latent-layer saturated model is necessary for its identifiability. We next show that this is not the case, and prove that identifiability of  $\mathbf{G}$  can be established under two more flexible nonlinear (in terms of the dependence on  $\mathbf{A}$ ) parametric models commonly used in psychometrics, using the exact same conditions A and B. Here, to handle different parametrizations, define  $\eta_{j,\alpha}$  to be the nonlinear parameter for  $Y_j \mid \mathbf{A}$ :

$$Y_j \mid (\mathbf{A} = \alpha) \sim \text{ParFam}_j(\eta_{j,\alpha}),$$

and rewrite condition B as follows:

B'. For any  $\alpha \neq \alpha'$ , there exists  $j > 2K$  such that  $\eta_{j,\alpha} \neq \eta_{j,\alpha'}$ .

We first consider the *ExpDINA model* (see Definition 4 in [Lee and Gu, 2024](#))<sup>1</sup>, which considers the following conjunctive form of  $\eta_{j,\alpha}$ :

$$Y_j \mid (\mathbf{A} = \alpha) \sim \text{ParFam}_j\left(g_j\left(\beta_{j,0} + \beta_{j,1} \prod_{k=1}^K \alpha_k^{q_{j,k}}, \gamma_j\right)\right). \quad (\text{S.27})$$

In other words, the conditional distribution has two possible parameter values based on whether  $\prod_{k=1}^K \alpha_k^{q_{j,k}} = 1$  (or equivalently, whether  $\mathbf{A} \succeq \mathbf{q}_j$ ). To resolve the sign flipping ambiguity, let us assume  $\beta_{j,1} > 0$  for all  $j$  instead of Assumption 1(c). Under this model,

---

<sup>1</sup>While this model is originally named ‘‘Exponential-family based’’, this is not required for our identifiability conclusion. In other words, the family  $\text{Parfam}_j$  in (S.27) can be any parametric family.

both parts of Lemma S.2 does not hold since  $|\mathcal{S}_j| = 2$  whenever  $|H_j| \geq 1$ . Hence, we focus on partitioning  $\{0, 1\}^K$  by grouping the binary patterns  $\boldsymbol{\alpha}$  that takes the same values of (S.7), instead of just looking at the cardinality of  $\mathcal{S}_j$ . We formally state this claim in the following Lemma. Consequently, this Lemma can be used in place of Lemma S.2 to prove identifiability of the exploratory ExpDINA model. The proof is a direct modification of Step 2 above (first, use part (a) of Lemma S.6 to construct a permutation  $\sigma \in S_{[K]}$  based on the first  $K$  rows, and use part (b) to prove  $\tilde{g}_{j,k} = g_{j,\sigma(k)}$  for the other rows), and we omit the details.

**Lemma S.6.** *Consider an ExpDINA model. Fix any  $j$  such that  $|H_j| \geq 1$ , and partition  $\{0, 1\}^K$  into two sets  $T_j$  and  $T_j^c$  based on the value of  $\mathcal{S}_j = \{\mathbf{s}_j(\boldsymbol{\alpha})\}_{\boldsymbol{\alpha}}$ , so that  $|T_j| \leq |T_j^c|$ . If  $|T_j| = |T_j^c|$ , we break the symmetry by additionally assuming that  $\mathbf{1}_K \in T_j$ . Then, the following holds.*

(a)  $T_j = \{\boldsymbol{\alpha} : \boldsymbol{\alpha} \succeq \mathbf{g}_j\}$  and  $|T_j| = 2^{K-|H_j|}$ .

(b) *Suppose that the first  $K$  rows of  $\mathbf{G}$  is a row-permutation of  $\mathbf{I}_K$ , in other words, there exists  $\sigma \in S_{[K]}$  such that  $\mathbf{g}_k = \mathbf{e}_{\sigma(k)}$  for all  $k$ . Then, for any  $j$ ,  $T_j \subseteq T_k$  if and only if  $g_{j,\sigma(k)} = 1$ .*

*Proof.* (a) Note that the parameter of the ExpDINA model takes two values, depending on the value of  $\prod_k \alpha_k^{g_{j,k}} = \mathbf{1}(\boldsymbol{\alpha} \succeq \mathbf{g}_j)$ . This value is equal to one for the  $2^{K-|H_j|}$  configurations of  $\boldsymbol{\alpha}$  such that  $\boldsymbol{\alpha} \succeq \mathbf{g}_j$ , and these are exactly the elements of  $T_j$ .

(b) The “if” part is immediate since  $g_{j,\sigma(k)} = 1$  implies  $\mathbf{g}_j \succeq \mathbf{g}_k$ .

For the “only if” part, we prove the contrapositive. Suppose  $g_{j,\sigma(k)} = 0$ . Then,  $\boldsymbol{\alpha} = \mathbf{1}_K$  and  $\boldsymbol{\alpha}' := (\alpha_1, \dots, \alpha_{\sigma(k)-1}, 0, \alpha_{\sigma(k)+1}, \dots, \alpha_K)$  have the same conditional distribution as in (S.27). Hence,  $\boldsymbol{\alpha}$  and  $\boldsymbol{\alpha}'$  must both belong in  $T_j$  but  $\boldsymbol{\alpha}' \notin T_k$ , so  $T_j \not\subseteq T_k$ .

□

Next, as a second example, we consider the flexible *ExpGDM* (see Definition 1 in the Supplementary Material of Lee and Gu, 2024) and prove its identifiability under the same conditions A and B'. This model considers all possible linear and interaction effects between the latent variables:

$$Y_j \mid \mathbf{A} \sim \text{ParFam}(\eta_{j,\boldsymbol{\alpha}}, \gamma_j),$$

where  $\eta_{j,\boldsymbol{\alpha}} = \beta_{j,\emptyset} + \sum_{k=1}^K \beta_{j,k} \{q_{j,k}\alpha_k\} + \sum_{1 \leq k_1 < k_2 \leq K} \beta_{j,k_1 k_2} \{q_{j,k_1}\alpha_{k_1}\} \{q_{j,k_2}\alpha_{k_2}\} + \cdots + \beta_{j,H_j} \prod_{k \in H_j} \{q_{j,k}\alpha_k\}.$

The above model incorporates all possible main and interaction effects of the parent latent variables in the conditional distribution of  $Y_j \mid \mathbf{A}$ . It is clear that this model generalizes both the one-latent-layer saturated model in Definition S.1 and the ExpDINA model. To address the sign-flipping issue, we assume that

$$\eta_{j,\boldsymbol{\alpha}} > \eta_{j,\boldsymbol{\alpha}'} \quad \text{for } \boldsymbol{\alpha} \succeq \mathbf{g}_j, \boldsymbol{\alpha}' \not\succeq \mathbf{g}_j. \quad (\text{S.28})$$

This is a stronger assumption compared to Assumption 1(c). We impose this modified monotonicity condition as Assumption 1(c) cannot resolve the sign-flipping ambiguity, as we illustrate this in the following example.

**Example S.1.** Consider a toy setting of  $J = K = 2$  and  $\mathbf{G} = \mathbf{I}_2$  with  $\beta_{1,1} = \beta_{2,2} = 1$ . Suppose that there all intercepts and interaction effects are zero for each  $j = 1, 2$ :  $\beta_{j,0} = \beta_{j,12} = 0$ . Consider a stronger monotonicity assumption that all main-effects are nonnegative, that is  $\beta_{j,k} \geq 0$ . Define an alternative model with  $\tilde{\mathbf{G}} = \begin{pmatrix} 1 & 0 \\ 1 & 1 \end{pmatrix}$  and positive main-effects:  $\tilde{\beta}_{1,1} = 1, \tilde{\beta}_{2,1} = \tilde{\beta}_{2,2} = 1$  and no intercepts, but with a negative interaction effect  $\tilde{\beta}_{2,12} = -2$ . Then, the matrix  $\{\eta_{j,\boldsymbol{\alpha}}\}_{j,\boldsymbol{\alpha}}$  and  $\{\tilde{\eta}_{j,\boldsymbol{\alpha}}\}_{j,\boldsymbol{\alpha}}$  are identical up to column permutation, so these two distinct parameters are non-distinguishable.

Also assuming a monotone condition on the parametric family (see below), we can modify

Lemma S.6 as follows. Consequently, under all these assumptions, the ExpGDM is also identifiable under conditions A and B’.

**Definition S.3** (Monotone family). *We say that a parametric family  $p(\cdot | \eta)$  is a monotone family with a monotone set  $U$  when there exists a measurable set  $U \subset \mathcal{Y}$  not depending on  $\eta$  such that  $\mathbb{P}(Y \in U | \eta)$  (or  $\mathbb{P}(Y \in U | \eta, \gamma)$ ) is a strictly increasing function in  $\eta$ .*

Note that all parametric families considered in this paper are monotone families. For example, we can take  $U = \{1\}, \{1, 2, \dots\}, (0, \infty)$  for the Bernoulli/Poisson/Normal distribution with mean  $\eta$ , respectively.

**Lemma S.7.** *Consider an ExpGDM. Suppose all  $p_j$ s are monotone families with monotone sets  $U_j$ , and the monotonicity condition (S.28) holds. Let  $T_j := \{\boldsymbol{\alpha} : \mathbb{P}_{j,\boldsymbol{\alpha}}(U_j) = \max_{\boldsymbol{\alpha}'} \mathbb{P}_{j,\boldsymbol{\alpha}'}(U_j)\}$ . Then, the same conclusions as in Lemma S.6 hold.*

*Proof.* (a) Since we consider a monotone family, we can write  $T_j = \{\boldsymbol{\alpha} : \eta_{j,\boldsymbol{\alpha}} = \max_{\boldsymbol{\alpha}'} \eta_{j,\boldsymbol{\alpha}'}\}$ .

Then, by assumption (S.28),  $\boldsymbol{\alpha} \notin T_j$  for  $\boldsymbol{\alpha} \not\preceq \mathbf{g}_j$ . Also, by the faithfulness assumption, we have  $\boldsymbol{\alpha} \in T_j$  for all  $\boldsymbol{\alpha} \succeq \mathbf{g}_j$ .

(b) Assuming part (a), the argument in Lemma S.6 can be applied.

□

## S.2 Details of the Layerwise Double-SVD Initialization

### S.2.1 Details of Algorithm 2

We describe full details of the layerwise double-SVD initialization in Algorithm 2. We first consider the noiseless scenario to motivate the general procedure. The setting is that we are given a  $N \times J$  matrix  $\mathbb{E}[\mathbf{Y}]$ , and wish to recover  $\mathbf{A}, \mathbf{B}$ . For simplicity, we consider the one-latent-layer saturated model, and omit the layer-wise superscript to simplify the notation.

We also assume identical parametric families in the observed layer and a nonlinear function  $\mu \circ g$ .

The first step involves denoising the nonlinearity and rewriting the data matrix as a low-rank approximation. Recall that  $\mu : H \rightarrow \mathbb{R}$  computes the mean of the observed-layer parametric family,  $g : \mathbb{R} \rightarrow H$  is the link function, and define a function  $\tilde{g} := \mu \circ g$ . Since

$$\mathbb{E}(Y_{i,j} \mid \mathbf{A}_i) = \mu(g(\beta_{j,0} + \sum_k \beta_{j,k} A_{i,k}, \gamma_j)) = \tilde{g}(\beta_{j,0} + \sum_k \beta_{j,k} A_{i,k}),$$

we have

$$\mathbf{Z} := \tilde{g}^{-1}(\mathbb{E}(\mathbf{Y} \mid \mathbf{A})) = [\mathbf{1}_N, \mathbf{A}]\mathbf{B}_1^\top.$$

Let  $\mathbf{Z}_0$  be the centered version of  $\mathbf{Z}$  so that the column sums are zero, in other words,  $z_0(i, j) := z(i, j) - \frac{1}{N} \sum_{i'=1}^N z(i', j)$ . Similarly, let  $\mathbf{A}_0$  be the column-centered version of  $\mathbf{A}$  with  $A_0(i, k) := A(i, k) - \frac{1}{N} \sum_{i'=1}^N A(i', l)$ . Then, we have

$$\mathbf{Z}_0 = \mathbf{A}_0 \mathbf{B}^\top. \tag{S.29}$$

This is a rank  $K$  decomposition, and we can write the SVD of  $\mathbf{Z}_0$  as  $\mathbf{Z}_0 = \mathbf{U}\mathbf{\Sigma}\mathbf{V}^\top$ . Here,  $\mathbf{U}, \mathbf{\Sigma}, \mathbf{V}$  are  $N \times K, K \times K, J \times K$  matrices, respectively.

The second step addresses the rotation invariance of the SVD by finding the sparse representation in (S.29). Motivated by the sparsity of  $\mathbf{B}$ , we perform the Varimax rotation on  $\mathbf{V}$ . As Varimax finds a sparse rotation (see [Rohe and Zeng, 2023](#), for a theoretical justification), we expect it to find a rotation matrix  $\mathbf{R}$  such that  $\widehat{\mathbf{B}} := \mathbf{V}\mathbf{R}$  has the same sparsity pattern as  $\mathbf{B}$  (and the graphical matrix  $\mathbf{G}$ ). Consequently, we can use  $\widehat{\mathbf{B}}$  as a rough estimate for  $\mathbf{B}$ , and the sparsity pattern of  $\widehat{\mathbf{B}}$  to estimate  $\mathbf{G}$ . The estimate for  $\mathbf{A}$  follows from solving (S.29) for  $\mathbf{A}_0$ , using the estimated  $\widehat{\mathbf{B}}$ .

There are several subtleties to address when extending this procedure to the sample-based setting. One immediate issue is applying the inverse-link function  $\tilde{g}^{-1}$ . For discrete samples, observed data may take values in the boundary of the sample space, such as  $Y_j = 0$

when  $\mathcal{Y} = \mathbb{N} \cup \{0\}$ . This makes the inverse function not well-defined. To resolve this, we apply the double SVD-based procedure in [Zhang et al. \(2020\)](#) as mentioned in the main text, which denoises and truncates the data into a subset of the sample space. The final output of this procedure is the sample-version SVD for the matrix  $\mathbf{Z}_0$  (see step 6 in [Algorithm 4](#)).

Another subtlety arises while estimating  $\mathbf{A}$  and  $\mathbf{B}$  after rotating  $\mathbf{V}$ , since Varimax does not account for the scaling of the row/columns. Here, we exploit the discreteness of the latent variables in  $\mathbf{A}$  to rescale  $\mathbf{B}$ . Using the decomposition [\(S.29\)](#), we can crudely estimate  $\mathbf{A}_0$  using the sparse Varimax output  $\widehat{\mathbf{B}}$ . While the estimates  $\widehat{\mathbf{A}}_0$  also suffer from the same scaling issue, we can still estimate the *binary*  $\mathbf{A}$  by noting that  $A_0(i, k) < 0$  if and only if  $A(i, k) = 0$ . Finally, using the estimated  $\widehat{\mathbf{A}}$ , we re-estimate  $\mathbf{B}$  via [\(S.29\)](#), now with correct scaling; see steps 9-10 in [Algorithm 4](#).

The entire procedure is summarized in [Algorithm 4](#), where we also specify the choice of tuning parameters.

**Remark S.1** (Truncating  $\widehat{\mathbf{Y}}$ ). *We explain more on the truncation details in Step 3 by considering specific response types. For Normal responses, the original sample space is  $\mathbb{R}$  and the truncation (Steps 1-4 in [Algorithm 4](#)) may be omitted. For Binary responses, we set*

$$\widehat{y}_{K^{(1)}}(i, j) = \begin{cases} \epsilon, & \text{if } y_{K^{(1)}}(i, j) = 0, \\ 1 - \epsilon, & \text{if } y_{K^{(1)}}(i, j) = 1. \end{cases}$$

*For Poisson responses, we set*

$$\widehat{y}_{K^{(1)}}(i, j) = \begin{cases} \epsilon, & \text{if } y_{K^{(1)}}(i, j) < \epsilon, \\ y_{K^{(1)}}(i, j), & \text{otherwise.} \end{cases}$$

*In terms of implementing the method, we follow the suggestions of [Zhang et al. \(2020\)](#) with  $\epsilon = 10^{-4}$ .*

**Remark S.2** (Constant  $C_g$ ). *In Step 10 of [Algorithm 4](#),  $C_g > 0$  is an artificial scaling*



---

**Algorithm 4:** Spectral initialization for Algorithm 1
 

---

**Data:**  $\mathbf{Y}$ ,  $\{K^{(d)}\}_d$ ,  $D$ , function  $\tilde{g}$ , truncation parameters  $\epsilon = 10^{-4}$ ,  $\delta = \frac{1}{2.5\sqrt{J}}$

1. Apply SVD to  $\mathbf{Y}$  and write  $\mathbf{Y} = \mathbf{U}\Sigma\mathbf{V}^\top$ , where  $\Sigma = \text{diag}(\sigma_i)$  and  $\sigma_1 \geq \dots \geq \sigma_J$ .
2. Let  $\mathbf{Y}_{\widehat{K}^{(1)}} = \sum_{k=1}^{\widehat{K}^{(1)}} \sigma_k \mathbf{u}_k \mathbf{v}_k^\top$ , where  $\widehat{K}^{(1)} := \max\{K^{(1)} + 1, \arg \max_k \{\sigma_k \geq 1.01\sqrt{N}\}\}$ .
3. Define  $\widehat{\mathbf{Y}}_{\widehat{K}^{(1)}}$  by truncating  $\mathbf{Y}_{\widehat{K}^{(1)}}$  to the range of responses, at level  $\epsilon$ . See Remark S.1 for details.
4. Define  $\widehat{\mathbf{Z}}$  by letting  $\widehat{z}(i, j) = \tilde{g}^{-1}(\widehat{y}_{\widehat{K}^{(1)}}(i, j))$ .
5. Let  $\widehat{\mathbf{Z}}_0$  be the centered version of  $\widehat{\mathbf{Z}}$ , that is,  $\widehat{z}_0(i, j) = \widehat{z}(i, j) - \frac{1}{N} \sum_{k=1}^N \widehat{z}(k, j)$ .
6. Apply SVD to  $\widehat{\mathbf{Z}}_0$  and write its rank- $K^{(1)}$  approximation as  $\widehat{\mathbf{Z}}_0 \approx \widehat{\mathbf{U}}\widehat{\Sigma}\widehat{\mathbf{V}}$ .
7. Let  $\widetilde{\mathbf{V}}$  be the rotated version of  $\widehat{\mathbf{V}}$  according to the Varimax criteria.
8. Entrywise threshold  $\widetilde{\mathbf{V}}$  at  $\delta$  to induce sparsity, and flip the sign of each column so that all columns have positive mean. Let  $\widehat{\mathbf{G}}^1$  be the estimated sparsity pattern.
9. Estimate the centered  $\mathbf{A}_0$  by  $\widehat{\mathbf{A}}_0 := \widehat{\mathbf{Z}}_0 \widetilde{\mathbf{V}} (\widetilde{\mathbf{V}}^\top \widetilde{\mathbf{V}})^{-1}$ , and estimate  $\mathbf{A}$  by reading off the signs:  $\widehat{A}(i, k) = \mathbb{1}(A_0(i, k) > 0)$ .
10. Let  $\widehat{\mathbf{A}}_{\text{long}} := [\mathbf{1}, \widehat{\mathbf{A}}]$ . Estimate  $\mathbf{B}_1$  by  $\widehat{\mathbf{B}}_1 := C_g ((\widehat{\mathbf{A}}_{\text{long}}^\top \widehat{\mathbf{A}}_{\text{long}})^{-1} \widehat{\mathbf{A}}_{\text{long}}^\top \widehat{\mathbf{Z}}_0) \cdot \widehat{\mathbf{G}}^1$ , where  $\cdot$  is the element-wise product and  $C_g$  is a positive constant that is defined in Remark S.2
11. Let  $\mathbf{Y} = \widehat{\mathbf{A}}$  and  $g$  be the logistic function. Go back to Step 1 to estimate the next layer coefficient matrix. Continue until reaching the deepest layer.
12. For the deepest layer, estimate  $\mathbf{p}$  by setting  $\widehat{\mathbf{p}}_k := \frac{1}{N} \sum_{i=1}^N \widehat{A}(i, k)$ .

**Output:**  $\widehat{\mathbf{p}}, \{\widehat{\mathbf{B}}^{(d)}\}_d$ .

---

constant that depends on the link function  $\tilde{g}$ . This is introduced to better adjust the scaling of  $\mathbf{B}$ , as the nonlinear transform  $\tilde{g}^{-1}$  leads to a potentially biased estimate for  $\widehat{\mathbf{Z}}_0$ . This adjustment is unnecessary for Normal-based DDEs, where  $g$  is the identity link, and in such cases, one can simply set  $C_g = 1$ . For the Bernoulli or Poisson-based DDE where  $\tilde{g}$  is the logistic or exponential function, we choose  $C_g = \frac{1}{2}$  as the scaling factor based on simulation results.

## S.2.2 Estimation Accuracy Without the Spectral Initialization

We illustrate the effectiveness of our spectral initialization for by comparing it with EM parameter estimates obtained under random initialization. We show that even for the low dimensional setting  $(J, K^{(1)}, K^{(2)}) = (18, 6, 2)$ , the overall model complexity may be too large for an EM algorithm with random initialization to converge to the global optimum. In contrast, the spectral initialization provides a reliable starting point. In Table S.1, we compare the accuracy of the PEM estimates under (a) random initialization and (b) spectral initialization. Here, we consider the same three parametric families as the main paper, the identifiable true parameter values  $\mathcal{B}_s$  (see eq. (13)), and two sample sizes  $N = 1000, 4000$ . We set the random initialization as follows:

$$p_k, B_{j,k}^{(1)}, B_{k,l}^{(2)} \sim \text{Unif}(0, 1), \quad \text{for all } k \in [K^{(1)}], j \in [J], l \in [K^{(2)}],$$

$$B_{j,0}^{(1)}, B_{k,0}^{(2)} \sim \text{Unif}(-1, 0), \quad \gamma_j \sim \text{Unif}(0.5, 1.5),$$

where  $\text{Unif}(a, b)$  denotes the uniform distribution on the interval  $(a, b)$ .

ParFam	Initialization \ N	Accuracy( $\mathcal{G}$ )		RMSE( $\Theta$ )		Time (s)		# iterations	
		1000	4000	1000	4000	1000	4000	1000	4000
Bernoulli	Random	0.617	0.547	1.37	1.32	23.6	48.4	20.1	27.11
	<b>Spectral</b>	0.966	0.992	0.30	0.20	6.7	37.5	4.1	4.2
Poisson	Random	0.743	0.725	1.47	1.49	20.4	26.8	21.9	23.2
	<b>Spectral</b>	0.999	1	0.16	0.08	3.6	6.4	4.4	4.0
Normal	Random	0.595	0.581	1.71	1.83	36.6	347.7	14.7	16.9
	<b>Spectral</b>	0.996	1	0.13	0.06	1.2	3.0	4.1	4.4

Table S.1: Accuracy measures for  $\mathcal{G}$  and  $\Theta$ , computation time and iterations for 2-layer DDE estimates under different initializations. For the Accuracy( $\mathcal{G}$ ) column, larger is better. For the other columns, smaller is better.

The results in Table S.1 clearly illustrates that random initialization does not effectively converge to the true parameter values. In contrast, the spectral initialization results in a significantly smaller estimator error as well as shorter time and smaller numbers of iterations,

demonstrating its superior performance.

It may be worth mentioning that a significant proportion of local optimizers arise from boundary cases of the identifiability condition. For example, in the Normal case, the local optimizers emptied out one or more columns in the  $\mathbf{B}^{(1)}$  and  $\mathbf{B}^{(2)}$  matrices, or exhibit two linearly dependent columns. This corresponds to the set of parameters excluded by Assumption 1.

## S.3 Additional Algorithm Details

### S.3.1 Detailed Update Formulas

**Simplified M-step for the PEM Algorithm.** We display more explicit expressions for the M-step in Algorithm 1. Recall that we need to solve three optimizations detailed in equations (8)-(10). By plugging-in the distributional formulas from Section 2, we can simplify each equation as follows. The computations are straightforward and we just display the simplified formulas.

First, the maximization in (8) simplifies to updating

$$p_l^{[t+1]} = \frac{\sum_{i, \alpha^{(1)}, \alpha^{(2)}} \alpha_l^{(2)} \varphi_{i, \alpha^{(1)}, \alpha^{(2)}}^{[t+1]}}{N},$$

for  $l \in [K^{(2)}]$ . The maximization in (9) simplifies to maximizing the  $k$ th row of  $\mathbf{B}^{(2)}$  for each  $k \in [K^{(1)}]$ :

$$\begin{aligned} & \boldsymbol{\beta}_k^{(2), [t+1]} \\ &= \operatorname{argmax}_{\boldsymbol{\beta}^{(2)} \in \mathbb{R}^{K^{(2)}+1}} \sum_{i, \alpha^{(1)}, \alpha^{(2)}} \log \mathbb{P}(\mathbf{A}_{i,k} = \alpha_k^{(1)}; g_{\text{logistic}}(\beta_0^{(2)} + \sum_{l=1}^{K^{(2)}} \alpha_l^{(2)} \beta_l^{(2)})) \varphi_{i, \alpha^{(1)}, \alpha^{(2)}}^{[t+1]} - p_{\lambda_2, \tau}(\boldsymbol{\beta}^{(2)}). \end{aligned}$$

Finally, the maximization in (10) boils down to maximizing the  $j$ th row of  $\mathbf{B}^{(1)}$  and  $\gamma_j$  for each  $j \in [J]$ :

$$(\boldsymbol{\beta}_j^{(1), [t+1]}, \gamma_j^{[t+1]})$$

$$= \operatorname{argmax}_{\boldsymbol{\beta}^{(1)} \in \mathbb{R}^{K^{(1)}+1}, \gamma > 0} \sum_{i, \boldsymbol{\alpha}^{(1)}, \boldsymbol{\alpha}^{(2)}} \log \mathbb{P}(Y_{i,j}; \beta_0^{(1)} + \sum_{k=1}^{K^{(1)}} \alpha_k^{(1)} \beta_k^{(1)}, \gamma) \varphi_{i, \boldsymbol{\alpha}^{(1)}, \boldsymbol{\alpha}^{(2)}}^{[t+1]} - p_{\lambda_1, N, \tau}(\boldsymbol{\beta}^{(1)}),$$

**Simplified Simulation Step for the SAEM Algorithm.** We display the complete conditionals for the simulation step in the  $(t+1)$ th iteration of the SAEM (see Algorithm 3).

First, we sample each  $A_{i,l}^{(2),[t+1]}$  from the following distribution:

$$\begin{aligned} \mathbb{P}(A_{i,l}^{(2)} = \alpha_l^{(2)} \mid (-)) &\propto p_l^{[t]\alpha_l^{(2)}} (1 - p_l^{[t]})^{1-\alpha_l^{(2)}} \prod_{k=1}^{K^{(1)}} g_{\text{logistic}}(A_{i,k}^{(1),[t]}; e^{\eta_{k, \mathbf{A}_i^{(2),[t]}}}) \\ &\propto p_l^{[t]\alpha_l^{(2)}} (1 - p_l^{[t]})^{1-\alpha_l^{(2)}} \prod_{k=1}^{K^{(1)}} \frac{e^{A_{i,k}^{(1),[t]} \beta_{k,l}^{(2),[t]} \alpha_l^{(2)}}}{1 + e^{\eta_{k, \mathbf{A}_i^{(2),[t]}}}}. \end{aligned}$$

Here,  $(-)$  denotes the samples/parameter values computed in the previous ( $t$ th) iteration, excluding the random variable of interest,  $A_{i,l}^{(2),[t]}$ . The notation

$$\eta_{k, \mathbf{A}_i^{(2),[t]}} := \beta_{k,0}^{(2),[t]} + \sum_{l' \neq l} \beta_{k,l'}^{(2),[t]} A_{i,l'}^{(2),[t]} + \beta_{k,l}^{(2),[t]} \alpha_l^{(2)}$$

denotes the linear combinations computed under  $\Theta^{[t]}, \mathbf{A}^{(2),[t]}$ . As  $\alpha_l^{(2)} = 0/1$ , sampling from this distribution is straightforward by computing the above expression.

Next, we sample each  $A_{i,k}^{(1),[t+1]}$  similarly from the complete conditionals:

$$\mathbb{P}(A_{i,k}^{(1)} = \alpha_k^{(1)} \mid (-)) \propto e^{\alpha_k^{(1)} \eta_{k, \mathbf{A}_i^{(2),[t]}}} \prod_{j=1}^J \mathbb{P}\left(Y_{i,j}; g(\eta_{j, \mathbf{A}_i^{(1),[t]}}, \gamma_j^{[t]})\right).$$

Here,  $\eta_{j, \mathbf{A}_i^{(1),[t]}}$  is similarly defined as  $\beta_{j,0}^{(1),[t]} + \sum_{k' \neq k} \beta_{j,k'}^{(1),[t]} A_{i,k'}^{(1),[t]} + \beta_{j,k}^{(1),[t]} \alpha_k^{(1)}$ .

**Simplified M-step for the SAEM Algorithm.** In the main paper, we have motivated the SAEM M-step in terms of the parameter  $\mathbf{B}^{(2)}$  (see (12)). Here, for completeness, we present the fully expanded formulas for updating each parameter.

First, for each  $l \in [K^{(2)}]$ , we update  $p_l$  in closed form as follows:

$$p_l^{[t+1]} := \frac{\sum_i A_{i,l}^{(2),[t+1]}}{N}.$$

Next, for  $k \in [K^{(1)}]$ , we update the  $k$ th row of  $\mathbf{B}^{(2)}$  (denoted as  $\boldsymbol{\beta}_k^{(2)}$ ) as follows:

$$Q_k^{(2),[t+1]}(\boldsymbol{\beta}_k^{(2)}) := (1 - \theta_{t+1})Q_k^{(2),[t]}(\boldsymbol{\beta}_k^{(2)}) + \theta_{t+1} \sum_{i=1}^N \log \mathbb{P}(A_{i,k}^{(1)} = A_{i,k}^{(1),[t+1]} \mid \mathbf{A}_i^{(2)} = \mathbf{A}_i^{(2),[t+1]}; \boldsymbol{\beta}_k^{(2)}),$$

$$\boldsymbol{\beta}_k^{(2),[t+1]} := \operatorname{argmax}_{\boldsymbol{\beta}_k^{(2)}} \left[ Q_k^{(2),[t+1]}(\boldsymbol{\beta}_k^{(2)}) - p_{\lambda_N, \tau_N}(\boldsymbol{\beta}_k^{(2)}) \right],$$

Finally, for each  $j \in [J]$ , we update the  $j$ th row of  $\mathbf{B}^{(1)}$  (denoted as  $\boldsymbol{\beta}_j^{(1)}$ ) and  $\gamma_j$  (if it exists) as follows:

$$Q_j^{(1),[t+1]}(\boldsymbol{\beta}_j^{(1)}, \gamma_j) := (1 - \theta_{t+1})Q_j^{(1),[t]}(\boldsymbol{\beta}_j^{(1)}, \gamma_j) + \theta_{t+1} \sum_{i=1}^N \log \mathbb{P}(Y_{i,j} \mid \mathbf{A}_i^{(1)} = \mathbf{A}_i^{(1),[t+1]}; \boldsymbol{\beta}_j^{(1)}, \gamma_j),$$

$$(\boldsymbol{\beta}_j^{(1),[t+1]}, \gamma_j^{[t+1]}) := \operatorname{argmax}_{\boldsymbol{\beta}_j^{(1)}, \gamma_j} \left[ Q_j^{(1),[t+1]}(\boldsymbol{\beta}_j^{(1)}, \gamma_j) - p_{\lambda_N, \tau_N}(\boldsymbol{\beta}_j^{(1)}) \right]. \quad (\text{S.30})$$

### S.3.2 Estimating the Number of Latent Variables

Recall that we have proposed a spectral-ratio estimator to select the latent dimension  $\mathcal{K}$  in Section 4.3. In this supplement, we propose two alternative estimators motivated by popular methods for selecting the number of latent variables in other statistical problems (Shen and Wong, 1994; Melnykov and Melnykov, 2012; Chen and Li, 2022). The performance of these will be later assessed in a simulation study in Section S.4.3.

Continuing from the setup in Section 4.3, we address the estimation of  $\mathcal{K}$  under the two-latent-layer DDE. We first focus on the scenario where the number of deepest latent variables,  $K^{(2)}$ , is known, and our goal is to select  $K^{(1)}$  from a candidate grid  $\mathfrak{K}$ . This assumption is often justified in real-world applications where prior knowledge of the number of latent labels or classes in the dataset is available. The objective is to uncover finer-grained latent structures that capture additional generative information beyond the known labels.

- EBIC: We compute the extended BIC (EBIC; Chen and Chen, 2008) for each  $k \in \mathfrak{K}$ , and select the model with the smallest EBIC:

$$K^{(1)} := \operatorname{argmin}_{k \in \mathfrak{K}} \text{EBIC}(k).$$

We postpone the details of the formula of  $\text{EBIC}(k)$  to Section S.3.4. Here, we consider EBIC instead of more traditional information criteria such as AIC and BIC since it is designed to handle large parameter spaces.

- LRT: The class of models with  $k \in \mathfrak{K}$  can be viewed as a nested set of regular parametric models, and one can apply the method of sieves to select  $K^{(1)}$  (Shen and Wong, 1994). In other words, we start from the smallest  $k$  and sequentially conduct level- $\alpha$  likelihood ratio tests for  $H_0 : K^{(1)} = k$  v.s.  $H_1 : K^{(1)} = k + 1$  using the  $\chi^2$  limiting distributions, until when we cannot reject the alternative; define  $\widehat{K}^{(1)}$  as this  $k$ .

Below is a discussion regarding the theoretical and computational properties of the three proposed estimators (spectral-ratio, EBIC, LRT). Theoretically, consistency of all three methods can be justified under varying assumptions. Additionally assuming that  $K^{(1)}$  is identifiable, the EBIC is known to be consistent even under a diverging  $J$  (Chen and Chen, 2008). The LRT estimator can be justified by standard arguments invoking Wilk’s theorem (Wilks, 1938). Finally, under the asymptotic regime  $N, J \rightarrow \infty$  and assuming that  $\mu \circ g$  is linear,  $\sigma_1, \dots, \sigma_r$  is close to the top  $r$  singular values of  $\mathbf{Y}$  and standard eigenvalue perturbation arguments (Weyl’s theorem) guarantee that the spectral ratio estimator for  $K^{(1)}$  is consistent.

In terms of computation, the spectral-ratio estimator is the most desirable as it just requires computing the SVD of the denoised data matrix once. The other two methods (EBIC, LRT) require re-fitting the model (using Algorithm 3) for each candidate value of  $K^{(1)}$  as well as computing the likelihood. This limits their usage when the upper bound for  $K^{(1)}$  is large. Furthermore, the model re-fitting issue for EBIC and LRT is amplified when the number of the top layer latent variables  $K^{(2)}$  is also unknown, as the cardinality of the candidate set for  $\mathcal{K} = (K^{(1)}, K^{(2)})$  increases. On the other hand, the spectral-ratio estimates the number of latent variables in a layerwise manner, and is computationally efficient even under an unknown  $K^{(2)}$ .

For analyzing real data, we recommend making the final selection of  $\mathcal{K}$  by also incorporating qualitative aspects of the data such as domain knowledge and interpretability.

### S.3.3 Implementation Details

We elaborate on the choices made to implement the EM Algorithms 1 and 3.

**Tuning parameter selection.** For practical implementation, the penalty function and the tuning parameters  $\lambda_N, \tau_N$  must be specified. In this work, we consider the truncated Lasso penalty function (TLP) proposed by Shen et al. (2012), that is  $p_{\lambda, \tau}(b) := \lambda \min(|b|, \tau)$ . Preliminary simulations revealed that the results are very similar under other penalties such as SCAD.

Based on the consistency result in Theorem 3, we consider  $\lambda_N = N^{1/4}, \tau_N = 3N^{-0.3}$  for the simulation studies. For real data analysis, tuning parameters were selected from the following grid:

$$\lambda_{1,N}, \lambda_{2,N} \in \{N^{1/8}, N^{2/8}, N^{3/8}\}, \quad \tau_N \in 2\{N^{-1/8}, N^{-2/8}, N^{-3/8}\}.$$

Here,  $\lambda_{a,N}$  ( $a = 1, 2$ ) denotes the penalty size for the  $a$ th latent layer coefficient  $\mathbf{B}^{(a)}$ . Note that distinct  $\lambda_N$ -values are used for each layer, which is to better accommodate the larger uncertainty in the deeper layer.

While there are many ways to select tuning parameters such as exact or approximate cross-validation and information criteria-based methods, we choose to use the latter in order to encourage sparsity. We select the model with the smallest extended Bayesian information criterion (EBIC). This approach is preferred over cross-validation in unsupervised settings, where likelihood-based loss functions often yield non-sparse, overfitted models (Chetverikov et al., 2021).

Additionally, to implement the SAEM, the step size  $\theta_t$  that determines the weight of the stochastic averaging needs to be specified. Here, following the standard Robbins-Monro

condition (Robbins and Monro, 1951), we set  $\theta_t = 1/t$ .

**Convergence criteria.** For the penalized EM algorithm, we set the convergence criteria such that we terminate the algorithm when the difference between the log-likelihood function values of two consecutive iterations is less than  $N/500$ , as the log-likelihood is proportional to  $N$ . For the SAEM, since we do not directly compute the log-likelihood, convergence is declared when the difference of the vectorized  $L^2$  norm of the continuous parameters is smaller than  $K^{(2)}/2$ . Under the spectral initialization, the PEM and SAEM generally took less than 10 and 5 iterations until convergence, respectively.

In terms of implementing the PEM algorithm to select the number of latent variables,  $K^{(1)}$  or  $K^{(2)}$ , we consider a more generous threshold of  $3 \times N/500$ . This is for the sake of faster implementation, as we only use the resulting likelihood to implement the EBIC and LRT method.

**M-step implementation.** As our M-step in both algorithms (PEM and SAEM) boils down to solving multiple lower-dimensional maximization of dimensions less or equal to  $K^{(1)} + 1$ , we choose to simply apply a built-in optimizing package that directly computes the global maximizers. This is because there are already other approximations being made in the SAEM, and we did not want to increase the randomness for our simulation studies.

For practical implementation for a larger dataset, we recommend the user to modify the M-step to a faster but approximate optimization procedure. For example, one may choose to do a one-step gradient ascent in each iteration of the M-step.

**Additional latent variable permutation for simulations.** In our simulations, resolving the latent variable permutation is necessary to accurately compute the errors. A naive approach involves computing the error across all possible permutations, but this quickly becomes computationally infeasible, even for moderate values of  $K^{(1)} = 18, K^{(2)} = 6$ . To



address this, we formulate the optimal latent variable permutation as an assignment problem and solve it efficiently using the following bottom-up approach as follows.

First, we construct a  $K^{(1)} \times K^{(1)}$  cost matrix, where each entry is the squared  $L^2$  norm between the corresponding column vectors of  $\mathbf{B}^{(1)}$  and  $\widehat{\mathbf{B}}^{(1)}$ . Next, use the Hungarian algorithm (Kuhn, 1955) to find a column permutation that minimizes the total assignment cost. As the column indices of  $\mathbf{B}^{(1)}$  correspond to the row indices of  $\mathbf{B}^{(2)}$ , we permute the rows of  $\mathbf{B}^{(2)}$  accordingly. Finally, we apply the same procedure to find an optimal permutation of the  $\mathbf{B}^{(2)}$  columns. This method ensures computational efficiency while accurately resolving the latent variable permutation.

### S.3.4 Definition of EBIC

Consider a 2-latent layer DDE with  $\mathcal{K} = (K^{(1)}, K^{(2)})$  latent variables. This is a parametric model with  $|\Theta| = J(K^{(1)} + 1) + K^{(1)}(K^{(2)} + 1) + K^{(2)} + J$  (if there exists a dispersion parameter) or  $J(K^{(1)} + 1) + K^{(1)}(K^{(2)} + 1) + K^{(2)}$  (otherwise) parameters. Here, we do not count the discrete parameters  $\mathcal{G}$ , as they are implied by the coefficients  $\mathcal{B}$ . Let  $\widehat{\Theta}_{\mathcal{K}}$  and  $\ell_{\mathcal{K}}(\widehat{\Theta}_{\mathcal{K}}; \mathbf{Y})$  respectively denote the MLE and the log-likelihood under the 2-layer DDE with  $\mathcal{K}$  parameters. Also, let  $\text{df}(\mathcal{K})$  be the number of non-zero parameters in  $\widehat{\Theta}_{\mathcal{K}}$ . Then, following Chen and Chen (2008), the EBIC objective in Section S.3.2 is defined as follows:

$$EBIC(\mathcal{K}) := -2\ell_{\mathcal{K}}(\widehat{\Theta}_{\mathcal{K}}; \mathbf{Y}) + \text{df}(\mathcal{K}) \log N + 2 \binom{|\Theta|}{\text{df}(\mathcal{K})}.$$

## S.4 Additional Simulation Results

### S.4.1 Simulation Results Under the Generic Identifiable Parameters $\mathcal{B}_g$ and Computation Time

Here, we present the omitted details from Section 5 in the main paper, regarding (a) the estimation accuracy under generically identifiable parameters, (b) performance of the PEM algorithm, and (c) computation time.

**Estimation accuracy under generically identifiable parameters.** We present the analogs of Figure 3 under the generically identifiable true parameters  $\mathcal{B}_g$  defined as:

$$\mathbf{B}_g^{(d)} = \begin{pmatrix} -2\mathbf{1}_{K^{(d)}} & \mathbf{B}_2^{(d)} \\ -4\mathbf{1}_{K^{(d)}} & \mathbf{B}_2^{(d)\top} \\ -2\mathbf{1}_{K^{(d)}} & \mathbf{B}_1^{(d)} \end{pmatrix}, \quad \text{where } \beta_{2;j,k}^{(d)} := \begin{cases} 4 & \text{if } k = j, \\ 4/3 & \text{else if } 0 < k - j \leq \lceil K^{(d)}/3 \rceil, \\ 0 & \text{otherwise,} \end{cases} \quad (\text{S.31})$$

and  $\mathbf{B}_1^{(d)}$  is the matrix defined in Equation (13). Note that  $\mathbf{B}_g^{(d)}$  is a less sparse version of  $\mathbf{B}_s^{(d)}$ , where the identity matrices are modified to  $\mathbf{B}_2^{(d)}$ . While  $\mathbf{B}_2^{(d)}$  and  $\mathcal{B}_g$  have the same value of 4 on the main diagonals,  $\mathcal{B}_s$  is sparser. In particular,  $\mathcal{B}_s$  has two exclusive children per latent variable whereas  $\mathcal{B}_g$  has none.

While all other simulation settings are identical to that described in the main text, we make the following two changes. First, we do not consider the largest parameter dimension of  $(J, K^{(1)}, K^{(2)}) = (90, 30, 10)$  in this generically identifiable setting. This is because the layerwise initialization turned out to be less effective in this high-dimensional but less-sparse scenario. Second, for Poisson-based-DDEs, we modify the intercept values to be smaller compared to the values in (13) as follows. When  $K^{(2)} = 2$ , we consider a smaller intercept parameter for  $\mathbf{B}_g^{(1)}$  as follows:

$$\beta_{2;j,0}^{(1)} := \begin{cases} -3 & \text{if } k \leq K^{(1)}, \\ -5 & \text{else if } K^{(1)} < k \leq 2K^{(1)}, \\ -2 & \text{otherwise.} \end{cases}$$

Similarly for  $K^{(2)} = 6$ , we work under the smaller intercept values of

$$\beta_{2;j,0}^{(1)} := \begin{cases} -10 & \text{if } \sum_{k=1}^{K^{(1)}} \beta_{j,k} \geq 8, \\ -5 & \text{otherwise.} \end{cases}$$

This adjustment is to make the Poisson parameters not explode, as using the original in-

tercept values in (S.31) makes some Poisson parameters for  $Y_j \mid \mathbf{A}$  very large and generates unrealistic data.

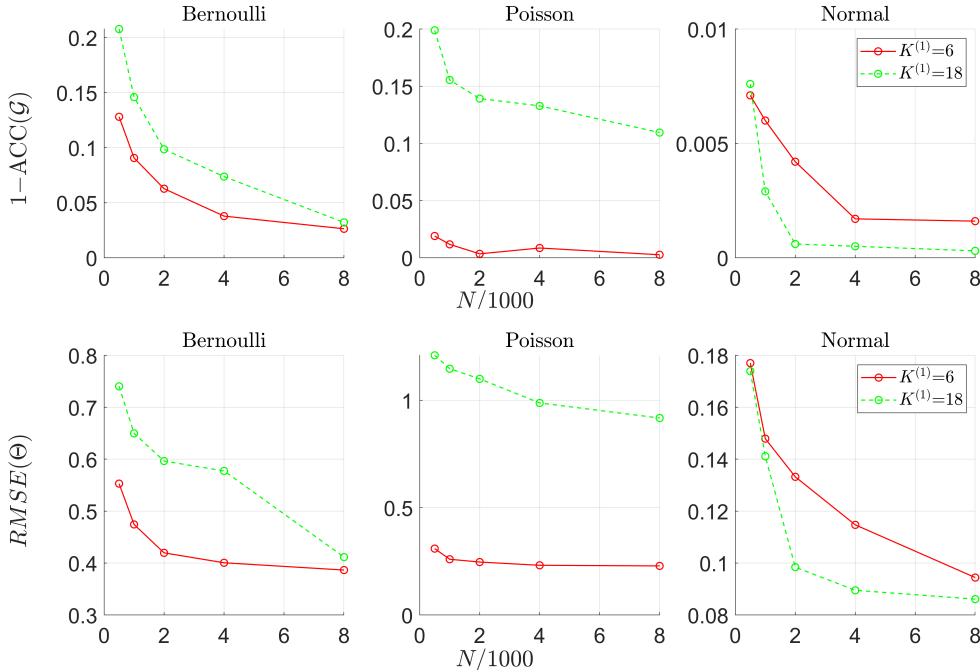


Figure S.1: Estimation error for  $\mathcal{G}$  and  $\Theta$  under the 2-layer DDE with parameters  $\mathcal{B}_g$  and various observed-layer parametric families. Note that the y-axis varies across plots.

The estimation accuracy for  $\mathcal{G}$  and  $\Theta$  is displayed in Figure S.1. While we see a similar trend as in the results under the true parameters  $\mathcal{B}_s$  (Figure 3), the overall error values are larger and indicate that estimation under the less sparse model is more challenging. Recall that we are considering a different Poisson intercept compared to that under  $\mathcal{B}_s$ , so we cannot directly compare the Poisson results.

**Estimation accuracy of the PEM algorithm.** We compare the performance of PEM (Algorithm 1) and SAEM (Algorithm 3) for each parametric family. We implement the PEM under the same simulation setup as SAEM, described in Section 5. However, the PEM implementation failed for higher latent dimensions, specifically under the latent dimension of  $(J, K^{(1)}, K^{(2)}) = (54, 18, 6)$  or higher, due to memory allocation issues. As a result, PEM was only applied in the low-dimensional scenario with with  $(J, K^{(1)}, K^{(2)}) = (18, 6, 2)$ .

The results, presented in Tables S.3-S.5 (error of estimating  $\mathcal{G}$ ) and S.6-S.8 (error of estimating  $\Theta$ ) in Section S.4.4, show that the PEM estimates exhibit a faster rate of convergence as  $N$  increases. In particular, the RMSE values decrease at the parametric rate  $1/\sqrt{N}$ , as established in Theorem 3. We believe that the lower estimation accuracy under SAEM is due to multiple approximations within the SAEM algorithm such as approximate sampling and the objective function updates. We recommend using PEM instead of SAEM to estimate DDEs when the latent dimension is small.

**Computation time.** Figure S.2 reports the computation times for all simulations in Section 5.1 and Section S.4.1. The results show that computation time varies across parametric families. A common trend is that both SAEM and PEM slow down as the sample size  $N$  increases. Additionally, SAEM becomes slower as the parameter dimension increases. Comparing SAEM and PEM is somewhat subtle, as their relative computation times depend on the response type and different convergence criteria. However, preliminary simulations under the dimension  $(J, K^{(1)}, K^{(2)}) = (45, 15, 5)$  indicate that PEM is slower than SAEM across all three responses types. Furthermore, PEM fails to operate under larger dimensions due to high memory requirements. These observations support the conclusion in the main paper that SAEM is desirable for scenarios involving large latent dimensions.

## S.4.2 Experiments With Varying Numbers of Gibbs Samples in

### Algorithm 3

Here, we conduct additional experiments to assess the effect of the number of Gibbs samples,  $C$ , on both estimation accuracy and computation time. These experiments follow the setup in Section S.2.2, but we implement the SAEM algorithm (Algorithm 3) varying  $C = 1, 5, 25$ .

The simulation results in Table S.2 indicate that smaller values of  $C$  result in faster computation across all parametric families, with minimal loss in estimation accuracy. Here, the dependence of computation time on  $C$  arises at the M-step, where the maximization

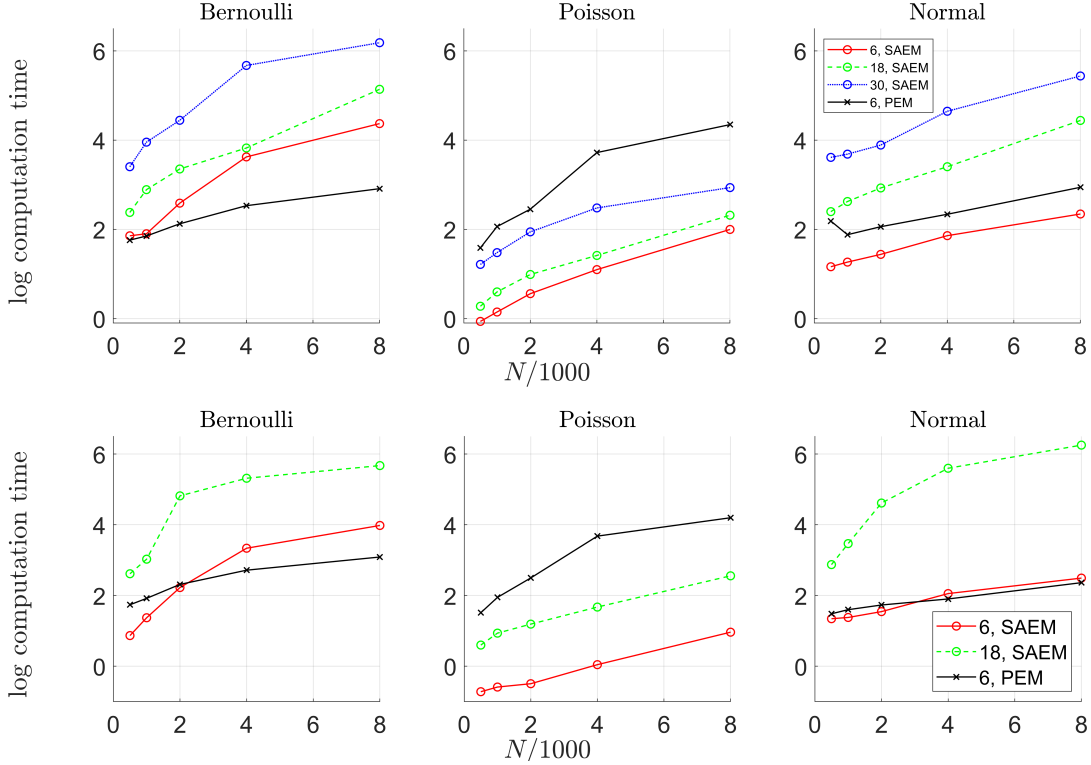


Figure S.2: Log computation time (in seconds) for the simulation results in Section 5 and Section S.4.1, under true parameters  $\mathcal{B}_s$  (top row) and  $\mathcal{B}_g$  (bottom row). The legends indicate the value of  $K^{(1)}$  and estimation algorithm.

objective is a sum of  $O(C)$  functions. A larger  $C$  complicates the objective function and makes the optimization slower. Based on these findings, we selected  $C = 1$  as a baseline for the SAEM procedure.

### S.4.3 Simulations for Selecting the Number of Latent Variables

We first evaluate the performance of the three estimators (denoted as EBIC, LRT, Spectral) for selecting  $K^{(1)}$ , as introduced in Section S.3.2, assuming the knowledge of  $K^{(2)}$ . Since the EBIC and LRT estimators require likelihood computation, we restrict the simulations to the configuration  $(J, K^{(1)}, K^{(2)}) = (18, 6, 2)$ . For each candidate model with  $k \in \mathfrak{K}$  first-latent-layer variables, the likelihood is computed using parameter estimates from the PEM algorithm. For the LRT estimator, we have set the significance level to be  $\alpha = 0.01$  and used the  $\chi^2$  limiting distribution for each sequential test. Continuing from the simulation settings

ParFam	# Gibbs $C \setminus N$	Accuracy( $\mathcal{G}$ )		RMSE( $\Theta$ )		time (s)		# iterations	
		1000	4000	1000	4000	1000	4000	1000	4000
Bernoulli	1	0.916	0.962	0.43	0.36	3.1	10.0	3.0	3.6
	5	0.920	0.961	0.43	0.38	5.3	41.4	2.6	3.2
	25	0.923	0.962	0.43	0.37	26.0	198.5	2.5	3.1
Poisson	1	0.993	0.999	0.26	0.24	3.5	7.0	3.2	3.2
	5	0.999	1	0.24	0.24	6.5	25.4	3.3	3.2
	25	0.998	1	0.24	0.24	34.7	120.3	3.4	3.2
Normal	1	0.994	1	0.16	0.14	0.5	1.1	2.0	2.0
	5	0.995	1	0.15	0.13	1.0	2.2	2.0	2.0
	25	0.994	1	0.16	0.13	2.2	8.8	2.0	2.0

Table S.2: Accuracy measures for  $\mathcal{G}$  and  $\Theta$ , computation time and iterations for 2-layer DDE estimates under varying number of Gibbs samples  $C$ . For the first column, larger is better. For the other columns, smaller is better.

in Section 5, we consider two sets of true parameters:  $\mathcal{B}_s, \mathcal{B}_g$  and three sets of observed-layer parametric families: Bernoulli, Poisson, and Normal. In addition to the sample sizes  $N$  in the previous section,  $N = 6000$  is also considered to better assess the large-sample accuracy. Here, we assume that the number of the top layer latent variables  $K^{(2)} = 2$  is known, and select  $K^{(1)}$  from the candidate set  $\mathfrak{K} = [2K^{(2)}, J/2) \cap \mathbb{N} = \{4, 5, 6, 7, 8\}$ . The equality in  $2K^{(2)} \leq K^{(1)}$  is allowed to consider an equal number of underfitted/overfitted models.

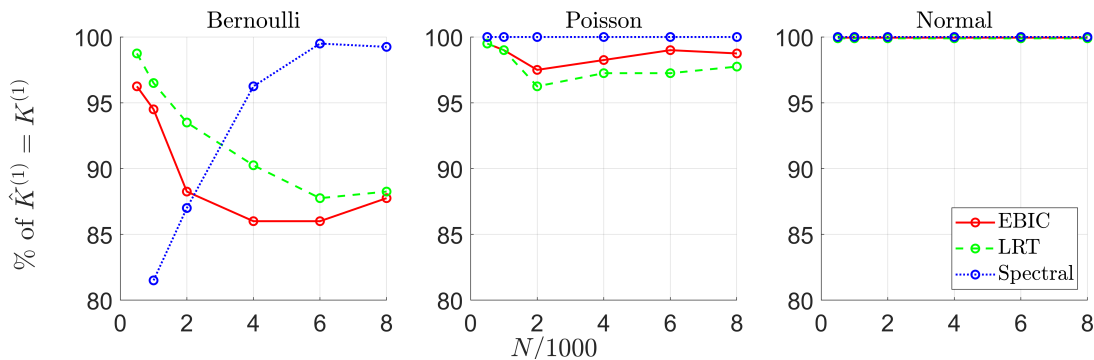


Figure S.3: Selection accuracy of  $K^{(1)}$  under the two-latent-layer DDE with true parameters  $\mathcal{B}_s$ . The spectral ratio estimator shows near-perfect accuracy for large  $N$ .

We fit the three estimators 400 times for each scenario, and display the correct selection percentage for the Bernoulli, Poisson, and Normal-based DDEs with true parameters  $\mathcal{B}_s/\mathcal{B}_g$

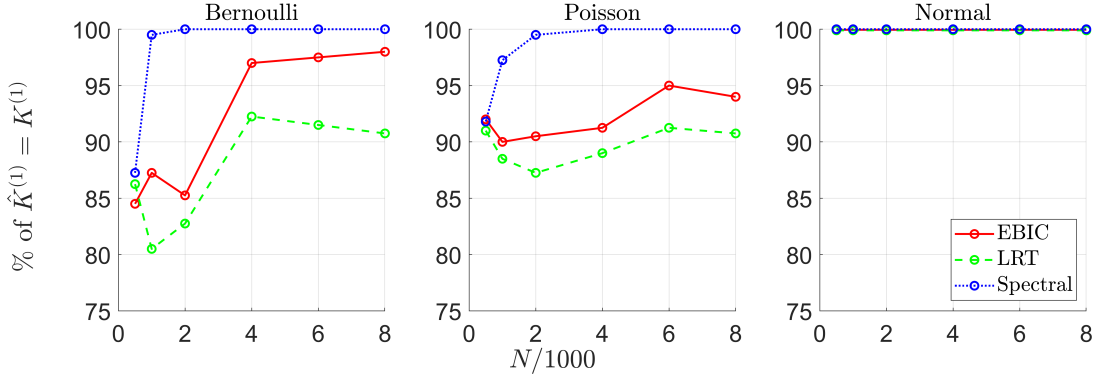


Figure S.4: Simulation results for selecting  $K^{(1)}$  under the 2-layer DDE with true parameters  $\mathcal{B}_g$ .

in Figure S.3/Figure S.4. Comparing the three estimators, the spectral ratio-based estimator has near-perfect accuracy when  $N$  is large enough, say 4000. This demonstrates the empirical consistency of the spectral ratio estimator. In contrast, the consistency of the EBIC and LRT estimators is not clear for Bernoulli and Poisson responses<sup>2</sup>. Thus, we conclude that for a large enough  $N$ , it is desirable to select  $K^{(1)}$  using the spectral ratio estimator. Among the three response types, the Bernoulli case with its nonlinear link function and limited response values is the most challenging. In contrast, the Normal case with a linear observed layer and continuous responses achieves near-perfect selection accuracy, which is consistent with earlier observations regarding parameter estimation accuracy.

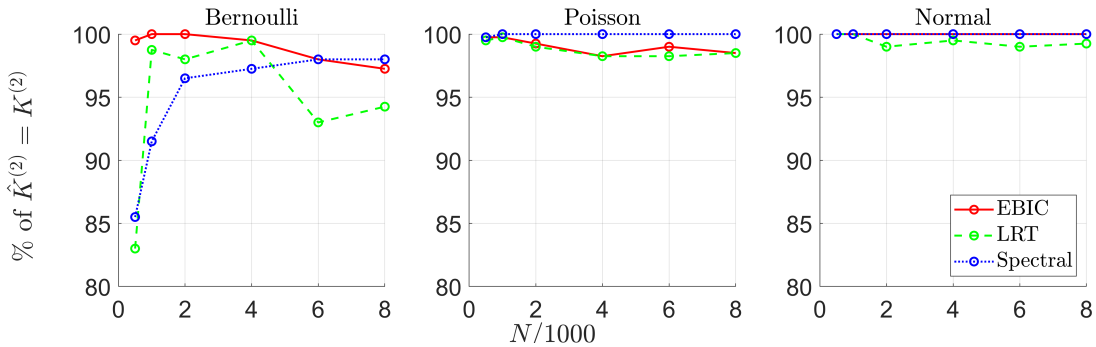


Figure S.5: Selection accuracy of  $K^{(2)}$  under two-latent-layer DDEs with true parameters  $\mathcal{B}_s$ .

<sup>2</sup>To be more precise, as we are using approximate level  $\alpha = 0.01$  tests, the correct selection percentage of the LRT estimator should converge to 0.99.

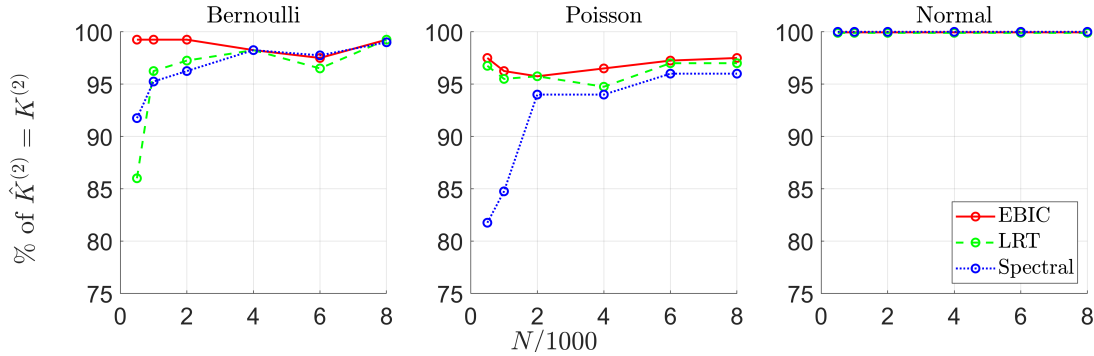


Figure S.6: Simulation results for selecting  $K^{(2)}$  under the 2-layer DDE with true parameters  $\mathcal{B}_g$ .

We also apply these three estimators to select  $K^{(2)}$ , assuming that  $K^{(1)} = 6$  is correctly estimated or known. The candidate set for  $K^{(2)}$  is  $\mathfrak{K} := \{1, 2, 3\}$ . Figure S.5/Figure S.6 displays the correct selection percentage under the true parameters  $\mathcal{B}_s/\mathcal{B}_g$ . Here, we implement the LRT estimator by naively assuming that Wilk’s theorem holds. The overall trends are similar to those observed in the previous figures for selecting  $K^{(1)}$ . Under the sparse true parameter  $\mathcal{B}_s$ , the spectral ratio estimator performs well across all response types and the LRT estimator has the lowest, but still decent accuracy. Interestingly, the EBIC estimator outperforms the spectral ratio estimator in more challenging scenarios, such as Bernoulli responses with small  $N$  or under the Poisson responses with less sparse true parameters  $\mathcal{B}_g$ . Unlike the case for selecting  $K^{(1)}$ , it is not clear that the spectral ratio estimator outperforms the EBIC estimator for selecting  $K^{(2)}$ .

Based on these experiments, we conclude that in the most general setting of a two-latent-layer DDE where both  $K^{(1)}$  and  $K^{(2)}$  are unknown, a two-step approach is effective. First, the spectral ratio estimator can be used to select  $K^{(1)}$ . Then,  $K^{(2)}$  can be determined using either the EBIC or the spectral ratio estimator, incorporating domain knowledge if needed.

#### S.4.4 Exact Values of Estimation Errors

We display the complete results of the simulation outputs corresponding to plots in Section 5, Section S.4.1, and Section S.4.3.



**Accuracy of Estimating  $\mathcal{G}$ .** Tables S.3-S.5 display the average entrywise estimation accuracy for  $\mathcal{G}$  under each parametric family. These values correspond to the upper rows of Figures 3 and S.1.

Parfam	True parameter	$(J, K^{(1)}, K^{(2)})$	Algorithm\N	500	1000	2000	4000	8000
Bernoulli	$\mathcal{B}_s$	(18,6,2)	SAEM	0.899	0.931	0.956	0.974	0.985
			PEM	0.926	0.966	0.986	0.992	0.992
		(54,18,6)	SAEM	0.910	0.967	0.990	0.996	0.998
	$\mathcal{B}_g$	(18,6,2)	SAEM	0.872	0.909	0.937	0.962	0.974
			PEM	0.891	0.937	0.970	0.986	0.992
		(54,18,6)	SAEM	0.792	0.854	0.902	0.926	0.968

Table S.3: Acc( $\mathcal{G}$ ) under the Bernoulli 2-layer DDE.

Parfam	True parameter	$(J, K^{(1)}, K^{(2)})$	Algorithm\N	500	1000	2000	4000	8000
Poisson	$\mathcal{B}_s$	(18,6,2)	SAEM	0.985	0.993	0.999	0.999	0.999
			PEM	0.994	0.999	1	1	1
		(54,18,6)	SAEM	0.987	0.996	0.999	1	1
	$\mathcal{B}_g$	(18,6,2)	SAEM	0.981	0.988	0.997	0.992	0.997
			PEM	0.994	0.995	0.998	0.998	1
		(54,18,6)	SAEM	0.801	0.845	0.861	0.867	0.891

Table S.4: Acc( $\mathcal{G}$ ) under the Poisson 2-layer DDE.

Parfam	True parameter	$(J, K^{(1)}, K^{(2)})$	Algorithm	500	1000	2000	4000	8000
Normal	$\mathcal{B}_s$	(18,6,2)	SAEM	0.985	0.993	0.999	0.999	0.999
			PEM	0.992	0.996	1	1	1
		(54,18,6)	SAEM	0.996	0.998	0.999	1	1
	$\mathcal{B}_g$	(18,6,2)	SAEM	0.993	0.994	0.996	0.998	0.998
			PEM	0.992	0.997	0.999	1	1
		(54,18,6)	SAEM	0.993	0.995	0.998	0.999	1

Table S.5: Acc( $\mathcal{G}$ ) under the Normal 2-layer DDE.

**Accuracy of Estimating  $\Theta$ .** Tables S.6–S.8 reports the RMSE values for estimating continuous parameters  $\Theta$ . These values correspond to the bottom rows of Figures 3 and S.1.

Parfam	True parameter	$(J, K^{(1)}, K^{(2)})$	Algorithm\N	500	1000	2000	4000	8000
Bernoulli	$\mathcal{B}_s$	(18,6,2)	SAEM	0.498	0.431	0.386	0.359	0.341
			PEM	0.404	0.304	0.231	0.203	0.184
		(54,18,6)	SAEM	0.392	0.289	0.231	0.213	0.208
		(90,30,10)	SAEM	0.356	0.240	0.204	0.185	0.177
	$\mathcal{B}_g$	(18,6,2)	SAEM	0.553	0.474	0.420	0.400	0.387
			PEM	0.520	0.398	0.288	0.206	0.165
		(54,18,6)	SAEM	0.740	0.650	0.596	0.577	0.412

Table S.6: RMSE( $\Theta$ ) under the Bernoulli 2-layer DDE.

Parfam	True parameter	$(J, K^{(1)}, K^{(2)})$	Algorithm\N	500	1000	2000	4000	8000
Poisson	$\mathcal{B}_s$	(18,6,2)	SAEM	0.281	0.258	0.245	0.243	0.242
			PEM	0.219	0.158	0.108	0.080	0.061
		(54,18,6)	SAEM	0.289	0.168	0.153	0.147	0.145
		(90,30,10)	SAEM	0.281	0.195	0.125	0.117	0.116
	$\mathcal{B}_g$	(18,6,2)	SAEM	0.309	0.260	0.247	0.231	0.229
			PEM	0.206	0.145	0.101	0.072	0.053
		(54,18,6)	SAEM	1.210	1.147	1.100	0.988	0.918

Table S.7: RMSE( $\Theta$ ) under the Poisson 2-layer DDE.

Parfam	True parameter	$(J, K^{(1)}, K^{(2)})$	Algorithm\N	500	1000	2000	4000	8000
Normal	$\mathcal{B}_s$	(18,6,2)	SAEM	0.189	0.156	0.147	0.137	0.133
			PEM	0.170	0.128	0.080	0.063	0.054
		(54,18,6)	SAEM	0.117	0.090	0.072	0.063	0.057
		(90,30,10)	SAEM	0.108	0.074	0.054	0.045	0.041
	$\mathcal{B}_g$	(18,6,2)	SAEM	0.177	0.148	0.133	0.115	0.094
			PEM	0.179	0.137	0.094	0.069	0.055
		(54,18,6)	SAEM	0.174	0.141	0.098	0.090	0.086

Table S.8: RMSE( $\Theta$ ) under the Normal 2-layer DDE.

**Accuracy of selecting  $\mathcal{K}$ .** Tables S.9-S.10 reports the accuracy of selecting  $\mathcal{K}$  under Bernoulli and Poisson-based DDEs, which correspond to Figure S.3 and Figure S.4. Accu-

racy values for Normal-based DDEs are omitted, as all methods demonstrated near-perfect accuracy in this setting. Similarly, Tables S.11-S.12 display the results for selecting  $K^{(2)}$ , which corresponds to Figures S.5 and S.6.

These tables provide additional insights beyond those presented in figures, which only display the correct selection probability for the events  $\widehat{K}^{(1)} = 6$  and  $\widehat{K}^{(2)} = 2$ . The percentage of incorrect estimates in the tables reveal systematic tendencies of the estimators: the EBIC and LRT estimators frequently *overselect* ( $\widehat{K}^{(1)} \geq K^{(1)}$ ) whereas the spectral estimator sometimes *underselects* ( $\widehat{K}^{(1)} \leq K^{(1)}$ ).

ParFam, value	$N$	Method \ $\widehat{K}^{(1)}$	4	5	6	7	8	
Bernoulli, $\mathcal{B}_s$	500	EBIC		0.25	96.25	3.5		
		LRT	0.5		<b>98.75</b>	0.75		
		Spectral	1.75	30.0	67.5	0.75		
	1000	EBIC				94.5	5.5	
		LRT				<b>96.5</b>	3.5	
		Spectral	0.25	18.25	81.5			
	2000	EBIC				88.25	11.75	
		LRT				<b>93.5</b>	6.25	0.25
		Spectral		13.0	87.0			
	4000	EBIC				86.0	12.25	1.75
		LRT				90.25	9.25	0.5
		Spectral		3.75	<b>96.25</b>			
	6000	EBIC				86.0	13.5	1.5
		LRT				87.75	12.25	
		Spectral		0.5	<b>99.5</b>			
	8000	EBIC				87.75	11.0	1.25
		LRT				88.25	10.75	1.00
		Spectral		0.75	<b>99.25</b>			
Bernoulli, $\mathcal{B}_g$	500	EBIC			84.5	13.75	1.75	
		LRT	0.75	1.0	86.25	12.0		
		Spectral	8.5	4.25	<b>87.25</b>			
	1000	EBIC				87.25	10.5	2.5
		LRT				80.5	18.5	1.0
		Spectral	0.5		<b>99.5</b>			
	2000	EBIC				85.25	11.5	3.25
		LRT				82.75	16.25	1.0
		Spectral			<b>100.0</b>			
	4000	EBIC				97.0	3.0	
		LRT				92.25	7.75	
		Spectral			<b>100.0</b>			
	6000	EBIC				97.5	2.5	
		LRT				91.5	8.5	
		Spectral			<b>100.0</b>			
	8000	EBIC				98.0	2.0	
		LRT				90.75	9.25	
		Spectral			<b>100.0</b>			

Table S.9: Empirical distribution of the estimated  $\widehat{K}^{(1)}$  values under the Bernoulli DDE with true  $K^{(1)} = 6$  and parameters  $\mathcal{B}_s, \mathcal{B}_g$ . For each sample size, we present the method with the highest accuracy in bold. “ParFam” is short for “parametric family”.

ParFam, value	$N$	Method \ $\widehat{K}^{(1)}$	4	5	6	7	8	
Poisson, $\mathcal{B}_s$	500	EBIC			99.5	0.5		
		LRT			99.5	0.5		
		Spectral			<b>100.0</b>			
	1000	EBIC				99.0	1.0	
		LRT				99.0	1.0	
		Spectral				<b>100.0</b>		
	2000	EBIC				97.5	2.5	
		LRT				96.25	3.75	
		Spectral				<b>100.0</b>		
	4000	EBIC				98.25	1.5	0.25
		LRT				97.25	2.75	
		Spectral				<b>100.0</b>		
	6000	EBIC				99.0	1.0	
		LRT				97.25	2.75	
		Spectral				<b>100.0</b>		
	8000	EBIC				98.75	0.75	0.5
		LRT				97.75	1.75	0.5
		Spectral				<b>100.0</b>		
Poisson, $\mathcal{B}_g$	500	EBIC			<b>92.0</b>	7.75	0.25	
		LRT		1.0	91.0	8.0		
		Spectral	8.5		91.5			
	1000	EBIC				90.0	9.5	0.5
		LRT				88.5	10.75	0.75
		Spectral	2.75		<b>97.25</b>			
	2000	EBIC				90.5	8.5	1.0
		LRT		0.25	87.25	11.5	1.0	
		Spectral	0.5		<b>99.5</b>			
	4000	EBIC				91.25	7.25	1.5
		LRT				89.0	9.25	1.75
		Spectral				<b>100.0</b>		
	6000	EBIC				95.0	4.5	0.5
		LRT				91.25	7.75	1.0
		Spectral				<b>100.0</b>		
	8000	EBIC				94.0	5.0	1.0
		LRT				90.75	8.25	1.0
		Spectral				<b>100.0</b>		

Table S.10: Empirical distribution of the estimated  $\widehat{K}^{(1)}$  values under the Poisson DDE with true  $K^{(1)} = 6$  and parameters  $\mathcal{B}_s, \mathcal{B}_g$ . For each sample size, we present the method with the highest accuracy in bold. “ParFam” is short for “parametric family”.

ParFam, value	$N$	Method \ $\widehat{K}^{(2)}$	1	2	3	
Bernoulli, $\mathcal{B}_s$	500	EBIC	0.5	<b>99.5</b>		
		LRT	16.75	83.0	0.25	
		Spectral	12.0	85.5	2.5	
	1000	EBIC			<b>100.0</b>	
		LRT	0.5	98.75	0.75	
		Spectral	6.5	91.5	2.0	
	2000	EBIC			<b>100.0</b>	
		LRT		98.0	2.0	
		Spectral	3.25	96.5	0.25	
	4000	EBIC			<b>99.5</b>	0.5
		LRT		96.0	4.0	
		Spectral	2.75	97.25		
	6000	EBIC			<b>98.0</b>	2.0
		LRT		93.0	7.0	
		Spectral	2.0	<b>98.0</b>		
	8000	EBIC			97.25	2.75
		LRT			94.25	5.75
		Spectral	2.0	<b>98.0</b>		
Bernoulli, $\mathcal{B}_g$	500	EBIC	0.75	<b>99.25</b>		
		LRT	13.5	86.0	0.5	
		Spectral	7.0	91.75	1.25	
	1000	EBIC			<b>99.25</b>	0.75
		LRT	1.5	96.25	2.25	
		Spectral	3.5	95.25	1.25	
	2000	EBIC			<b>99.25</b>	0.75
		LRT	0.5	94.0	5.5	
		Spectral	8.75	90.75	0.5	
	4000	EBIC			<b>98.25</b>	1.75
		LRT			<b>98.25</b>	1.75
		Spectral	2.75	96.25	1.0	
	6000	EBIC			<b>97.5</b>	2.5
		LRT		96.5	3.5	
		Spectral	1.75	97.75	0.5	
	8000	EBIC			<b>99.25</b>	0.75
		LRT			<b>99.25</b>	0.75
		Spectral	0.5	99.0	0.5	

Table S.11: Empirical distribution of the estimated  $\widehat{K}^{(2)}$  values under the Bernoulli DDE with true  $K^{(2)} = 2$  and parameters  $\mathcal{B}_s, \mathcal{B}_g$ . For each sample size, we present the method with the highest accuracy in bold. “ParFam” is short for “parametric family”.

Parfam, value	$N$	Method \ $\widehat{K}^{(2)}$	1	2	3	
Poisson, $\mathcal{B}_s$	500	EBIC		<b>99.75</b>	0.25	
		LRT		99.5	0.5	
		Spectral	0.25	<b>99.75</b>		
	1000	EBIC			99.75	0.25
		LRT			99.75	0.25
		Spectral			<b>100.0</b>	
	2000	EBIC			99.25	0.75
		LRT			99.0	1.0
		Spectral			<b>100.0</b>	
	4000	EBIC			98.25	1.75
		LRT			98.25	1.75
		Spectral			<b>100.0</b>	
	6000	EBIC			99.0	1.0
		LRT			98.25	1.75
		Spectral			<b>100.0</b>	
	8000	EBIC			98.5	1.5
		LRT			98.5	1.5
		Spectral			<b>100.0</b>	
Poisson, $\mathcal{B}_g$	500	EBIC	1.0	<b>97.5</b>	1.5	
		LRT	1.75	96.75	1.5	
		Spectral	16.5	81.75	1.75	
	1000	EBIC	0.25	<b>96.25</b>	3.5	
		LRT	0.75	95.5	3.75	
		Spectral	13.75	84.75	1.5	
	2000	EBIC		<b>95.75</b>	4.25	
		LRT	0.5	94.0	5.5	
		Spectral	8.75	90.75	0.5	
	4000	EBIC	0.25	<b>96.5</b>	3.25	
		LRT	0.75	94.75	4.5	
		Spectral	5.5	94.0	0.5	
	6000	EBIC		<b>97.25</b>	2.75	
		LRT		97.0	3.0	
		Spectral	3.5	96.0	0.5	
	8000	EBIC	0.25	<b>97.5</b>	2.25	
		LRT	0.25	97.0	2.75	
		Spectral	3.5	96.0	0.5	

Table S.12: Empirical distribution of the estimated  $\widehat{K}^{(2)}$  values under the Poisson DDE with true  $K^{(2)} = 2$  and parameters  $\mathcal{B}_s, \mathcal{B}_g$ . For each sample size, we present the method with the highest accuracy in bold. “ParFam” is short for “parametric family”.

## S.5 Data Analysis Details and Additional Results

### S.5.1 Preprocessing

**MNIST Data.** We work with the preprocessed version of the default training set, which consists of 60,000 images, each containing information on the  $28^2$  pixel values. Initially, each pixel takes integer values between 0 and 255. As the data values are highly concentrated around values near 0 or larger than 200, we transform the data into binary responses by thresholding at a value of 128. In other words, pixels with values exceeding 128 are assigned a binary value of 1, while the rest are set to 0. For the sake of easier presentation and computational efficiency, we work on the subset of the dataset whose true digit labels are equal to 0, 1, 2, 3, and also discard some pixels with uniformly small values by selecting  $J = 264$  pixels whose average pixel values are larger than 40. After preprocessing, the training set consists of  $N = 20,679$  unlabeled images. We identically preprocess the test set, which leads to a total of  $N = 4,157$  images.

**20 Newsgroups Data.** The dataset provides a default partition of the train and test sets based on chronological order, and we use this partition. The preprocessing of the training data was carried out in three main steps. First, to reduce the signal-to-noise ratio and enhance interpretability, we focus on a subset of labels. To elaborate, we consider the newsgroup articles that belong to the large class of computer, recreation, and science (see the top-latent layer labels in Figure S.7). A manual inspection revealed that the newsgroup with label `sci.crypt` has a wide range of topics such as government and politics and was often cross-referenced to those newsgroups, so we did not include these documents in our dataset. Second, documents of extreme lengths were filtered out by removing the shortest 5% and longest 1% of all documents. This procedure is standard in the literature, and has been shown to increase the signal-to-noise ratio (Ke and Wang, 2024). Third, we construct our dictionary by excluding infrequent words (with less than 100 occurrences) and screening



out stop-words (such as the, he, in) and topic-irrelevant words (such as like, must, since) using the R package `tm`. As the original dataset consists of email texts, we performed a manual screening to remove uninformative email-related vocabulary, such as edu, com, net, and cmu. Finally, we conducted a secondary filtering of the short documents, as the removal of stop-words led to some documents being uninformative. The resulting processed train dataset is a sparse  $5883 \times 653$  count matrix.

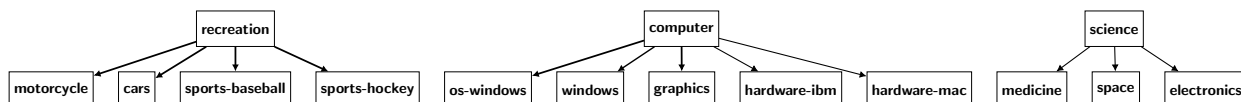


Figure S.7: Nested structure of the true held-out labels for the 20 newsgroups dataset.

To process the test dataset, we go through the same first and second steps described above. We continue using the dictionary constructed from the train set, with  $J = 653$  words. After filtering out the short/long documents, the resulting data matrix consists of  $N = 3320$  documents.

**TIMSS Response Time Data.** We use the preprocessed dataset provided in [Lee and Gu \(2024\)](#). Additionally, we remove all rows of the data matrix with missing values. While our estimation procedure can be modified to handle missing data (missing at random) by modifying the likelihood function, we take this additional preprocessing step for the sake of consistency with other parts of the paper.

### S.5.2 Selecting the Number of Latent Variables

**MNIST Data.** We select  $K^{(1)} = 5$  based on the spectral-gap estimator, as illustrated in the left panel of Figure S.8. Also, we set  $K^{(2)} = 2$  motivated by our identifiability requirement  $2K^{(2)} < K^{(1)}$ . This choice is also supported by the fact that there are four true labels. Each latent configuration  $\mathbf{A}^{(2)} = (A_1^{(2)}, A_2^{(2)}) \in \{0, 1\}^2$  uniquely corresponds to each digit, as illustrated in the center panel of Figure 4.

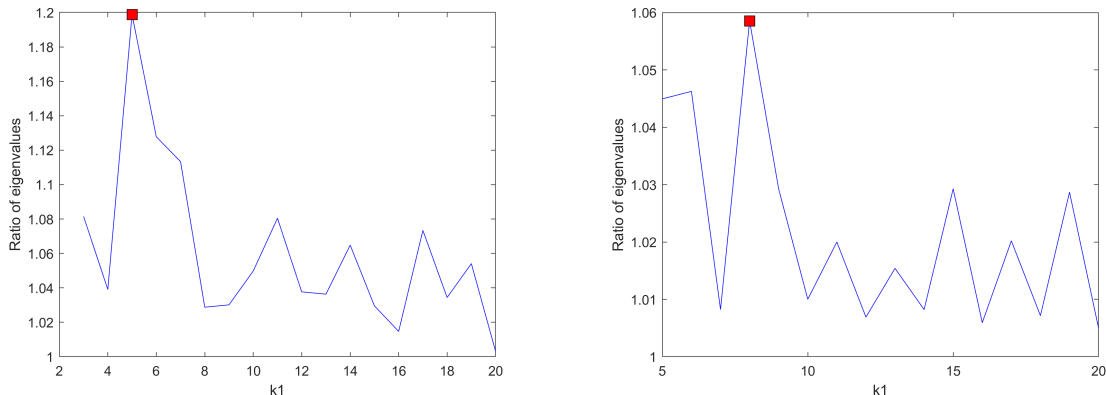


Figure S.8: Based on the spectral estimator for  $K^{(1)}$ , (left) we select  $K^{(1)} = 5$  for MNIST, and (right)  $K^{(1)} = 8$  for 20 newsgroups. The peak, highlighted in red, correspond to the selected values. We omit displaying the first few eigenvalue ratios for better illustration.

**20 Newsgroups Data.** We select  $K^{(1)} = 8$  based on the spectral-gap estimator, as illustrated in the right panel of Figure S.8. For  $K^{(2)}$ , the EBIC values are quite similar for  $K^{(2)} = 2, 3$  with values of  $1.3273 \times 10^6$  and  $1.3277 \times 10^6$ , respectively. Also, the spectral-gap is similar for both values  $K^{(2)} = 2, 3$ . Hence, we select  $K^{(2)}$  based on the interpretability of the inferred latent structure. The estimated latent structure with  $K^{(2)} = 3$  is displayed in Figure S.9. Compared to Figure 5 in the main text, the ‘technology’ topic has split into two groups whose interpretation is somewhat blurry. Notably, these two ‘technology’ latent variables do not match the labels of ‘computer’ and ‘science’ provided by the dataset (see Figure S.7). For instance, the ‘technology 2’ variable has arrows to the finer topics of motorcycle, software, and space. Hence, we select  $K^{(2)} = 2$  based on this lack of semantic distinction.

**TIMSS Response Time Data.** The dataset comes with a rough classification of the seven latent skills into  $K^{(2)} = 2$  categories: content skills and cognitive skills. However, we observed that fitting  $K^{(2)} = 2$  results in one of the proportion parameters exhibiting an unusually large value of  $p_2 = 0.96$ . This indicates that  $A_2^{(2)} = 1$  for 96% of the students, and this skill is redundant. Hence, we have adjusted the number of higher-order latent variables

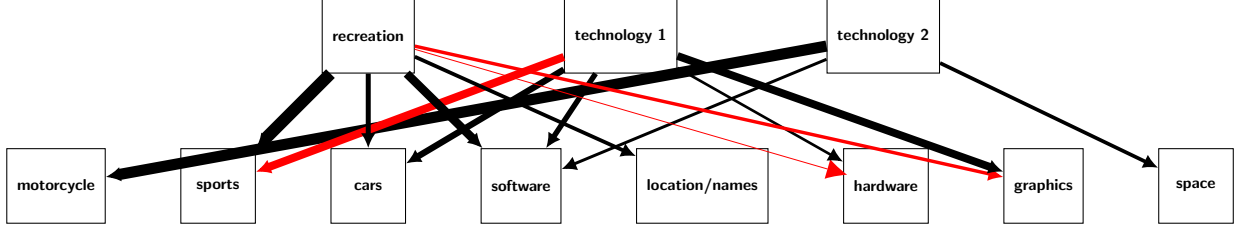


Figure S.9: Graphical structure of the latent topics, where we fit the 2-layer DDE with  $K^{(2)} = 3, K^{(1)} = 8$ . The width of the upper layer arrows is proportional to the corresponding coefficients and the red arrow indicates negative values.

to  $K^{(2)} = 1$ , which partitions the students into two groups based on the value of  $A_1^{(2)}$ . The EBIC for the two cases were also comparable and justified this choice.

### S.5.3 Performance Evaluation for the 20 Newsgroups Dataset

**Perplexity.** Perplexity is a very popular measure to evaluate topic models and many other machine learning models. Following the original definition from Blei et al. (2003) that considers each word as an individual sample, we define

$$\text{perplexity}(\mathbf{Y} \mid \mathbf{A}, \Theta) := \exp \left[ -\frac{\sum_{i,j} Y_{i,j} \log \left( \frac{\lambda_{i,j}}{\sum_{j'} \lambda_{i,j'}} \right)}{\sum_{i,j} Y_{i,j}} \right]. \quad (\text{S.32})$$

Here,  $\lambda_{i,j} = \exp \left( \beta_{j,0}^{(1)} + \sum_{k \in [K^{(1)}]} \beta_{j,k}^{(1)} A_{i,k}^{(1)} \right)$  is the Poisson parameter for the conditional distribution  $Y_{i,j} \mid \mathbf{A}_i^{(1)}$ . The motivation for (S.32) is that under the Poisson likelihood for (4), the joint distribution of  $(Y_{i,1}, \dots, Y_{i,J}) \mid \mathbf{A}_i$  follows a Multinomial distribution

$$\text{Multi} \left( \sum_j Y_{i,j}, \left( \frac{\lambda_{i,1}}{\sum_{j'} \lambda_{i,j'}}, \dots, \frac{\lambda_{i,J}}{\sum_{j'} \lambda_{i,j'}} \right) \right).$$

This definition is consistent with that used for Poisson factor analysis (Zhou et al., 2012; Gan et al., 2015) as well as LDA (Blei et al., 2003).

To evaluate (S.32), we use the parameter estimates  $\hat{\Theta}$  from our proposed method. As (S.32) also requires the knowledge of each latent variable  $\mathbf{A}_i^{(1)}$ , latent variable estimates needs to be computed. To compute train perplexity, we use the estimator (14) from the main text. For test perplexity, we adopt the approach of Gan et al. (2015), first computing the posterior

distribution of  $\mathbf{A}_i^{(1)}$  by using 80% of the words in each document, and evaluating perplexity based on the remaining 20% words.

**Implementations of existing topic modeling algorithms.** We describe the implementation details of alternative topic modeling algorithms that were used for model comparison in Table 4. LDA is implemented by the function `LDA` in the R package `topicmodels` (Grün and Hornik, 2011), using the variational EM algorithm. For DPFA, we have used the original MATLAB codes that were publicly available on the first author’s GitHub page<sup>3</sup> (Gan et al., 2015). Based on the empirical findings in Gan et al. (2015), which indicate that the DPFA-SBN model optimized using the SGNHT method performs the best among their proposed methods, we chose this implementation. The method was run using the default tuning parameters. Note while Gan et al. (2015) also analyzed the 20 Newsgroups dataset (see Table 1 in the cited paper), their reported perplexity values are not directly comparable to our results due to preprocessing. Notably, our preprocessing steps enhanced the signal-to-noise ratio and leads to a smaller perplexity.

### S.5.4 Additional Visualization of MNIST Dataset

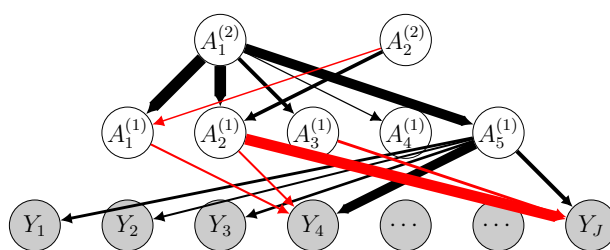


Figure S.10: Graphical model representation of the learned latent structure. The edge widths are proportional to coefficients’ absolute values. The edge colors (black/red) imply positive/negative coefficients, respectively.

In Figure S.10, we visualize the learned latent structure of the MNIST dataset. The corresponding graphical matrix  $\mathbf{G}^{(2)}$  was used to interpret the top layer latent variables in the

<sup>3</sup>[https://github.com/zhegan27/dpfa\\_icml2015/tree/master](https://github.com/zhegan27/dpfa_icml2015/tree/master)





















Label	True	LCM	1-layer DDE	Spectral init	2-layer DDE
0					
1					
2					
3					

Table S.13: True (first column) and reconstructed (other columns) images under various estimators. Here, each pixel takes values in  $[0, 1]$ , where a darker shade indicates a larger value.

main text. For example,  $A_1^{(2)}$  is connected to all lower-layer variables, and we interpret this as an indicator for the *pixel density* of the image.

We additionally visualize examples of reconstructed images under various models in Table S.13, which have been used to compute the pixel-wise reconstruction accuracy in Table 3 in the main paper. The reconstructions are based on the corresponding conditional mean  $\mathbb{E}(\mathbf{Y} \mid \mathbf{A}^{(1)})$  for each latent representation  $\mathbf{A}^{(1)}$ , which is rearranged in the original  $28 \times 28$  grid. The visualization illustrates that the reconstructions from the 2-layer DDE exhibit greater clarity compared to those from alternative models.